

UNCLASSIFIED

AD NUMBER

AD823181

LIMITATION CHANGES

TO:

Approved for public release; distribution is unlimited. Document partially illegible.

FROM:

Distribution authorized to U.S. Gov't. agencies and their contractors;
Administrative/Operational Use; NOV 1967. Other requests shall be referred to Arnold Engineering Development Center, Arnold AFB, TN. Document partially illegible.

AUTHORITY

AEDC ltr, 12 Sep 1968

THIS PAGE IS UNCLASSIFIED

Cy 1



INVESTIGATION OF DYNAMIC ROCKET THRUST MEASUREMENT TECHNIQUES

F. L. Crosswy and H. T. Kalb

ARO, Inc.

This document is approved for public release
and its distribution is unlimited. *Per AF Letter dtd
12 Sept. 1968 signed
William O. Cole.*

November 1967

*ADD (AET)
Released to AFTR Sept 1968*

This document is subject to special export controls
and each transmittal to foreign governments or foreign
nationals may be made only with prior approval of
Arnold Engineering Development Center (AEDC),
Arnold Air Force Station, Tennessee.

**ARNOLD ENGINEERING DEVELOPMENT CENTER
AIR FORCE SYSTEMS COMMAND
ARNOLD AIR FORCE STATION, TENNESSEE**

PROPERTY OF U. S. AIR FORCE
AEDC LIBRARY
AF 40(600)1200

AEDC TECHNICAL LIBRARY



5 0720 0031 5913

NOTICES

When U. S. Government drawings, specifications, or other data are used for any purpose other than a definitely related Government procurement operation, the Government thereby incurs no responsibility nor any obligation whatsoever, and the fact that the Government may have formulated, furnished, or in any way supplied the said drawings, specifications, or other data, is not to be regarded by implication or otherwise, or in any manner licensing the holder or any other person or corporation, or conveying any rights or permission to manufacture, use, or sell any patented invention that may in any way be related thereto.

Qualified users may obtain copies of this report from the Defense Documentation Center.

References to named commercial products in this report are not to be considered in any sense as an endorsement of the product by the United States Air Force or the Government.

DEPARTMENT OF THE AIR FORCE
HEADQUARTERS ARNOLD ENGINEERING DEVELOPMENT CENTER (AFSC)
ARNOLD AIR FORCE STATION, TENNESSEE 37369



REPLY TO
ATTN OF:

AETS

12 September 1968

SUBJECT:

Distribution Statement for AEDC-TR-67-202, "Investigation of
Dynamic Rocket Thrust Measurement Techniques," (AD 823 181)

TO:

ALL RECIPIENTS

1. Subject report has been reviewed for applicable distribution
limitations and has been determined releasable to the general
public. Correct distribution statement for this report is:

This document has been approved for public
release and sale; its distribution is unlimited.

2. Previous distribution statement should be deleted.

William O. Cole
WILLIAM O. COLE
STINFO Officer
Directorate of Test

INVESTIGATION OF DYNAMIC
ROCKET THRUST MEASUREMENT
TECHNIQUES

F. L. Crosswy and H. T. Kalb
ARO, Inc.

This document is subject to special export controls and each transmittal to foreign governments or foreign nationals may be made only with prior approval of Arnold Engineering Development Center (AEDC), Arnold Air Force Station, Tennessee.

This document has been approved for public release
and its distribution is unlimited. Per AF letter dtd
12 Sept., 1968 Signed
William O. Cole.

FOREWORD

The work presented herein was sponsored by Arnold Engineering Development Center (AEDC), Air Force Systems Command (AFSC), Arnold Air Force Station, Tennessee, under Program Element 6240518F, Project 5730, and Task 573004.

The work was obtained by ARO, Inc. (a subsidiary of Sverdrup & Parcel and Associates, Inc.), contract operator of the AEDC under Contract AF40(600)-1200. The research and testing was performed from June 1966 to August 1967 under ARO Project No. BC2703, and the manuscript was submitted for publication on August 30, 1967.

Information in this report is embargoed under the Department of State International Traffic in Arms Regulations. This report may be released to foreign governments by departments or agencies of the U. S. Government subject to approval of the Arnold Engineering Development Center (AEDC), or higher authority within the Department of the Air Force. Private individuals or firms require a Department of State export license.

This technical report has been reviewed and is approved.

Forrest B. Smith, Jr.
Research Division
Directorate of Plans
and Technology

Edward R. Feicht
Colonel, USAF
Director of Plans
and Technology

ABSTRACT

The dynamic rocket thrust measurement is set forth as a part of the overall ground test problem. Dynamic thrust data obtained with conventional thrust measurement techniques can be distorted because of the transient response of the thrust stand-rocket engine mechanical structure. Distortionless dynamic thrust measurement is shown to be possible if the transfer function of the measurement system satisfies certain criteria. Three independent techniques satisfying the distortionless measurement criteria were investigated both analytically and experimentally, and the results are presented and discussed. The development and use of several dynamic force calibrators are also discussed.

This document is subject to special export controls and each transmittal to foreign governments or foreign nationals may be made only with prior approval of Arnold Engineering Development Center (AEDC), Arnold Air Force Station, Tennessee.

This document has been approved for public release
its distribution is unlimited.

*Per AF Letter dtd
12 Sept, 1968 signed
William O. Cole*

CONTENTS

	<u>Page</u>
ABSTRACT	iii
NOMENCLATURE	viii
I. INTRODUCTION	
1.1 Scope of the Ground Test Problem.	1
1.2 Thrust Measurement Problem	2
II. FUNDAMENTAL CONSIDERATION OF MECHANICAL STRUCTURE TRANSIENT RESPONSE	
2.1 Analytical Calculation of System Response	3
2.2 Experimental Determination of System Response	5
III. THRUST TRANSDUCTION AND INFORMATION TRANSMISSION	
3.1 Requirements for Distortionless Measurements.	6
3.2 Time Domain Specification of Measurement Error	9
IV. DYNAMIC FORCE CALIBRATORS	
4.1 Impact Force Generators.	10
4.2 Step Function Force Generator	11
4.3 Electrodynamic Actuator Force Generator	11
V. DYNAMIC THRUST MEASUREMENT TECHNIQUES FOR SINGLE-DEGREE-OF-FREEDOM MECHANICAL SYSTEMS	
5.1 Dynamic Thrust Measurement by Mechanical System Response Optimization	13
5.2 Dynamic Thrust Measurement by Reaction Force Summation	20
5.3 Dynamic Thrust Measurement by Analog Computer Compensation.	25
5.4 Correlation of Dynamic Thrust Data by Reaction Force Summation and Computer Compensation	29
VI. DYNAMIC THRUST MEASUREMENT TECHNIQUES FOR MULTI-DEGREE-OF-FREEDOM MECHANICAL SYSTEMS.	30
VII. SUMMARY OF RESULTS AND CONCLUSION	32
REFERENCES.	36

APPENDIXES

I. ILLUSTRATIONS

<u>Figure</u>	<u>Page</u>
1. Representation of the Dynamic Thrust Measurement Problem	43
2. Relationship of Input Thrust, Thrust Measurement System Transfer Function, and Output Signal.	46
3. Ideal Time Delayed, Distortionless Reproduction of Thrust Information	46
4. Tandem Operation of Basic Thrust Measurement System and Compensation System to Obtain Distortionless Transmission of Thrust Information	47
5. Ideal Low Pass Filter Characteristics.	47
6. Comparison of Amplitude Characteristics of Common Filter Types	48
7. Comparison of Transient Responses of the Butterworth and Bessel Function-Type Filters.	49
8. Instantaneous Tracking Error	50
9. Schematic of Exploding Wire Device.	51
10. Force to Armature Coil Current Calibration of Electrodynamic Actuator.	52
11. Block Diagram of Current Function Generator for the Dynamic Force Calibrator	53
12. Typical Performance of the Current Function Generator for the Dynamic Force Calibrator.	54
13. Rocket Engine Test Data Illustrating Single-Degree-of-Freedom Dynamic Response of the Thrust Measurement System	55
14. Step Function Response of Single-Degree-of-Freedom Thrust Measurement System	56
15. Amplitude and Phase Response of Single-Degree-of-Freedom Thrust Measurement System.	57
16. Mechanical Component Schematic of Optimally Damped Dynamic Thrust Measurement System.	58

<u>Figure</u>		<u>Page</u>
17.	Block Diagram of Single-Degree-of-Freedom Mechanical System with Velocity Feedback Damping	59
18.	Root Locus Plot of Open Loop Transfer Function of Velocity Feedback Damped Single-Degree-of-Freedom Mechanical System	60
19.	Transfer Mechanical Impedance Plot (Amplitude Only) for System Shown in Fig. 16	61
20.	Analytical Model and Block Diagram of Single Axis, Three-Degree-of-Freedom Mechanical System with Velocity Feedback Damping	62
21.	Root Locus Plot of Open Loop Transfer Function of Velocity Feedback Damped Three-Degree-of-Freedom Mechanical System	63
22.	Optimally Damped Servomechanism System Typical Performance	64
23.	Optimally Damped Servomechanism System Response to a 300-lb Step Function Force.	65
24.	Optimally Damped Servomechanism System Response to a 500-lb Step Function Force.	66
25.	Reaction Force Summation System	67
26.	Reaction Force Summation System Typical Performance	68
27.	Analytical Model of a Thrust Measurement System with a Dynamic Degree of Freedom of the Thrust Butt.	69
28.	S-Plane Pole-Zero Plot for Mechanical System and Compensator	70
29.	Frequency Response of Mechanical System, Compensator, and Compensated System	71
30.	Operational Block Diagram of General Three-Amplifier Analog Computer Compensator	72
31.	Operational Block Diagram of Simulated Thrust Stand-Feedback-Type Compensator	73
32.	Simplified Functional Block Diagram of Differentiator-Type Analog Computer Compensator	74

<u>Figure</u>		<u>Page</u>
33.	System for Comparison of Data by Reaction Force Summation and Computer Compensation Techniques	75
34.	Computer Compensation System Typical Performance	76
35.	Comparison of Performance of Reaction Force Summation and Computer Compensation Techniques	77
36.	Comparison of Performance of Reaction Force Summation and Computer Compensation Techniques for a High Peak Force Input	78
37.	Conceptual Drawing of Static and Dynamic Thrust Measurement System	79
II.	ANALYTICAL CALCULATION OF MECHANICAL STRUCTURE TRANSIENT RESPONSE	80



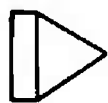


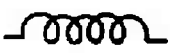
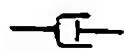
NOMENCLATURE

A	Amplifier gain
B_{LC}	Dissipation coefficient of the load cell
B_{TB}	Dissipation coefficient of the thrust butt
\bar{B}	Magnetic field strength
db	Decibel
e	Base of the natural logarithm
$e(t_r)$	Instantaneous tracking error
$e_{in}(t)$	Instantaneous input voltage
$e_{in}(\omega)$	Sinusoidal steady state input voltage
$e_{out}(t)$	Instantaneous output voltage
$e_{out}(\omega)$	Sinusoidal steady state output voltage
$F(s)$	Laplace transform of $F(t)$
$F(t)$	Instantaneous force (including thrust force)
$F(j\omega)$	Fourier transform of $F(t)$

$\bar{F}(\omega)$	Sinusoidal vector force
f_t	Mechanical system damped natural frequency
$G_1(j\omega)$	Fourier transform transfer function
$G_1(s)$	Thrust measurement system transfer function
$G_2(j\omega)$	Fourier transform transfer function
$G_2(s)$	Compensator transfer function
$G_F(j\omega)$	Fourier transformed filter transfer function
$H(s)$	Feedback loop transfer function
h	Scale factor
h_A	Accelerometer sensitivity
h_D	Displacement transducer sensitivity
h_V	Velocity transducer sensitivity
K_{LC}	Spring constant of the load cell
K_{TB}	Spring constant of the thrust butt
M_E	Mass of rocket engine and mounting structure
M_{TB}	Moving mass of the thrust butt
$q(s)$	Laplace transform of $q(t)$
$q(t)$	Cartesian coordinate displacement variable
$\dot{q}(t)$	First time derivative of $q(t)$
$\ddot{q}(t)$	Second time derivative of $q(t)$
$\bar{q}(\omega)$	Sinusoidal steady state vector displacement
$\dot{\bar{q}}(\omega)$	First time derivative of $\bar{q}(\omega)$
$\ddot{\bar{q}}(\omega)$	Second time derivative of $\bar{q}(\omega)$
s	Laplace transform variable, $s = \sigma + j\omega$
t	Time
t_d	Delay time
t_r	Reference time
$X(s)$	Laplace transform of $X(t)$
$X(t)$	Load cell output signal
$\dot{X}(t)$	First time derivative of $X(t)$

$\ddot{X}(t)$	Second time derivative of $X(t)$
$X(j\omega)$	Fourier transform of $X(t)$
$X(\omega)$	Sinusoidal steady state load cell signal
$\bar{Z}(\omega)$	System mechanical impedance
α	Damping time constant
ξ_c	Compensator damping ratio
ξ_o	Mechanical system damping ratio
ψ	Phase shift
ω	Radian frequency
ω_c	Compensator undamped natural radian frequency
ω_{co}	Filter cutoff radian frequency
ω_o	Mechanical system undamped natural radian frequency
ω_r	Mechanical system resonant radian frequency
ω_t	Mechanical system damped natural radian frequency

SYMBOLS

	Operational amplifier
	Gain and/or summing amplifier
	Integrating amplifier
	Potentiometer
	Summing junction
	Mechanical spring
	Viscous damping mechanism

SECTION I INTRODUCTION

1.1 SCOPE OF THE GROUND TEST PROBLEM

Important data to be gathered during rocket engine ground tests are engine thrust and total and/or specific impulse. At the present time, acceptably accurate static thrust and total impulse measurements are possible with well-designed thrust measurement systems¹ over the entire force range from 10^{-6} through 10^6 lb (Refs. 1-7). Recent research efforts have yielded several feasible approaches for performing relatively accurate dynamic thrust measurements (Refs. 8-11). Although of utmost importance, static and dynamic thrust measurement is but a portion of the overall ground test problem.

In addition to thrust measurement accuracy, totally effective ground testing of rocket engines must provide environments (altitude, temperature, etc.) typical of that to be experienced by the engine in actual flight. The degree to which the flight environments can be simulated depends upon the characteristics of the test engine (size, exhaust efflux rate, etc.) and the levels to which particular simulation technologies have been advanced. For example, in the field of ion rocket engine testing, there have been recent significant development of test facilities capable of providing realistic launch to ultimate altitude ambient pressure simulation (atmosphere to 10^{-5} torr in 60 sec) and uninterrupted, long term (10,000 hr) ultimate altitude pressure simulation (10^{-7} torr) under the detrimental influence of the energetic ion rocket exhaust efflux (Refs. 12-15). In this particular case, pressure simulation is most important since the test cell background pressure profoundly affects the thrust performance of the ion engine.

The effort that should be expended to provide realistic environmental simulations while simultaneously performing thrust measurement is dependent upon the possible interactions between the environment variable and the thrust variable. For example, the effects of flight vehicle vibrations on the thrust performance of certain liquid-propellant rocket engines can be quite pronounced (Refs. 16-18). Structural, vibration-induced, propellant feedline pressure surges can result in undesirable surges of thrust. This process can be regenerative,

¹The phrase, thrust measurement system, is meant to include the rocket engine, its mounting structure, and all attached mechanical components, as well as all associated electronic components.

and large amplitude thrust surges are possible. It is generally not feasible to ground test entire flight vehicles because of the inadequacies of most test facilities. Even the ground testing of the entire vehicle may not reveal combustion instabilities that could be experienced in actual flight since the ground test vibration environment is generally not the same as that experienced in actual flight (Ref. 19). However, a recently proposed solution for the difficult problem of simulating flight vehicle dynamics is a controlled response, servo-mechanism-type, thrust measurement-vibration simulation system (Ref. 20).

1.2 THRUST MEASUREMENT PROBLEM

The major factors contributing to thrust measurement errors are (Ref. 21):

1. Hysteresis,
2. Initial alignment,
3. Deflection under load,
4. Redundancy of thrust restraint,
5. Pendulum effects,
6. Temperature effects, and
7. System dynamics.

Meaningful and accurate ground test thrust measurement requires evaluation or actual simulation of the expected flight environment variables and minimization of the error-producing mechanisms mentioned above.

Studies concerning thrust measurement error mechanisms, (1) through (6), listed above are extensively documented, and simulations of the various environments are studies in their own right. The following discussions will therefore be limited to assessment of thrust measurement error attributable to system dynamics and analytical and experimental investigations of dynamic thrust measurement techniques, since this still remains a subtle and sometimes formidable problem.

1.2.1 Thrust Measurement Error Attributable to Dynamics

During dynamic thrust periods, the thrust stand-rocket engine mechanical system natural frequencies may be excited, and large measurement errors are possible. The nature of the dynamic thrust measurement problem is illustrated in Fig. 1. Figure 1a shows three typical mounting configurations for rocket engine testing. Figure 1b is a general single-axis multi-degree-of-freedom analytical model representing any one of these mounting configurations. Under certain

circumstances, to be discussed, the analytical model shown in Fig. 1b can be simplified to that of Fig. 1c.

The entire thrust measurement system is actually a force transducer consisting of mechanical and electrical components as shown in Fig. 1d. Thrust force is the input variable, and an electrical analog signal is the output variable of this transducer.

Calculation (using the model of Fig. 1b or Fig. 1c) or experimental measurement of the system response to a thrust input, $F(t)$, would yield data as shown in Fig. 1e. It is seen that electronic noise is a possible source of degradation of $X(t)$ as the analog representation of $F(t)$ as well as distortion caused by the mechanical system transient response. The ideal thrust measurement system would yield an analog time-function output which is an exact scaled replica of the input thrust. The solution then to the dynamic thrust measurement problem depends upon the development of techniques which will yield an analog output which is an accurately scaled, undistorted, replica of the thrust force input.

One of the first successful techniques to yield an accurate analog output signal representative of the dynamic input thrust utilized mathematical operations involving experimentally determined thrust measurement system parameters and the distorted load cell signal (Ref. 22). This technique has been shown to yield accurate results though it necessarily involves post-firing computations and operations on the distorted load cell signal (Ref. 23). This computation technique has been followed by several successful "on-line" techniques which provide immediate analog representations of the input thrust.

The following discussions will deal mostly with thrust measurement systems capable of on-line dynamic measurements as opposed to systems requiring post-firing computations or operations.

SECTION II

FUNDAMENTAL CONSIDERATION OF MECHANICAL STRUCTURE TRANSIENT RESPONSE

2.1 ANALYTICAL CALCULATION OF SYSTEM RESPONSE

The degree of success in analytically predicting the responses of a complex mechanical structure to input forces is directly determined by the adequacy of the model used to approximate the particular structure. All mechanical systems are fabricated with continuous mass members and in some cases can be successfully analyzed only by distributed

parameter techniques since the motion response of each incremental mass point is a function of both position and time. However, for all practical purposes, the analysis of many systems is successfully carried out by considering the mass, elasticity, and energy dissipation mechanisms to be lumped quantities located at discrete points in the system model.

Assuming the adequacy of the lumped parameter model, several simplifying but oftentimes valid assumptions can be made before formulating the equations of motion. In particular, small oscillations of time invariant, lumped parameter mechanical systems may be describable by ordinary, linear differential equations with constant coefficients. The energy dissipation mechanism is frequently represented as being viscous in nature with damping proportional to velocity. Under these conditions, the equations of motion of the system are conveniently derivable by application of D'Alembert's principle or by the Lagrangian formalism. The analytical expression for the natural frequency displacement response of mass point M_i of an n -degree-of-freedom structure is given by (Appendix II):

$$q_i^* = \sum_{r=1}^n C_{ir} e^{-\alpha_r t} \cos(\omega_r t + \psi_{ir}), \quad i = 1, 2, \dots, n, \quad (1)$$

where C_{ir} is the peak displacement response of mass point M_i attributable to the natural frequency r , and α_r is the damping time constant associated with the natural frequency r .

When the energy dissipation of a linear system is negligible, normal mode theory can be used to determine the response of the M_i mass points attributable to the r natural frequencies. The natural frequency displacement response is given by the following general expression (Appendix II):

$$q_i^* = \sum_{r=1}^n A_{ir} \sin(\omega_r t + \psi_{ir}), \quad i = 1, 2, \dots, n, \quad (2)$$

where A_{ir} is the peak displacement response of mass point M_i attributable to the natural frequency r .

The discussions to follow will consider principally single-axis thrust measurement systems with small displacements so that the generalized coordinate q_i^* becomes the cartesian coordinate $q_i(t)$.

The analytical prediction of the transient structural response of a rocket thrust stand in the design stage will yield expressions of the form

of Eq. (1) or (2). However, once the stand is built the actual response of the thrust stand-rocket engine system will include the transient response characteristics of the engine structure.

A recent analytical and experimental motion response study of a large space vehicle has demonstrated the validity of using lumped parameter model formulation and normal mode theory (Ref. 24). In this particular study, it was found that a lumped parameter model of the space vehicle yielded analytically predicted responses as accurate as those predicted by a distributed parameter model, since both models produced analytical results in good agreement with experimentally determined responses.

2.2 EXPERIMENTAL DETERMINATION OF SYSTEM RESPONSE

The adequacy of any model formulation and subsequent calculation of response can only be verified by correlation with the experimentally determined system response. The experimental determination of motion response at a particular coordinate in a multi-degree-of-freedom system can be conveniently carried out by applying mechanical impedance techniques (Refs. 25-26). In general, any portion of a structure has six degrees of freedom: three orthogonal rectilinear motions and three possible rotational motions. Therefore, the complete specification of the mechanical impedance would require six impedance components. However, for the present discussion, only one rectilinear impedance component will be specified.

The unidirectional, rectilinear, mechanical impedance measured at any coordinate point of a structure at any particular radian frequency, ω , is defined by the following equations:

$$\bar{Z}(\omega) = \frac{\bar{F}(\omega)}{\dot{\bar{q}}(\omega)} e^{j\psi} \quad (3)$$

or

$$\bar{Z}(\omega) = \frac{\bar{F}(\omega)}{\omega \bar{q}(\omega)} e^{j(\psi + \pi/2)} \quad (4)$$

or

$$\bar{Z}(\omega) = \frac{\omega \bar{F}(\omega)}{\ddot{\bar{q}}(\omega)} e^{j(\psi - \pi/2)} \quad (5)$$

If $\bar{F}(\omega)$ and $\bar{q}(\omega)$ or $\dot{\bar{q}}(\omega)$ or $\ddot{\bar{q}}(\omega)$ are experimentally measured at the same point on the structure, the calculated impedance is termed the

driving point impedance. The measurement of a motion response variable at a point other than the point at which the force is applied results in a calculation of a transfer impedance.

A graphical plot of the magnitude and phase of the mechanical impedance results in a useful presentation of the effects of the resonant and antiresonant frequencies of the structure at the point in question. A mechanical impedance plot for a thrust stand-rocket engine structure would indicate the natural frequencies to be contended with during transient response periods since, for a lightly damped structure, the resonant and natural frequencies are practically the same. The excitation of the structural natural frequencies during transient response periods is the essence of the dynamic thrust measurement problem, the solution of which must necessarily yield techniques to determine the true thrust function input in spite of the effects of the excited natural frequencies.

SECTION III THRUST TRANSDUCTION AND INFORMATION TRANSMISSION

3.1 REQUIREMENTS FOR DISTORTIONLESS MEASUREMENTS

The usual analytical or experimental motion response problem requires calculation or recording of a system response variable given a system model and specific forcing function input. The experimental determination of the thrust performance of a rocket engine requires solution of the inverse problem: a system model and response are given and the forcing function is to be determined.

Thrust measurement by conventional methods involves first a transduction of the thrust force to a mechanical motion response and then a transduction of the particular motion response to an electrical analog signal. However, only under certain special circumstances does the motion transducer yield an output which is a true time replica of the thrust input.

The thrust function input to a linear thrust measurement system can be related analytically to the analog output signal by the system transfer function. Using Fourier transformed quantities, the system transfer function is related to the thrust function and the analog output signal by the following relationship (see Fig. 2):

$$F(j\omega) G_t(j\omega) = X(j\omega) \quad (6)$$

From Eq. (6) it can be seen that the most desirable system transfer function would be:

$$G_1(j\omega) = h = \text{constant scale factor} \quad (7)$$

since in this case the output signal would be an exact scaled replica of the input force:

$$F(j\omega)h = X(j\omega). \quad (8)$$

The condition inferred by Eq. (7) is, in the strictest sense, unrealizable since the energy storage components of the mechanical system will cause $G_1(j\omega)$ to be frequency dependent. Also, from a practical point of view, it is certain that stochastic processes in the motion transducer and associated electronics as well as other noise sources will degrade the fidelity of $X(j\omega)$ as the analog of $F(j\omega)$. In some cases, the transfer function characteristic of Eq. (7) can be approached by a physical system, as exemplified by a piezoelectric accelerometer operated well below its natural frequency (Ref. 27). It is conceivable that a thrust stand-rocket engine system could approach the response characteristics of Eq. (7) if the system natural frequencies are at least five times higher than the highest appreciable amplitude Fourier frequency component of the input thrust.

Under certain circumstances, practically distortionless transduction, transmission, and recording of thrust data can be attained even though the mechanical system response is frequency dependent. Distortionless but time-delayed thrust determinations can be achieved if the following condition is met (See Ref. 28 for analogous discussion of distortionless information transmission in electrical networks):

$$X(t) = hF(t - t_d), \quad t > t_d \quad (9)$$

If Eq. (9) is satisfied, then an idealized input-output relationship is illustrated in Fig. 3.

The form of $G_1(j\omega)$ to realize time-delayed but distortionless transmission of thrust information can be obtained by substituting Eq. (9) into the defining equation for the Fourier transform (Ref. 28):

$$X(j\omega) = h \int_{-\infty}^{\infty} F(t - t_d) e^{-j\omega t} dt = h \int_{-\infty}^{\infty} F(y) e^{-j\omega(y + t_d)} dy, \quad y = t - t_d \quad (10)$$

but

$$F(j\omega) = \int_{-\infty}^{\infty} F(y) e^{-j\omega y} dy$$

Therefore,

$$X(j\omega) = h e^{-j\omega t_d} F(j\omega) = G_1(j\omega) F(j\omega)$$

It can be seen that for delayed but distortionless transduction and transmission of the thrust data the system transfer function must be of the form:

$$G_1(j\omega) = h e^{-j\omega t_d} \quad (11)$$

Equation (11) requires that the system transfer function have a constant gain and linear phase shift characteristic for all frequencies with appreciable amplitudes in the Fourier series representation of the thrust function.

One practical solution to approach distortionless response is to ensure that the mechanical system itself conforms as closely as practical to the ideal requirements of Eq. (7) or (11). However, it is important to realize that a distorted mechanical system response recorded at the output of the load cell can be amplitude and/or phase compensated to obtain overall distortionless output. The compensation concept is illustrated in Fig. 4.

From the above discussion, it can be understood that regardless of the particular technique employed to determine input thrust, the mechanical and electronic components of the thrust measuring system should be designed and integrated to yield the transfer function of either Eq. (7) or (11).

3.1.1 Filter Characteristics for Distortionless Information Transmission

A complete thrust measurement system may include a low pass filter to attenuate spurious high frequency noise in the output signal (see Section V). The choice of a filter must meet the requirements for distortionless information transmission. The principal requirement is that the filter cutoff frequency be chosen so that none of the appreciable amplitude Fourier frequency components of the input thrust are amplitude or phase distorted. The desirable filter transfer function would be

$$G_F(j\omega) = G_F(\omega) e^{-j\psi(\omega)} \quad (12)$$

with

$$G_F(\omega) = G_F = \text{constant}, \omega \leq \omega_{co}$$

$$G_F(\omega) = 0, \omega > \omega_{co}$$

and

$$\psi(\omega) = 0$$

for all ω . These filter characteristics are physically unrealizable, and a more practical goal would be to select a filter which approximates a

maximally flat amplitude and time delay characteristic in its frequency passband (Ref. 29). The filter transfer function in this case would be

$$G_F(j\omega) = G_F(\omega) e^{-j\omega t_d} \quad (13)$$

with

$$G_F(\omega) = G_F = \text{constant}, \omega \leq \omega_{co}$$

$$G_F(\omega) = 0, \omega > \omega_{co}$$

and

$$t_d = \frac{\psi}{\omega} = \text{constant}$$

for all ω . The ideal filter characteristics are shown in Fig. 5.

The common filter types, Butterworth, Chebyshev, and Elliptic function filter, are designed for a maximally flat amplitude characteristic but inherently possess a nonlinear phase response, hence a nonlinear time delay. A Bessel function filter, on the other hand, is designed for a maximally flat time delay but exhibits an amplitude characteristic that is inferior to that of the three types listed above. The amplitude responses of several common filter types of comparable complexity are shown in Fig. 6 (Ref. 30).

The combination of the desirable amplitude characteristic of the Butterworth filter and the linear phase characteristic of the Bessel filter results in a compromise filter termed a transitional Butterworth-Thomson filter (Ref. 29).

Introduction of fast rise time thrust information should produce no distortion in the output signal because of transient overshoot and natural frequency response of the filter. The Bessel filter exhibits superior transient response characteristics compared to the other common filter types. Figure 7 shows a comparison of the typical transient responses of the Butterworth and Bessel filters of similar design complexity. The Bessel filter is seen to exhibit a larger t_d and lesser rate of rise than the Butterworth filter, but its transient overshoot characteristic is superior. However, regardless of the filter type used, filtering of thrust data will always increase the "instantaneous tracking error" during dynamic thrust periods. The term instantaneous tracking error is defined in Section 3.2.

3.2 TIME DOMAIN SPECIFICATION OF MEASUREMENT ERROR

The amount of distortion and time delay introduced by a thrust measurement system is descriptively specified by a time domain

quantity termed "instantaneous tracking error". Instantaneous tracking error is defined as the algebraic difference between $F(t)$ and $X(t)$ with both variables determined at a reference time t_r . The instantaneous tracking error concept is illustrated in Fig. 8.

The dynamic thrust measurement techniques to be discussed will be compared on the basis of the magnitudes of instantaneous tracking error to be expected with each technique. However, the actual determination of the instantaneous tracking error for a particular thrust measurement system requires the use of a dynamic force calibrator. These will be discussed in the following section.

SECTION IV DYNAMIC FORCE CALIBRATORS

The validity and accuracy of a particular dynamic thrust measurement technique must finally be proved by comparison of the measurement system output signal with an analog signal representative of a known dynamic input force. Known dynamic forces can be produced by exploiting several different physical principles. The production of dynamic as well as static forces with a Lorentz-type force generator is particularly versatile and accurate.

4.1 IMPACT FORCE GENERATORS

Impact-type dynamic force generators which require calculation of the time-function force, considering initial and final energy conditions of the impacting member and/or the impacted member, are not considered desirable for thrust stand calibration. The force input as a function of time is quite dependent upon the conditions of the impacting surfaces, since resilient surfaces yield longer force durations than hard surfaces. Metal-on-metal impacts produce impulse-type forces which excite virtually all the measurement-system natural frequencies and are a more severe force environment than that to be expected from a rocket engine. Impacts on resilient material require precise knowledge of the material properties before the time function force calculation can be attempted. A calculated force input is not as desirable as utilizing a scheme which yields an accurate instantaneous analog signal directly proportional to the force input.

An impact-type dynamic force generator with a very high natural frequency force transducer as the impacting member has been shown to

be an effective dynamic force calibrator (Ref. 9). The proper resilient material is placed on the impacting surfaces so that the natural frequency of the impacting force transducer is not excited by the impact force. The instantaneous tracking error of the impacting force transducer output signal, as an analog representation of the force, is negligibly small since this force measurement scheme very closely approaches the criterion of Eq. (7). The thrust stand output signal is then compared to the force transducer signal for dynamic force calibration.

4.2 STEP FUNCTION FORCE GENERATOR

Well-defined step functions of force can be imparted to a thrust stand by stressing the stand with a wire or cable, until the desired force level is obtained and then instantaneously severing the restraining wire. The precise definition of the time dependent force function depends upon prior, in-place, calibration of the load cell and application of the cable tension force along the same line of action as the static calibration force. The production of a true step function force depends upon instantaneous parting of the restraining wire. An electrical exploding wire device shown in schematic form in Fig. 9 was built for this purpose. This device is capable of completely vaporizing a 0.040-in. -diam tungsten wire in less than $10 \mu\text{sec}$ - appreciably faster than mechanically cutting the wire.

4.3 ELECTRODYNAMIC ACTUATOR FORCE GENERATOR

During the course of the experimental thrust measurement investigations, the most versatile dynamic force calibrator was found to be an electrodynamic actuator. The actuator output force (Lorentz force) is given by (Ref. 31):

$$\vec{F}(t) = nI(t) \vec{L} \times \vec{B} \quad (14)$$

where $I(t)$ is the armature current, \vec{L} is the spatial orientation of each armature coil (\vec{L} and \vec{B} are orthogonal), n is the number of armature coils, and \vec{B} is the field strength of the actuator magnetic field.

From Eq. (14) it can be seen that for a constant actuator magnetic field strength the output force is directly proportional to, and in phase with, the armature current.

Oscilloscope presentation of the armature current yields instantaneous knowledge of the force output from the actuator. A force to armature current calibration was performed by placing the actuator in

a vertical position, noting the null position of the armature, loading the armature with known deadweight, and then recording the armature current necessary to force the armature back to its original null position. A differential transformer capable of detecting 10^{-6} in. displacements was used to position the armature. The force-to-armature current calibration is plotted in Fig. 10. When coupled to the thrust measurement system and driven with sinusoidal armature currents, the actuator is useful for determining the mechanical impedance and resonant frequencies of the system.

To simulate rocket thrust buildup, duration, and termination, a current function generator was designed and built to drive the actuator armature. This device is capable of producing preselected linear current rise times from 0.5 to 20 msec, constant level current flow from 25 to 300 msec, and current fall times from 0.6 to 20 msec. The maximum current amplitude is variable from 0 to 12 amp giving a peak force range from 0 to 75 lb. The function generator is shown schematically in Fig. 11.

Abrupt current changes in the actuator armature produce appreciable inductive voltage transients, and motion of the armature with respect to the actuator magnetic field generates a back electromotive force. Both of these phenomena oppose the desired control of the actuator armature current by the function generator. However, the differential error control amplifier circuitry of the function generator possesses sufficient response characteristics to perform high speed corrections with the result that precisely controlled armature currents are possible. The back electromotive force produced in the field coil attributable to changing current in the armature was found to have a small effect in this particular case. However, even this small effect is eliminated by error amplifier control circuitry similar to that used for armature current control and by operation of the field magnetic circuit in the saturation region of its magnetization characteristic. Several typical armature current functions are shown in Fig. 12.

Ideally, an electrodynamic actuator dynamic force generator should perform as a single mass body coupled rigidly to the thrust measurement system so that the generator contributes no additional degrees of freedom to the mechanical system. This requirement for fast rise time, high level forces presents a severe mechanical and electrical design problem. The commercially available actuator used in this study did exhibit several minor resonances which degraded the desired force-time function to a small degree. However, an electrodynamic actuator custom built for a dynamic thrust measurement system could undoubtedly be designed to satisfy the rigidity requirement.

The use of this type dynamic calibrator programmed to produce a time dependent force function approximating the expected thrust performance of the test engine permits an immediate evaluation of the measurement system instantaneous tracking error characteristics.

SECTION V

DYNAMIC THRUST MEASUREMENT TECHNIQUES FOR SINGLE-DEGREE-OF-FREEDOM MECHANICAL SYSTEMS

5.1 DYNAMIC THRUST MEASUREMENT BY MECHANICAL SYSTEM RESPONSE OPTIMIZATION

No thrust stand-rocket engine system is a single-degree-of-freedom system in the strictest sense of the definition, and in general the natural frequency response at any point of the system is given by Eq. (1). However, in certain cases, systems can be designed to exhibit predominantly single-degree-of-freedom response in that

$$q_i(t) = \sum_{r=1}^n C_{ir} e^{-\alpha_r t} \cos(\omega_r t + \psi_{ir}) \quad (15)$$

$i = 1, 2, \dots, n$

with

$$C_{i1} > C_{i2}, C_{i3}, \dots, C_{in}$$

Actual test data from a solid-propellant rocket engine test firing are shown in Fig. 13, and the single-degree-of-freedom nature of the thrust measurement system is evident (Ref. 32).

A single-axis, single-degree-of-freedom thrust measurement system is shown in simplified schematic form in Fig. 1, along with the linear, lumped and time invariant, analytical model. The equation of motion is:

$$M\ddot{q}(t) + B\dot{q}(t) - Kq(t) = F(t). \quad (16)$$

One of the most severe dynamic thrust inputs to a thrust measurement system is a step function. Solving the equation of motion (Eq. (16)) for a step function input force yields (Ref. 33):

$$\frac{X(t)}{A} = \frac{h_D q(t)}{A} = h_D \left[1 - \frac{e^{-\zeta_0 \omega_0 t}}{\sqrt{1 - \zeta_0^2}} \sin \left(\omega_0 \sqrt{1 - \zeta_0^2} t + \psi \right) \right] \quad (17)$$

where

$$\psi = \cos^{-1} \zeta_0, \quad \omega_0 = \sqrt{\frac{K}{M}}, \quad \zeta_0 = \frac{B}{2 \sqrt{KM}}$$

and A is the magnitude of the step function.

A time domain plot of Eq. (17) with ζ_0 as parameter is shown in Fig. 14. From Fig. 14, it is evident that only one natural frequency is excited by the step input (or any other dynamic input) as was expected since Eq. (1) for the single-degree-of-freedom system yields:

$$C_{11} \neq 0, \text{ with } C_{12} = C_{13} = \dots C_{1n} = 0 \quad (18)$$

The inextricable relationship of time and frequency domain responses of physical systems provided by the trigonometric Fourier series, Fourier transform pair, and Laplace transform pair is quite useful in the study of dynamic thrust measurement techniques. The sinusoidal steady state frequency response of the system shown in Fig. 1c is plotted in Fig. 15 for several values of the damping ratio, ζ_0 .

The undamped natural frequency, ω_0 , damped natural frequency, ω_t , and the resonant frequency, ω_r , are related by the following expressions (Ref. 34):

$$\omega_t = \sqrt{1 - \zeta_0^2} \omega_0 \quad (19)$$

and

$$\omega_r = \sqrt{1 - 2\zeta_0^2} \omega_0 \quad (20)$$

For small ζ_0 it is evident that the undamped natural frequency, damped natural frequency, and resonant frequency of the system are practically the same.

5.1.1 Effect of Large ω_r

Any periodic time function satisfying the Dirichlet conditions can be represented by a Fourier trigonometric series. Specifically, the rocket thrust input to a thrust measurement system can be so represented. Most conventional thrust measurement systems utilizing load cell force transducers possess small values of damping ratio ($\omega_0 \approx \omega_r$). Examination of Fig. 15 reveals that if the highest appreciable amplitude Fourier frequency component of the thrust function is several times less than the measurement system resonant frequency then the system transfer function will approach the criterion set forth in Eq. (7), since there will be negligible amplitude and phase distortion of the thrust signal. The equivalent time domain statement would be that the instantaneous tracking error for any t_r will be small, since the system natural frequency would not be excited, and the load cell signal will closely "track" any dynamic changes of thrust.

To physically realize a system of this nature for short rise time, high level, thrust inputs with appreciable measurement system moving

mass presents quite stringent demands upon the K and h_D parameters of the system spring member and displacement measurement scheme (h_D = volts output per inch displacement). Since the system natural frequency is given by

$$\omega_o = \sqrt{\frac{K}{M}} \quad (21)$$

a requirement for large ω_o given a large M necessitates a correspondingly large K . Large K in turn requires a large h_D for which there is a definite limitation with the conventional strain-gage load cell. Although the strain-gage load cell is a high resolution device, it and associated electronics do have a definite signal-to-noise ratio limitation.

The successful realization of this type system depends upon whether h_D is large enough to provide an adequate signal-to-noise ratio for small displacements. Piezoresistive strain-gage elements offer a significantly larger h_D than that of the metallic foil gages, and recently developed temperature compensating techniques have resulted in usable semiconductor strain-gage load cells (Ref. 35). The higher h_D allows a larger K and, therefore, a larger ω_o for a given system M . Piezoelectric displacement sensing elements have quite high h_D values but are limited to dynamic measurements since there is no electrical output for static deflections. Other displacement sensing devices with higher h_D values than the strain gage can be used. It is not particularly difficult to detect dynamic displacement changes on the order of 10^{-7} in. with the linear variable differential transformer. Capacitive-type displacement transducers have been shown to detect displacements on the order of 10^{-9} in. (Ref. 10).

5.1.2 Effect of Optimum Damping

In many cases the system moving mass is large, and it is quite impractical if not impossible to provide a system K large enough to yield ω_o several times larger than the highest appreciable amplitude Fourier frequency component of the input thrust. In this situation, short rise time thrust inputs would be expected to excite the system natural frequency with resulting large instantaneous tracking errors. However, tracking error can be confined to the initial portion of the measurement system response by optimally damping the mechanical system (Refs. 36-37). The optimum damping ratio is defined as that which just eliminates transient overshoot and natural frequency "ringing". Perusal of Fig. 14 shows that a damping ratio in the range 0.65 to 0.707 is optimum. The realization of a thrust measurement system with an optimum damping ratio approaches the criterion for distortionless measurement set forth in Eq. (11), since this system possesses a nearly constant amplitude

and approximately linear phase characteristic throughout its frequency passband (see Fig. 15).

Even though optimum damping is provided, it is still desirable to maintain ω_0 as large as possible to minimize tracking error during the initial portion of the system response following a thrust level change. For example, the rise time of a single-degree-of-freedom system is inversely proportional to its undamped natural frequency (for a step function input):

$$t_{\text{rise time}} \approx \frac{3}{\omega_0} \quad (22)$$

where rise time in this case is defined as the time required for the system to respond from 0 to 100 percent of the final static steady state value.

5.1.2.1 Optimum Damping by Servomechanism Techniques

An experimental servomechanism device simulating an optimally damped thrust measurement system was built and is schematically shown in Fig. 16. The effective moving mass of the simulated rocket engine and mounting cradle is 150 lb. Known dynamic forces are imparted to the system by the electrodynamic actuator (0-75 lb) and pull wire device (75-2000 lb). System damping is accomplished by precise control of the armature current of an electrodynamic actuator rated for 3600-lb maximum force. A practical thrust measurement system would employ a high quality load cell in conjunction with the damping mechanism. The system shown in Fig. 16 did not readily permit the use of a load cell, since the two electrodynamic actuators occupied both possible load cell positions. Therefore, the spring constant was provided by proper design of the four plate flexures shown in Fig. 16. Displacement of the system is measured by a linear variable differential transformer. A deadweight static force calibrator was used to determine the displacement transducer characteristic (volts output/lbf input) and the spring constant.

To achieve simple dynamic response, the system was designed to respond predominantly in a single-degree-of-freedom manner for which the design of the damping servomechanism is straightforward. The damper actuating signal can be provided by either lead network compensation of the displacement signal or by a velocity transducer signal. The velocity transducer was found to produce more nearly optimum damping than the lead network. A block diagram of the servomechanism damped system is shown in Fig. 17. The Laplace transformed output signal is given by

$$X(s) = \left(\frac{h_D}{M} \right) \left(\frac{F(s) + n_P A_F + n_A A_P A_F + n_V A_V A_P A_F}{s^2 + 2\zeta_c \omega_0 s + \omega_0^2} \right) - n_D \quad (23)$$

where

$$\omega_o = \sqrt{\frac{K}{M}}$$

$$\zeta_o = \frac{B + h_V A_V A_P A_F}{2 \sqrt{KM}}$$

and B is the practically negligible damping coefficient of the mechanical system.

The effect of noise signals is evident, since they all directly introduce error into X(s) as the analog representation of F(s).

The system open loop transfer function is given by

$$G(s) H(s) = N \left(\frac{s}{s^2 + 2\zeta_o \omega_o s + \omega_o^2} \right) \quad (24)$$

where

$$\zeta_o = \frac{B}{2 \sqrt{KM}}$$

$$\omega_o = \sqrt{\frac{K}{M}}$$

and

$$N = \frac{h_V A_V A_P A_F}{M}$$

The root locus plot of this transfer function is shown in Fig. 18 and indicates that the system should be stable for all values of open loop gain, N.

However, as stated previously, no complex mechanical structure such as a thrust measurement system can be expected to respond strictly as a single-degree-of-freedom system for an unlimited range of excitation frequencies. Multi-degree-of-freedom mechanical system response becomes a particular problem when feedback damping is employed, since the servomechanism may become unstable and oscillate at one of the natural frequencies (Ref. 37). Initial operation of the system shown in Fig. 16 was unsatisfactory because of sustained oscillations that were produced as the loop gain was increased. Optimum damping was not possible because of the instability of the servomechanism. It was found that the system could exhibit a sustained oscillation at about 550 Hz or 1000 Hz depending upon the rise time of the input force produced by the electrodynamic-type force generator.

The slower rise time forces excited the 550-Hz oscillation, whereas the fast rise time forces excited the 1000-Hz oscillation. Reduction of loop gain resulted in stable but undamped system response. The frequencies of oscillation were obtained from oscilloscope photographs.

To accurately determine the natural frequencies, a transfer mechanical impedance plot (amplitude only) was obtained by driving the dynamic force calibrator with a constant amplitude, variable frequency, sinusoidal current, and noting the resultant velocity transducer signal. The mechanical impedance plot is shown in Fig. 19. The predominant amplitude resonant frequency is seen to occur at 73.5 Hz with lesser amplitude resonances occurring at 555 and 1050 Hz. An almost continuous spectrum of small amplitude resonances was observed for excitation frequencies above 1050 Hz.

Once the mechanical impedance data were plotted, an analytical model of the mechanical system was formulated which yielded a transfer function capable of producing the observed resonant frequencies having appreciable amplitudes. This was done so that a more accurate root locus plot could be made which would reveal the nature of the observed servomechanism instabilities. Several three-degree-of-freedom models were analyzed, but only the one shown in Fig. 20a was capable of analytically predicting the observed instabilities. The application of D'Alembert's principle or the Lagrangian formulation yields the equations of motion, and with Laplace transformation of the variables and algebraic simplification the mechanical system transfer function is given by

$$\frac{q_1(s)}{F(s)} = \frac{K_2 K_3}{[(M_1 s^2 + K_1 + K_2)(M_2 s^2 + K_2 + K_3) - K_2^2] [M_3 s^2 + K_3] - K_3^2 [M_1 s^2 + K_1 + K_2]} \quad (25)$$

Negligible structural damping was assumed in deriving the equations of motion.

A revised block diagram of the velocity feedback damped system reflecting the multi-degree-of-freedom nature of the mechanical components is shown in Fig. 20b.

The three-degree-of-freedom, lumped parameter model of Fig. 20a is not a precisely accurate model of the system, since many minor resonances were detected during the recording of the mechanical impedance data. However, this lumped parameter model along with the experimentally determined natural frequency data yielded sufficient information to make the root locus plot shown in Fig. 21.

This plot predicts instability at the 555-Hz natural frequency which agrees with the observed instability for input force rise times of about 5 msec. However, forces having 1/2-msec rise time were observed to excite servomechanism instability with sustained oscillations at about 1050 Hz which is not predicted by the root locus plot of Fig. 21. This is an indication of the inadequacy of the model shown in Fig. 20a. However, the analytical model and the root locus plot do indicate the nature of servomechanism instability to be expected with this type system and illustrate the need to minimize the compliance of the mechanical structure between the point of application of the input force and the point of application of the damping force.

At this point in the investigation of the velocity feedback damped system, two alternatives were available to stabilize the servomechanism. Compensation circuitry could be designed for the feedback loop, or mechanical stiffeners could be added to the structure. Mechanical stiffeners were added with the result that stable operation of the servomechanism was possible. Operation of the system with an open loop gain sufficient to produce over-damped response of the predominant natural mode again resulted in instability at one of the higher natural frequencies. Practical application of this type system would require the proper design of compensation circuitry to enhance its stability characteristics; otherwise it would exist under the constant threat of instability. In general, rocket engines to be tested with this type system will contribute natural frequencies to the overall response characteristic, and compensation circuit design will be required for each dynamically dissimilar engine. Additional problems could be encountered if engine operation resulted in different natural frequencies during the test than those for which the compensation circuitry was initially designed.

5.1.2.2 Performance Characteristics of the Stable Servomechanism

Once stable operation was attained, the system shown in Fig. 16 was subjected to periodic force pulses from the dynamic calibrator to experimentally determine its dynamic force measurement capabilities. Figure 22a compares the input force to the system response with no feedback damping. The instantaneous tracking error is large for any t_r since the transient response persists throughout the duration of the input force. Figure 22b compares the input force and system response with optimum feedback damping. The improvement is obvious since tracking error is essentially zero during the static portion of the input force. Small tracking error during dynamic force changes (force rise and fall times as shown in Fig. 22) is directly related to large ω_0 . An infinite ω_0 with no damping would yield a system satisfying the criterion

of Eq. (7), whereas an infinite ω_0 with optimum damping ($\xi_0 = 0.707$) would yield a system satisfying the criterion of Eq. (11). The system shown in Fig. 16 approaches the criterion of Eq. (11) only for the frequencies included in its frequency passband.

Experimental determination of system response for dynamic forces greater than those provided by the electrodynamic actuator was accomplished by preloading the system with a restraining wire to the desired level and then instantaneously parting the wire to produce a step unload force. Figure 23 shows the system response for a 300-lb pre-load, and the effects of optimum damping are obvious. Figure 24 illustrates system response for a 500-lb preload. The distorted characteristic of the damped response following the rise time portion was caused by saturation of amplifier A_V (Fig. 20). If the gain of either A_P or A_F could have been increased, this distortion would have been reduced. The accuracy of static thrust measurements using this type system is dependent only on the accuracy and stability of the in-place calibrated displacement transducer and associated electronics.

5.2 DYNAMIC THRUST MEASUREMENT BY REACTION FORCE SUMMATION

A thrust measurement system can be represented by the single-degree-of-freedom model of Fig. 1c provided the following conditions pertain:

1. The rocket engine, engine mounting structure, and attached ancillary equipment (propellant feedlines, etc.) are considered as one lumped, time invariant mass,
2. The thrust butt is rigid,
3. The dynamic and static deflections are small,
4. The energy dissipation mechanism is linearly dependent upon velocity and is time invariant, and
5. The spring rate is a linear function of spring deflection and is also time invariant.

If the above conditions are realized, the equation of motion of the system is given by:

$$M\ddot{q}(t) + B\dot{q}(t) + Kq(t) = F(t) . \quad (26)$$

This equation is a mathematical statement of Newton's third law or D'Alembert's principle in that the external force is seen to be equal to the sum of the system reaction forces. If M , B , and K are accurately

determined and $q(t)$, $\dot{q}(t)$, and $\ddot{q}(t)$ are accurately measured and if the three reaction forces are properly summed, then $F(t)$ can be determined by reaction force summation. On first encounter, the practical application of this technique seems to present, at best, a subtle problem in regard to the accurate determination of the system parameters and variables and maintaining the proper phase relation between the reaction force signals to be summed. However, a practical reaction force summation system is readily attainable when the system is dynamically simple (predominantly single-degree-of-freedom), and the damping is negligible.

For all practical purposes, the transient response of many lightly damped, dynamically simple, thrust measurement devices is given by Eq. (2):

$$q_1(t) = \sum_{r=1}^n A_{1r} \sin(\omega_r t + \psi_{1r}), \quad i = 1, 2, \dots, n \quad (27)$$

but with

$$A_{11} \gg A_{12}, A_{13}, \dots, A_{1n}$$

The equation of motion for this case is given by:

$$M\ddot{q}(t) + Kq(t) = F(t) \quad (28)$$

For the case when B is negligible and Eq. (28) adequately represents the equation of motion, the application of reaction force summation techniques yields an accurate method for the determination of $F(t)$. A practical force measurement scheme employing reaction force summation techniques is shown in Fig. 25 (Refs. 9 and 38). From Fig. 25 it can be seen that the analog signal, representing the $Kq(t)$ reaction force, is furnished by a load cell which can be calibrated by deadweight loading. Here, it is not required that M be accurately determined or that $\ddot{q}(t)$ be accurately measured. The only requirement is that M be a lumped and time invariant mass and that the accelerometer used to determine $\ddot{q}(t)$ be a linear, constant sensitivity, and high natural frequency transducer with negligible phase shift throughout the range of excitation frequencies to be experienced. The gain of the accelerometer amplifier is adjusted until the two transducer signals sum to zero during the natural frequency ringing period following a dynamic excitation. This procedure is in accordance with the requirements of the homogeneous equation of motion given by:

$$M\ddot{X}(t) + KX(t) = 0 \quad (29)$$

5.2.1 Performance Characteristics of the Reaction Force Summation System

The system shown in Fig. 25 was subjected to sharp dynamic force inputs with a plastic tipped hammer. The load cell and accelerometer signals were recorded before summation and are shown in Fig. 26a. It can be seen that the load cell and accelerometer signals are equal in magnitude but 180 deg out of phase during the natural frequency ringing period. The load cell and reaction force summation signals are recorded in Fig. 26b, and the load cell error attributable to dynamic effects is evident. In this case the actual input force, as a function of time, is not known precisely, but the reaction force summation technique has been precisely correlated with force measurements by analog computer techniques (see Section 5.4). It is this precise correlation of data by two independent force measurement techniques that strengthens confidence in both techniques.

This force measurement system very closely approaches the criterion of Eq. (7) and the instantaneous tracking error can be made quite small for single-degree-of-freedom systems. Small time delays of the output signal referenced to input force are caused by (1) operational amplifier and signal cable lags, (2) time delays incurred by the propagation time of the compression wave from the point of application of the force to the accelerometer position, and (3) minor delay attributable to accelerometer response (Ref. 9).

5.2.2 Insensitivity to Thrust Butt Motion

A valuable property of this thrust measurement technique is its relative insensitivity to vibrations introduced through the thrust butt attributable to test cell background vibrations and/or thrust butt motions attributable to dynamic thrust inputs (Ref. 9). Considering the model of a nonrigid thrust butt shown in Fig. 27, the equations of motion are:

$$M_E \ddot{q}_E(t) + B_{LC} [\dot{q}_E(t) - \dot{q}_{TB}(t)] + K_{LC} [q_E(t) - q_{TB}(t)] = F(t) \quad (30)$$

and

$$\begin{aligned} M_{TB} \ddot{q}_{TB}(t) + B_{LC} [\dot{q}_{TB}(t) - \dot{q}_E(t)] + K_{LC} [q_{TB}(t) - q_E(t)] \\ + B_{TB} \dot{q}_{TB}(t) + K_{TB} q_{TB}(t) = 0 \end{aligned} \quad (31)$$

The insensitivity to thrust butt motion can be explained by examination of Eq. (30). For simplicity, assume $F(t)$ is zero and that external excitation of the system is provided by a sinusoidal thrust butt motion given by:

$$q_{TB}(t) = A \sin \omega t \quad (32)$$

Assuming negligible damping³, Eq. (30) reduces to:

$$M_E \ddot{q}_E(t) + K_{LC} [q_E(t) - q_{TB}(t)] = 0 \quad (33)$$

Substitution of Eq. (32) into Eq. (33), Laplace transforming all variables, and with algebraic simplification an expression for the engine displacement is obtained:

$$q_E(s) = \frac{A \omega_o^2 \omega}{(s^2 + \omega^2)(s^2 + \omega_o^2)} \quad (34)$$

where

$$\omega_o = \sqrt{\frac{K_{LC}}{M_E}}$$

Inverse Laplace transformation of Eq. (34) yields

$$q_E(t) = \left(\frac{A \omega_o^2 \omega}{\omega_o^2 - \omega^2} \right) \left(\frac{\sin \omega t}{\omega} + \frac{\sin \omega_o t}{\omega_o^2} \right) \quad (35)$$

from which the expression for engine acceleration is found

$$\ddot{q}_E(t) = \left(\frac{A \omega_o^2 \omega}{\omega_o^2 - \omega^2} \right) (-\omega \sin \omega t - \sin \omega_o t) \quad (36)$$

Substitution of Eqs. (32), (35), and (36) into Eq. (33) yields a zero identity which shows that the inertial reaction force, $M_E \ddot{q}_E(t)$, must be equal in magnitude but opposite in phase with respect to the load cell force, $K_{LC} [q_E(t) - q_{TB}(t)]$ for thrust butt motions. The proper summation of an accelerometer signal measuring $\ddot{q}_E(t)$ and a load cell signal measuring $[q_E(t) - q_{TB}(t)]$ should yield a zero output for any reasonable thrust butt motions. Also with negligible damping, this same summation should yield an analog signal representative of the input force in accordance with Eq. (30).

³This is a valid assumption for a large number of thrust measurement systems since contributions to B attributable to engine, engine mounting assembly, and load cell structural deformations are quite small. Contributions to B by dragging instrumentation leads and propellant feedlines can be minimized by good design practices. Mechanical energy dissipation attributable to stresses in solid propellants can represent a subtle but probably small contribution to B.

Any arbitrary thrust butt motion other than a sinusoid could have been assumed to illustrate the insensitivity to such motion. The arbitrary thrust butt motion function could be expanded in a Fourier series and substituted into Eq. (33) term by term. The principle of superposition could be used to illustrate that the summation of responses attributable to each Fourier component again yields the same result.

5.2.2.1 Experimental Verification of Insensitivity to Thrust Butt Motions

The isolation mass (thrust butt) of the system shown in Fig. 25 was placed on a compliant support permitting displacements of about one-eighth inch and then was subjected to very heavy hammer raps (approximately 500-lb peak force). No significant output signals were noted as predicted by Eq. (33). A practical consideration, to realize this insensitivity to thrust butt motion, is that the accelerometer frequency response must extend down to the frequency of the thrust butt motion.

5.2.3 Further Applications of Reaction Force Summation Techniques

The application of reaction force summation techniques for rocket engine-thrust stand systems exhibiting multi-degree-of-freedom response becomes quite complex. This is attributable to the nonconformance of physical systems to simple lumped parameter models and the resultant nebulous decision as to where the additional accelerometers should be located and to the practical impossibility of instrumenting the additional spring elements.

Significant structural damping in the rocket engine-thrust stand system results in a phase shift of the load cell and accelerometer signals other than 180 deg, which introduces error in the summation signal. However, it is feasible to provide a damping reaction force signal, $B_{LC}[\dot{q}_E(t) - \dot{q}_{TB}(t)]$, for summation and correction of this error by differentiating $[q_E(t) - q_{TB}(t)]$.

The static thrust measurement accuracy of the reaction force summation technique is dependent only on the accuracy of the load cell data, provided that the electronics associated with the $\dot{q}_E(t)$ and $[q_E(t) - q_{TB}(t)]$ variables remain stable and contribute no spurious signals.

5.3 DYNAMIC THRUST MEASUREMENT BY ANALOG COMPUTER COMPENSATION

5.3.1 Ideal Computer Compensator

In Section III, it was pointed out that under certain circumstances a distorted output signal from the thrust measurement system load cell could be amplitude and/or phase compensated to obtain a distortionless analog representation of the forcing function (see Fig. 4).

Using Laplace transform terminology, the response, $X(s)$, of a linear thrust measurement system is related to the input forcing function, $F(s)$, by the system transfer function, $G_1(s)$:

$$X(s) = F(s) G_1(s) \quad (37)$$

The ideal compensator transfer function, $G_2(s)$, is the inverse of the mechanical system transfer function so that:

$$\frac{AX(s)}{G_1(s)} = \frac{AF(s) G_1(s)}{G_1(s)} = AF(s) \quad (38)$$

where

$$G_2(s) = \frac{A}{G_1(s)}$$

and A is a constant.

The transfer function for a linear single-degree-of-freedom mechanical system with constant parameters is given by:

$$\frac{X(s)}{F(s)} = G_1(s) = \left(\frac{\omega_o^2}{K} \right) \left(\frac{h_D}{s^2 + 2\zeta_o \omega_o s + \omega_o^2} \right) \quad (39)$$

Therefore, ideally, the compensator transfer function is given by:

$$G_2(s) = A(s^2 + 2\zeta_o \omega_o s + \omega_o^2) \quad (40)$$

Theoretically, analog computer circuitry can be designed to yield the ideal compensator transfer function with resultant mechanical system-compensator conformance with Eq. (7). However, this requires the use of differentiators which are undesirable because of the following characteristics:

1. Differentiators decrease the signal-to-noise ratio, and
2. Operational amplifiers used as differentiators can easily be driven into saturation and overload by high frequency signals and noise.

The objection to differentiator circuitry leads to compensator circuitry utilizing approximate differentiators or circuitry which depends only on integrators, gain amplifiers, and summing amplifiers.

5.3.2 Characteristics of Practical Compensators

The transfer function of a realizable, practical compensator is given by:

$$G_2(s) = \frac{A(s^2 + 2\zeta_o\omega_o s + \omega_o^2)}{(s^2 + 2\zeta_c\omega_c s + \omega_c^2)} \quad (41)$$

where the subscript, o, refers to original system parameters and the subscript, c, refers to compensator parameters. The zeroes of the compensator are seen to "cancel" the poles of the mechanical system. The compensator poles ideally should be located on the s-plane such that $\omega_c \sqrt{1 - \zeta_c^2}$ is at least five times greater than the highest appreciable amplitude, Fourier frequency component of the input forcing function. In actuality, this is not always practical, in which case ω_c should be chosen such that $\omega_c \approx 10\omega_o$ with the compensator pole response a maximally flat amplitude, linear phase characteristic. The particular choice, $\omega_c \approx 10\omega_o$, is dictated by the signal-to-noise characteristics of the load cell signal. The s-plane characteristics of the practical compensator are shown in Fig. 28.

The frequency response characteristics of the compensator and mechanical system are shown in Fig. 29. It can be seen that the compensator possesses an inverse amplitude and phase characteristic to that of the mechanical system up to the frequency at which the compensator poles begin to appreciably affect its response.

The time domain response of the mechanical system-compensator combination approaches the criterion of Eq. (11), and slightly time delayed but distortionless response is to be expected. Compensator circuitry can be synthesized with passive circuit elements, but analog computer circuitry is more versatile in that the transfer function is easily changed by changing amplifier gains and potentiometer settings.

5.3.2.1 General Three-Amplifier Compensator

A general analog computer circuit to realize the transfer function of Eq. (41) is shown in Fig. 30. The transfer function of this general system is given by (Ref. 39):

$$G_2(s) = \frac{-[gs^2 + (bg + eg - ah - ck)s + (beg + dgq + chq + adk - aeh - bck)]}{[s^2 + (b + e - hr - fk)s + (be + dg + fhq + dkr - ehr - bfk)]} \quad (42)$$

where a-h and k, q, and r are potentiometer settings. The amplifier gains and potentiometer settings are adjusted to realize the desired transfer function. This circuitry has been shown to perform effectively when used to compensate transient data typical of that of a low natural frequency thrust measurement system (Ref. 40). The on-line capability of this computer circuitry is limited to low natural frequency thrust measurement systems attributable to gain and voltage levels requirements greater than the ratings of conventional computer amplifier stages. Generally, the use of this circuitry requires that the load cell data be recorded on magnetic tape. The recorded data are run at a slower speed than the original record speed, and the distorted thrust information is computer compensated. The compensated tape data are then run at the original record speed, and the analog representation of the input thrust is obtained.

5.3.2.2 Simulated Thrust Stand-Feedback-Type Compensator

Effective computer compensation is possible with yet another approach. The thrust measurement system transfer function, $X(s)/F(s)$, is simulated with computer circuitry. The difference between the load cell and simulated system outputs is made to approach the actual time representation of the input thrust (Ref. 41). A block diagram of the circuit is shown in Fig. 31. The transfer function of the compensator is seen to be:

$$G_2(s) = \frac{A_1 A_2 (s^2 + 2\zeta_o \omega_o s - \omega_o^2)}{(s^2 + 2\zeta_c \omega_c s + \omega_c^2)} \quad (43)$$

where

$$2\zeta_c \omega_c = \left(2\zeta_o \omega_o + \frac{A_2 A_3}{M} \right)$$

and

$$\omega_c^2 = \left(\omega_o^2 + \frac{A_1 A_2}{M} \right)$$

The on-line capability of this circuitry is limited to low natural frequency thrust measurement systems ($f_t < 2$ Hz) for the same reasons given for the first computer technique.

5.3.2.3 Approximate Differentiator Compensator

Analog computer circuitry utilizing approximate differentiators is capable of on-line compensation of systems with natural frequencies up to several hundred thousand Hz (Ref. 42). A simplified block diagram of this type compensation circuitry is shown in Fig. 32.

Approximate differentiators are used to circumvent the problems of the straight differentiator. The transfer function of the circuit shown in Fig. 32 is given by:

$$G_2(s) = \frac{A(s^2 + 2\zeta_0\omega_0 s + \omega_0^2)}{(s + 12\omega_0)^2} \quad (44)$$

Use of this circuitry effectively increases the bandwidth of the basic thrust measurement system by a factor of 12. The use of compensators does amplify high frequency noise, and their use requires an input signal with a good signal-to-noise ratio characteristic. The severity of the noise amplification problem increases as the mechanical system natural frequency decreases since spurious signals at power line frequencies and signals arising from background vibrations as well as random process noise may be amplified by the compensator. Noise frequencies higher than the highest appreciable amplitude Fourier frequency component of the thrust signal can be attenuated with filters. Filters should be chosen according to the criteria discussed in Section 3.1.1.

5.3.2.3.1 Performance Characteristics of the Approximate Differentiator

Differentiator-type circuitry was used to compensate the distorted load cell data and to recover the dynamic force imparted to the system shown in Fig. 33. Typical results are shown in Fig. 34, and it is concluded that an accurate recovery of the force is accomplished since the data have been precisely correlated with that of the reaction force summation technique (see Section 5.4).

The use of filters to suppress high frequency noise introduces phase shift and increases the instantaneous tracking error. However, the use of linear phase filters is still compatible with the criterion of Eq. (11) provided the cutoff frequency is chosen so that no thrust information is lost. The result is that time delayed but distortionless measurement is still possible.

Multi-degree-of-freedom response of a thrust measurement system with all the natural frequencies occurring in the same frequency decade can conceivably be computer compensated with one complete compensator circuit required for each degree of freedom. Successful computer compensation can be carried out regardless of the analytical model-lumped parameter, or distributed parameter. The only requirement for programming the computer is that the natural frequencies and associated damping characteristics be known. In contrast to this versatility, compensation for multi-degree-of-freedom response (excluding the degrees of dynamic freedom of the thrust butt) utilizing

reaction force summation techniques is practically impossible because of the uncertainty as to where the additional transducers should be located. The accuracy of static thrust measurements with computer compensation is dependent only on the in-place calibration accuracy of the load cell and the stability of the associated electronic equipment.

5.4 CORRELATION OF DYNAMIC THRUST DATA BY REACTION FORCE SUMMATION AND COMPUTER COMPENSATION

A critical evaluation of any dynamic force measurement technique must finally be effected by comparison with a known force input. The electrodynamic-type dynamic force generator discussed in Section 4.3 was not available at the time reaction force summation and computer compensation techniques were being evaluated. However, the precise correlation that was obtained with these two independent techniques with somewhat arbitrary force inputs (hammer raps) for a range of peak force amplitudes from 50 to 500 lb seemed to prove the validity of using either technique for a single-degree-of-freedom mechanical system with negligible damping.

The system shown in Fig. 33 was subjected to sharp hammer raps, and the outputs from the two measurement circuits were displayed simultaneously on a dual-beam oscilloscope. The computer compensation circuitry exhibited several microseconds delay as compared to the reaction force summation circuitry. This was caused mainly by the noise filter placed between the computer output and the oscilloscope input. The two oscilloscope presentations were positioned horizontally until the displayed signals were coincident, and then the system was subjected to the hammer raps.

Both force measurement circuits were adjusted for optimum transient response by repetitively rapping the system with a hammer and manipulating the amplifier gains and attenuator potentiometer settings until no natural frequency effects could be seen on the oscilloscope. The oscilloscope presentation scale factor, pounds input/centimeter, was determined for the entire force measurement system, including all electronic components, by deadweight calibration.

Figure 35 illustrates that the two techniques can produce precisely the same results even for high peak level and fast rise time forces. Identical linear phase filters (passband 0-5 kHz) were placed at both oscilloscope inputs for the data shown in Fig. 35a. In Fig. 35b the data were obtained when the filter was used with the computer, but the reaction force summation circuitry was unfiltered. The identical results

obtained in Figs. 35a and b show that no force information was lost by filtering the computer output signal. The recorded force information shown in Fig. 36 was obtained by a high peak force hammer rap with a less resilient material inserted between the impacting surfaces than that used to obtain the data shown in Fig. 35.

The fact that reaction force summation and computer compensation techniques can yield identical results enables the thrust measurement system designer to take advantage of the best qualities of each. The combination of the two techniques results in a "hybrid" system capable of dynamic thrust measurement with multi-degree-of-freedom mechanical system response.

SECTION VI

DYNAMIC THRUST MEASUREMENT TECHNIQUES FOR MULTI-DEGREE-OF-FREEDOM MECHANICAL SYSTEMS

The determination of the static thrust vector for a particular rocket engine requires a measurement system capable of resolving and measuring the component forces. The accurate determination of each force component requires particular attention of the thrust stand designer to minimize the sources of error listed in Section 1.2. The determination of the static interactions between the force component measurement mechanisms requires a well-designed and complex calibration procedure (Ref. 43).

The determination of the thrust vector during dynamic thrust periods would in general require compensation for at least as many natural modes as there are force components to be determined. A six-component thrust stand would possibly require compensation for six natural modes for each of the force component measurement mechanisms. Add the natural modes contributed by the dynamics of the thrust butts and multi-degree-of-freedom response of the rocket engine and mounting assembly, and the problem of accurate dynamic thrust determination becomes formidable. The magnitudes of the C_{ir} coefficients of Eq. (1) will determine if the particular r mode is significant enough to require compensation. Fortunately, some of the r modes are insignificant for well-designed thrust stands, and in many cases compensation for the effects of several significant natural modes is practical.

A multi-degree-of-freedom response problem that exists in a large number of conventional thrust stands is attributable to nonrigidity of the thrust butt (Refs. 20 and 22). The reaction force summation technique

was shown to be inherently insensitive to thrust butt motions regardless of the mechanical complexity of the thrust butt. However, this technique is not readily usable for compensation of rocket engine and engine mounting structure natural modes other than the predominant one.

Considering again the relatively simple two-degree-of-freedom model illustrating a nonrigid thrust butt shown in Fig. 27 and assuming negligible damping, the load cell force to thrust force transfer function can be shown to be:

$$\frac{K_{LC} [q_E(s) - q_{TB}(s)]}{F(s)} = \frac{[M_{TB} s^2 + K_{TB}]}{[M_E M_{TB}] s^4 + [M_E (K_{LC} + K_{TB}) + M_{TB} K_{LC}] s^2 + K_{LC} K_{TB}} \quad (45)$$

Solving the characteristic equation for s^2 yields the two natural frequencies, and for this simple model two tandem stages of computer compensation could be employed to recover the true input forcing function (provided the two natural frequencies occur in the same frequency decade). However, should the thrust butt respond dynamically in a more complex manner, introducing several natural frequencies, the tandem connection of computer compensation stages soon reaches a practical limit.

The combination of the unique properties of the reaction force summation technique (insensitivity to thrust butt motions regardless of complexity) and computer compensation technique (capable of compensating for rocket engine and mounting structure natural frequencies regardless of lumped parameter or continuous media origin) results in a versatile dynamic thrust measurement scheme superior to either technique alone.

The optimally damped servomechanism dynamic force measurement technique has been shown to be feasible for single-degree-of-freedom systems. Additional degrees of freedom can actually contribute to servomechanism instability unless proper compensation circuitry is included in the design. In general, each rocket engine to be tested will contribute different response characteristics to the overall mechanical system response, and the servomechanism control loop will have to be redesigned to ensure stable performance. If the system natural frequencies change appreciably during the firing (natural frequency change caused by mass loss of solid-propellant rocket engine, etc.), the servomechanism could become unstable. Regardless of the stability of the servomechanism, the force analog signal may contain the effects of multi-degree-of-freedom response of the mechanical system. However, with the servomechanism designed to optimally damp the largest amplitude natural

mode, computer compensation techniques could be used to compensate for the effects of the other natural modes. The damping action of the servomechanism, discussed previously, was completed within a very short period of time after the termination of a dynamic force change, and the system was quickly returned to the static steady state. A practical consideration of this fact, whether the mechanical system response is or is not multi-degree-of-freedom, linear or nonlinear, is that with optimum performance of an active damping device the system is quickly returned to the static steady state following an input force change, and the static force measurement accuracy of the load cell is available.

SECTION VII

SUMMARY OF RESULTS AND CONCLUSION

Three independent techniques, (1) mechanical system response optimization (optimization of system natural frequency, or optimally damped system), (2) reaction force summation, and (3) computer compensation, have been shown to be capable of performing dynamic thrust measurement in conjunction with predominantly single-degree-of-freedom, linear mechanical systems.

One possible solution to the dynamic thrust measurement problem for single-degree-of-freedom systems is to ensure that the thrust measurement system spring member is sufficiently stiff so that the system natural frequency is not excited. If this condition is met then the input thrust is balanced by a large spring reaction force and practically negligible inertial and damping reaction forces. A practical limit to increases in spring constant is dictated by the sensitivity of the transducer used to measure the displacement across the spring member. The displacement transducer signal is used as the analog signal representative of the input thrust.

The system spring constant can conceivably be furnished by a well-designed position servomechanism or by a conventional load cell, the choice being dictated by the (1) values of K possible with each approach, (2) reliability of the prime K mechanism and auxiliary equipment, (3) stability characteristics of the servomechanism, (4) compatibility of the K mechanism with the test environments, (5) complexity of maintenance procedures, (6) cost, and (7) ease of operation. However, the provision of the large spring constant does not necessarily ensure accurate dynamic thrust measurements since multi-degree-of-freedom response of the test engine and mounting structure may introduce significant amplitude natural modes producing spring member reactions

indistinguishable from the effects of true thrust forces. However, computer compensation circuitry could be used to compensate for these natural modes.

The optimally damped servomechanism system is feasible for single-degree-of-freedom mechanical systems but requires careful control loop design to ensure stability when multi-degree-of-freedom mechanical system response is encountered. The largest instantaneous tracking error occurs during rapid thrust level changes. However, computer compensation as an auxiliary component is capable of significantly reducing this error. Multi-degree-of-freedom mechanical system response produces tracking errors in the output signal of the optimally damped system. Computer circuitry can again be used to compensate for the effects of several natural frequencies to significantly reduce this tracking error.

Reaction force summation techniques are easily applied for single-degree-of-freedom mechanical systems with negligible damping. This technique has been shown to be insensitive to thrust butt motions but is not capable of compensating for multi-degree-of-freedom response of the rocket engine and engine mounting structure.

Computer compensation techniques can be applied in a straightforward manner for mechanical system response exhibiting several appreciable amplitude natural frequencies. Natural frequency and damping characteristics are easily programmed into the computer. This technique is not limited to on-line data compensation, since tape recorded data can also be computer compensated.

Taped load cell thrust data played back on a tape loop machine with the signal presented on an oscilloscope is easily computer compensated. One computer section could be used to compensate for several natural frequencies by running the tape loop machine, compensating for one natural frequency, recording this compensated data and then repeating the procedure on the new tape for the next natural frequency. There is a practical limit to the number of appreciable amplitude natural frequencies that can easily be compensated. Nearly equal amplitude, nearly equal frequency natural modes would be most difficult to compensate. Fortunately, a large number of existing thrust measurement systems exhibit one natural mode having a large amplitude with higher natural frequency, lesser amplitude responses superimposed.

Analog computer compensation circuitry can possibly be programmed to take into account the mass loss of solid-propellant rocket engines, thereby decreasing the compensation error attributable to the changing

natural frequency and damping ratio of the mechanical system. The time integral of combustion chamber pressure or a pre-programmed function of engine burn time could be used as the actuating signal to correct for the changing natural frequency and damping ratio.

Before any of the compensation techniques are attempted, the degree of linearity of the thrust stand response should be ascertained since some large stands exhibit decidedly nonlinear dynamic response characteristics (Ref. 44).

An essential component of a dynamic thrust measurement system is the dynamic force calibrator. A dynamic force generator of the electrodynamic actuator type has been shown to be an accurate and versatile dynamic calibrator. Driving the actuator with sinusoidal currents permits the determination of the mechanical system frequency response. The most useful feature of the actuator is realized when the armature is driven by a precise current function generator which produces a time function force simulating the expected thrust performance of the test engine. Repetitive production of this forcing function with simultaneous presentation of the actuator current waveform and measured force analog signal on an oscilloscope permits rapid optimization of the particular dynamic force measurement technique being employed. The tracking error can then be directly determined from the oscilloscope presentations. Experience has shown that it is possible to optimize any of the dynamic measurement techniques in such a short time that the temperature rating of the actuator armature coil is not exceeded so that forced cooling with attendant complexity is not required.

Assessment of the dynamic thrust measurement problem and the capabilities of the available dynamic compensation techniques vividly demonstrates the requirement for the simplest thrust stand dynamic response obtainable. Experience has shown that even the response characteristics of the thrust stand side load flexures can adversely affect the overall mechanical system dynamic response by introducing unwanted natural frequencies. Compact rigid mechanical design utilizing materials with a large value of Young's modulus is obviously conducive to desirable dynamic response, as is the minimization of the total moving mass and maximization of the spring constant of the force restraining spring member.

Considering the previously mentioned characteristics conducive to good dynamic measurements, a conceptual design of a single-axis thrust measurement system optimized for dynamic as well as static measurements is shown in Fig. 37.

The load cell is a temperature compensated piezoresistive strain-gage type and is bolted to a massive, braced, thrust butt. Inevitable, though possibly negligible (depending on peak thrust force and thrust rise time), thrust butt motions do not appreciably degrade the dynamic force measurements since reaction force summation techniques are employed to compensate for the predominant amplitude system natural frequency. Computer circuitry is used to compensate for the lesser amplitude natural frequencies contributed by the test engine and its mounting structure.

The electrodynamic actuator dynamic force calibrator is constructed as an integral part of the metal housing for the accelerometer. Dynamic calibration forces are thereby imparted, approximately, at the same point as thrust forces transmitted by the rocket engine structure.

A high temperature accelerometer is used because of the possible adverse effects caused by heat conduction from the engine. The water-cooled heat shield should practically eliminate problems of heat radiation from the engine and engine exhaust plume.

Figure 37 does not show the details of the static force calibrator. However, this device would consist of conventional pull rods which engage the plate stiffener at the rear of the fins supporting the dynamic calibrator armature coils. The pull rods would pass through the thrust butt to be mechanically coupled to a deadweight loading mechanism. When not in use, the pull rods would be disengaged from the plate stiffener.

This system would be directly usable with physically small engines which could be secured directly to the attachment adapter. Larger engines would require cradle mounting structure and weight support and side load flexures. Experience has shown that plate flexures provide a compact scheme for weight support with simultaneous restraint for side loads. The plate flexures would have to be "tuned" with movable horizontal clamps for best dynamic response.

REFERENCES

1. Conner, R. F., and Hyman, J., Jr. "Direct Thrust Measurement of Electrical Propulsion Devices." ARS Paper No. 2180-61, New York, October 1961.
2. Nelson, L. A. and Hansen, S. "Sensitive Ion-Engine Thrust Measuring Device." Hughes Research Laboratories Report No. 246, Malibu, California, June 1962.
3. Pearson, J. "Description of a Microthrust Stand for the Measurement of Small Forces." Republic Aviation Corporation Report No. RAC 1469, PCD-TN-63-26, Farmingdale, New York, June 1963.
4. Sinnette, J. T. and Stoner, W. A. "Some Innovations in Thrust Balance Design." AIAA Paper No. 66-228, New York, March 1966.
5. Smith, R. E., Jr. "Testing Techniques for Small Solid Rocket Motors at Simulated High Altitude Conditions." Joint Army-Navy-Air Force Solid Propellant Rocket Static Test Panel, Paper No. 143, Palo Alto, California, October 1962.
6. Fluidyne Engineering Corporation. "Multi-Component Rocket Motor Thrust Stands." Report No. P-358, Minneapolis, Minnesota, June 1963.
7. Ormand, A. N. "Rocket Thrust Measurement Systems." Technical lecture given at the Arnold Engineering Development Center, Arnold Air Force Station, Tennessee, February 1967.
8. Fritz, E. E. and Sterling, W. L. "An Impulse Measurement Technique for Ground Testing Attitude Control Pulse Rockets." AIAA Paper No. 64-202, New York, July 1964.
9. Postma, R. W. "Pulse Thrust Measuring Transducer." Rocket-dyne Division of North American Aviation, Inc., Report No. R-6044, Canoga Park, California, January 1965.
10. Republic Aviation Division of Fairchild Hiller Corporation. "High Response, Low Level Thrust Stand System." Report No. FHR 2621-2, PCD-TR-65-25, Farmingdale, New York, October 1965.
11. Couvillion, A. J., Smith, J. D., and Kuberek, R. "High Response, Low Level Pulse Engine Thrust Stand System." Hughes Research Laboratories Report No. AFRPL-TR-66-344, Malibu, California, December 1966.

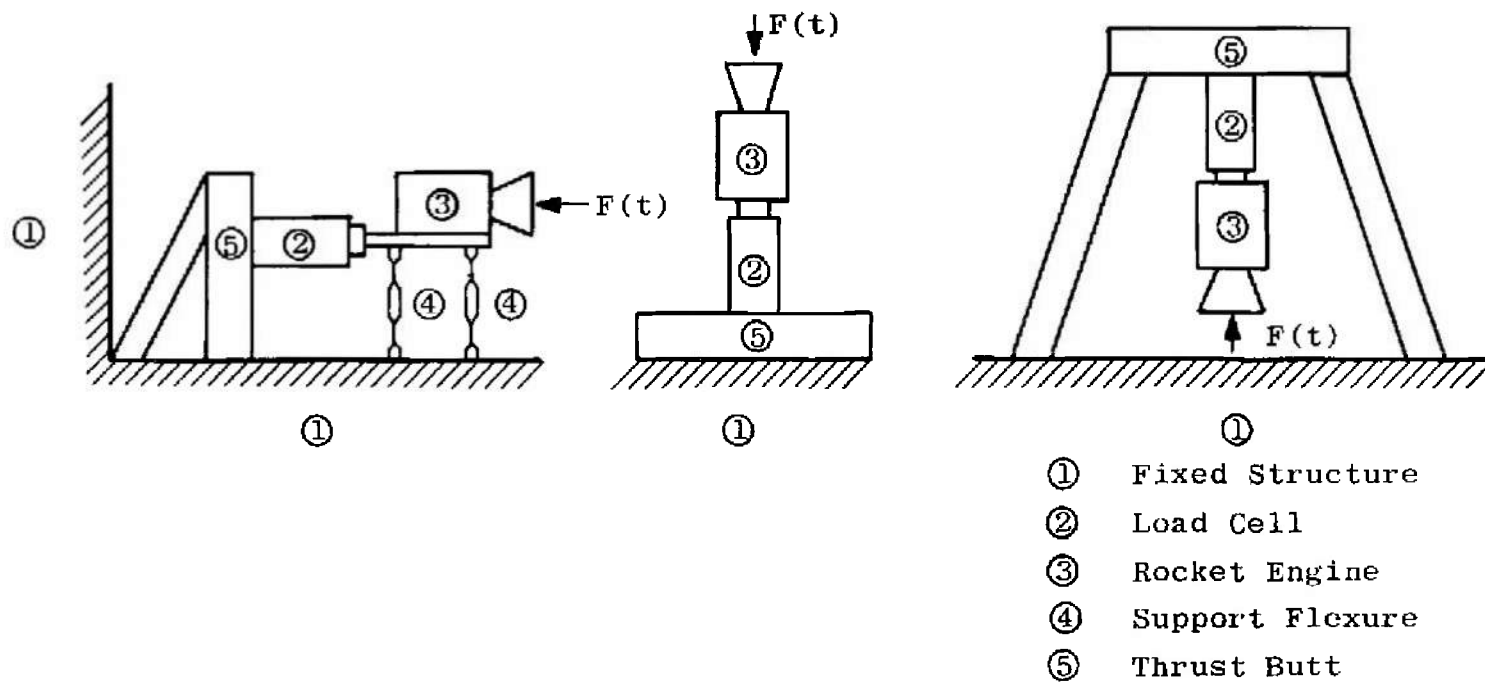
12. Lennert, A. E., Trolinger, J. D., and Shipp, J. I. "Ion Engine Outgassing Tests under Simulated Launch Conditions." AEDC-TDR-63-196 (AD433898), October 1963.
13. Wilton, W. D. "Improvements in Pressure Simulation from Launch to Low Altitude Orbit." AEDC-TR-65-208 (AD470310), September 1965.
14. Dunnill, W. A., Brayton, D. B., and Goethert, W. H. "Electrical Propulsion Test Facility Development Study Summary Report." AEDC-TR-67-106, July 1967.
15. Trolinger, J. D. and Shipp, J. I. "The Development of a Regenerative Collector Target for Long-Term Testing of Electrical Propulsion Systems." AIAA Paper No. 66-500, New York, June 1966.
16. Odgers, I. L., Van De Verg, N., and Wick, R. S. "Combustion-Stability Research." Jet Propulsion Laboratory Progress Report No. 20-203, January 1954.
17. Wick, R. S. "The Effect of Vehicle Structure on Combustion Stability in Liquid-Propellant Rockets." Jet Propulsion Laboratory Progress Report No. 20-248, December 1954.
18. Wick, R. S. "An Analysis of the Effect of Propellant Compressibility on the Dynamic Response of Structures Containing Propellant Feed Tanks." Jet Propulsion Laboratory Progress Report No. 20-267, April 1955.
19. Wick, R. S. "The Effect of Structure on Combustion Stability of Liquid-Propellant Rockets during Flight and during Static-Test-Stand Firings." Jet Propulsion Laboratory Progress Report No. 20-274, July 1955.
20. Kroeger, R. A. and Beckham, P. M. "Rocket Thrust Stand Simulation of Space Vehicle Flight Dynamics." AEDC-TDR-64-163 (AD446309), September 1964.
21. Ormand, A. N. "Six-Component Rocket Motor Thrust Stand Model MCT-1421-4K." Ormand, Inc., Technical Discussion No. 1421-1, Sante Fe Springs, California.
22. Goethert, B. H. "Some Selected Problems in Engine Altitude Testing." AEDC-TR-58-15 (AD203561), October 1958.
23. Irby, T. E. and Hung, J. C. "Optimum Correction of Thrust Transient Measurements." University of Tennessee, Report No. NASA CR-269, Washington, D. C., July 1965.

24. Carden, H. D. and Raney, J. P. "An Experimental and Analytical Study of the Longitudinal Vibration of a Simplified Thor Vehicle Structure." NASA TN D-3632, Washington, D. C., October 1966.
25. Plunkett, R. "Analytical Determination of Mechanical Impedance." Symposium on Shock, Vibration and Associated Environments, Bulletin No. 30, Part II. Washington, Office of Secretary of Defense, January 1962.
26. Bouche, R. R. "Instruments and Methods for Measuring Mechanical Impedance." Symposium on Shock, Vibration and Associated Environments, Bulletin No. 30, Part II. Washington, Office of Secretary of Defense, January 1962.
27. Bouche, R. R. "Instrumentation for Shock and Vibration Measurements." Endevco Corporation, Technical Publication No. 228, Pasadena, California.
28. Schwartz, M. Information Transmission, Modulation, and Noise. New York, McGraw-Hill Book Company, 1959.
29. Weinburg, L. Network Analysis and Synthesis. New York, McGraw-Hill Book Company, 1962.
30. ADC Products Company. "Wave Filters: Their Design and Specifications." Minneapolis, Minnesota, Division of Magnetic Controls Company.
31. Blass, G. A. Theoretical Physics. New York, Appleton-Century-Crafts, 1962.
32. Cimino, A. A. and Nelius, M. A. "Performance of the Amcel Modes A-1 and C-8 Solid-Propellant Rocket Motors at Simulated Altitudes." AEDC-TDR-62-106 (AD275640), May 1962.
33. Savant, C. J. Control System Design. New York, McGraw-Hill Book Company, 1964.
34. Thaler, G. J. and Brown, R. G. Analysis and Design of Feedback Control Systems. New York, McGraw-Hill Book Company, 1960.
35. Chelner, H. "Some Recent Developments in the Semiconductor Transducer Field." Rocketdyne Division of North American Aviation, Inc., Canoga Park, California.
36. Yu, Ying-Nien, Van Lerberg, D. H., and Price, P. "Research Studies and Modification of Thrust Measuring System." Inca Engineering Corporation, Job No. 343, Pasadena, California, December 1963.

37. Republic Aviation Corporation. "High Response, Low Level Thrust Measurement System." Report No. RAC 2601, PCD-TR-64-17, Farmingdale, New York, September 1964.
38. Ward, J. S. "A System for Correcting for Spurious Natural Frequency Ringing of Rocket Thrust Stands." U. S. Naval Ordnance Test Station NOTS TP 2541, NAV WEPS 7569, China Lake, California, September 1960.
39. Jackson, A. S. Analog Computation. New York, McGraw-Hill Book Company, 1960.
40. Lee, O. B. "The Analog Computer as a Compensator for Rocket Thrust Data." Master's thesis, The University of Tennessee, Knoxville, Tennessee, 1965.
41. Sprouse, J. A. and McGregor, W. K. "Investigations of Thrust Compensation Methods." AEDC-TDR-63-85 (AD411841), August 1963.
42. Liu, F. F. and Berwin, T. W. "Extending Transducer Transient Response by Electronic Compensation for High-Speed Physical Measurements." The Review of Scientific Instruments, Vol. 29, No. 14-22, January 1958.
43. Robinson, C. E. and Runyan, R. B. "Thrust Vector Determination for the Apollo Service Propulsion Engine Using a Six-Component Force Balance." AEDC-TR-65-250 (AD475564), December 1965.
44. Ankeney, D. P. and Woods, C. E. "Design Criteria for Large Accurate Solid-Propellant Static-Thrust Stands." U. S. Naval Ordnance Test Station NOTS TP 3240, NAV WEPS 8353, China Lake, California, June 1963.
45. Chen, Y. Vibrations: Theoretical Methods. Reading, Massachusetts, Addison-Wesley Publishing Company, 1966.
46. Den Hartog, J. P. Mechanical Vibrations. New York, McGraw-Hill Book Company, 1956.

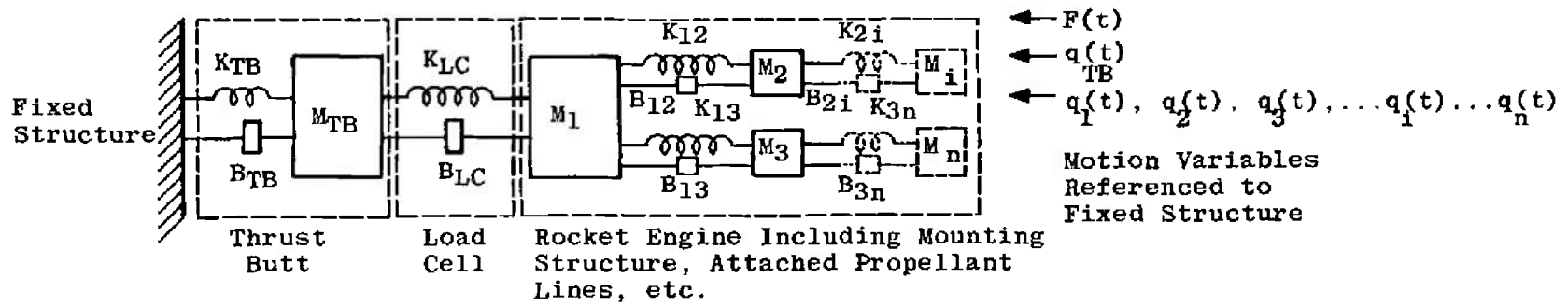
APPENDIXES

- I. ILLUSTRATIONS**
- II. ANALYTICAL CALCULATION OF MECHANICAL STRUCTURE
TRANSIENT RESPONSE**

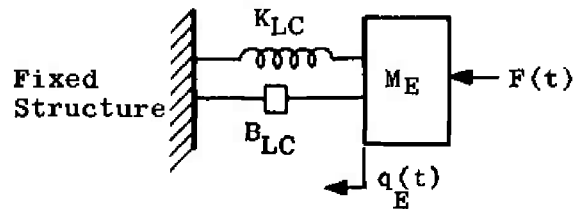


a. Representation of Typical Engine Mounting Configurations

Fig. 1 Representation of the Dynamic Thrust Measurement Problem

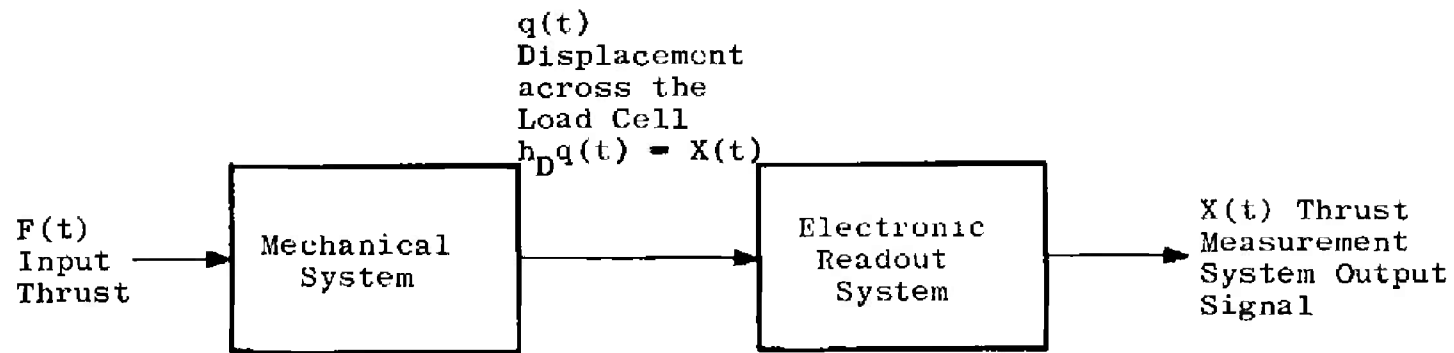


b. Analytical Model Single Axis, Multi-Degree-of-Freedom Mechanical System

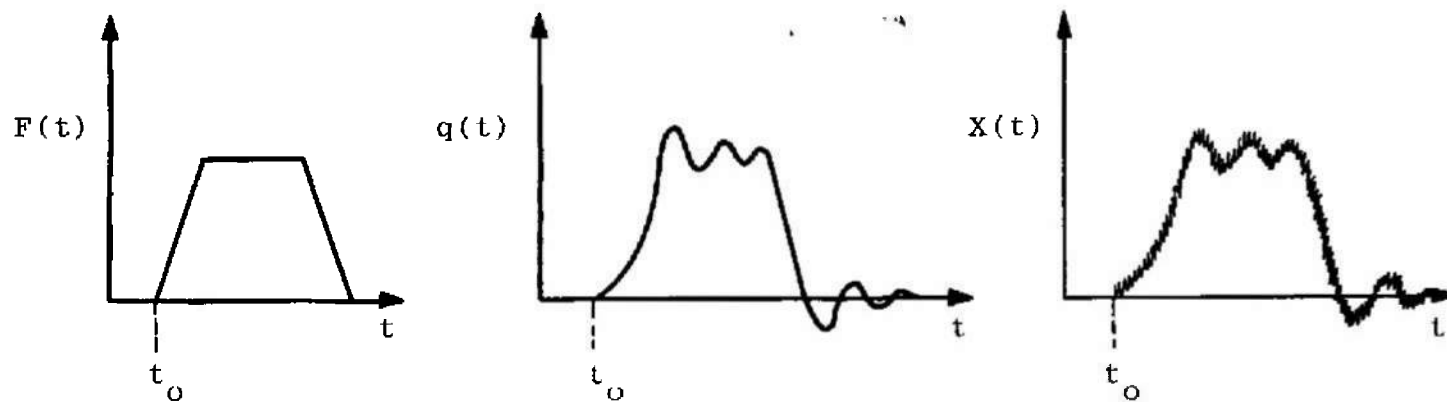


c. Analytical Model Single Axis, Single-Degree-of-Freedom Mechanical System

Fig. 1 Continued



d. Block Diagram Model



e. Time Representation of Variables Shown in (d) Illustrating the Effects of Mechanical System Amplitude and Phase Distortion and Electronic System Noise Distortion

Fig. 1 Concluded

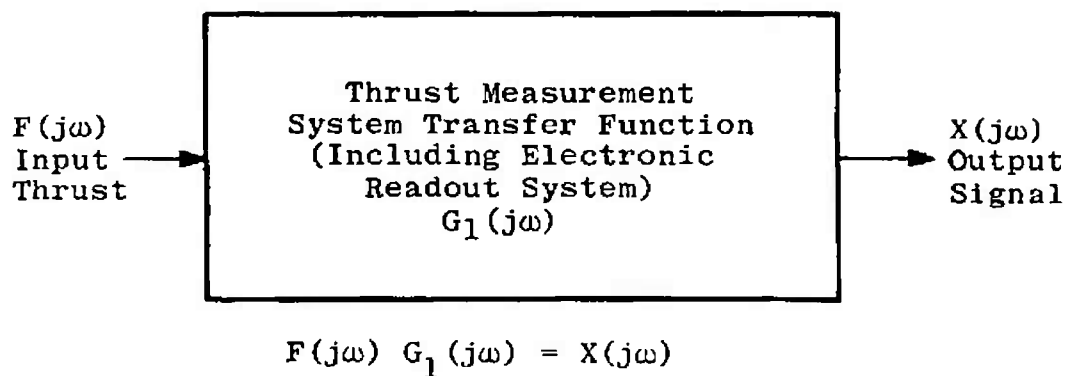


Fig. 2 Relationship of Input Thrust, Thrust Measurement System Transfer Function, and Output Signal

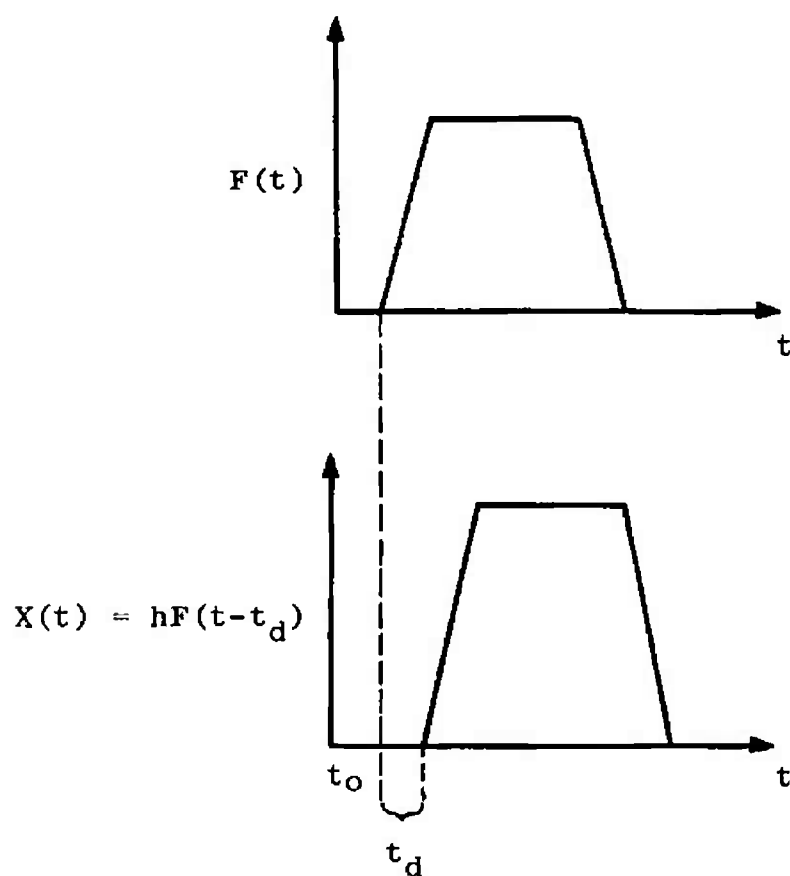


Fig. 3 Ideal Time Delayed, Distortionless Reproduction of Thrust Information

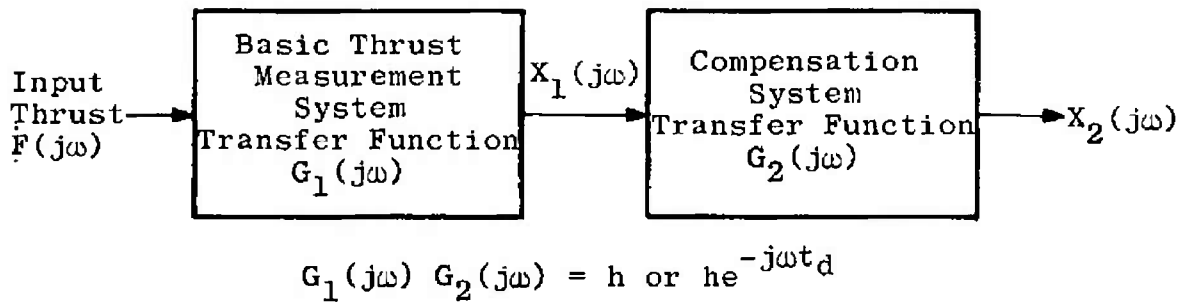


Fig. 4 Tandem Operation of Basic Thrust Measurement System and Compensation System to Obtain Distortionless Transmission of Thrust Information

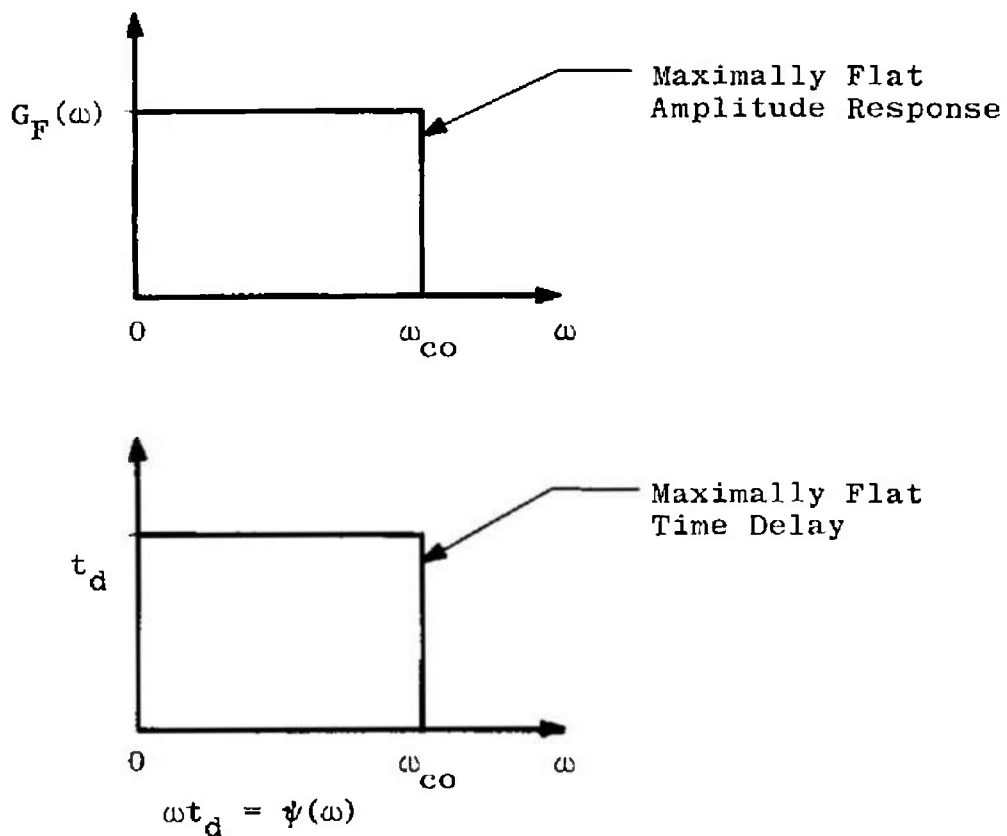


Fig. 5 Ideal Low Pass Filter Characteristics

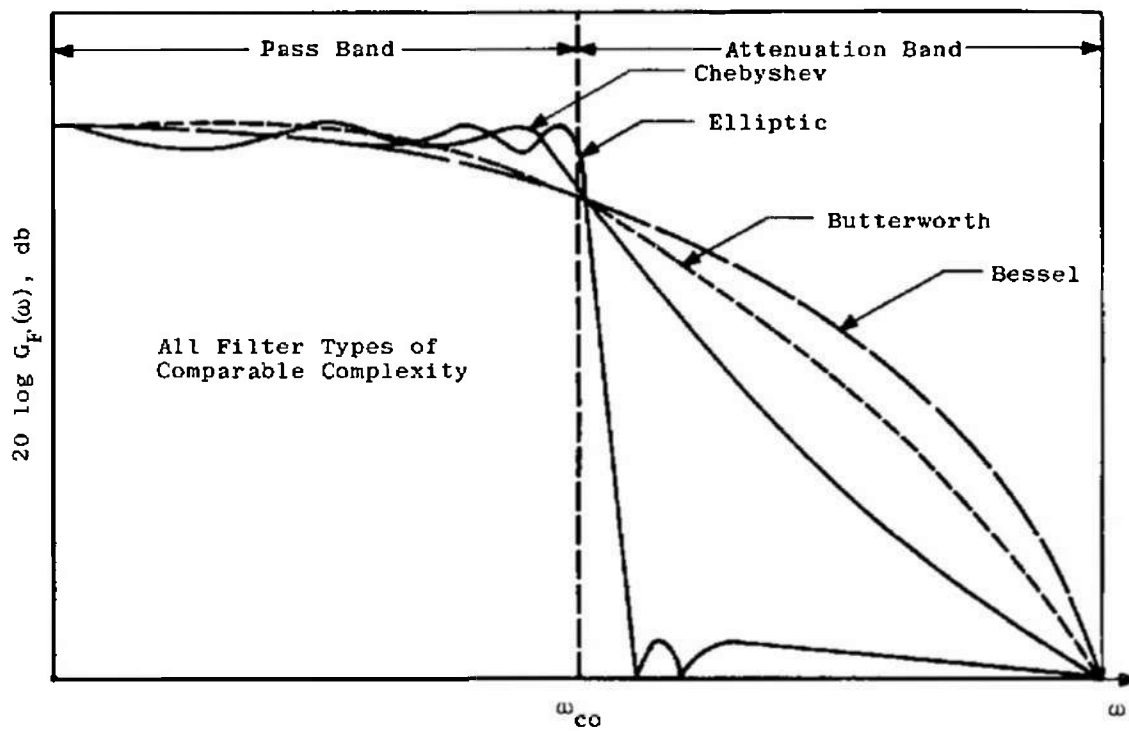


Fig. 6 Comparison of Amplitude Characteristics of Common Filter Types

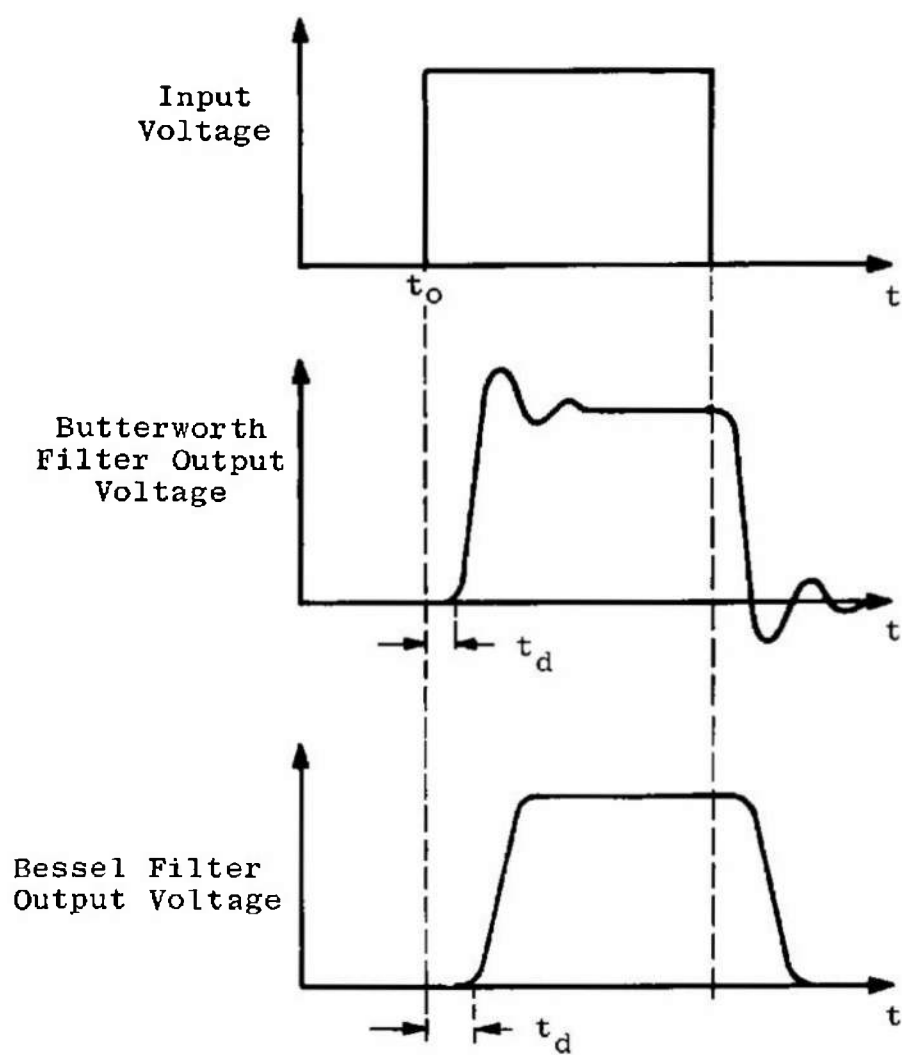


Fig. 7 Comparison of Transient Responses of the Butterworth and Bessel Function-Type Filters

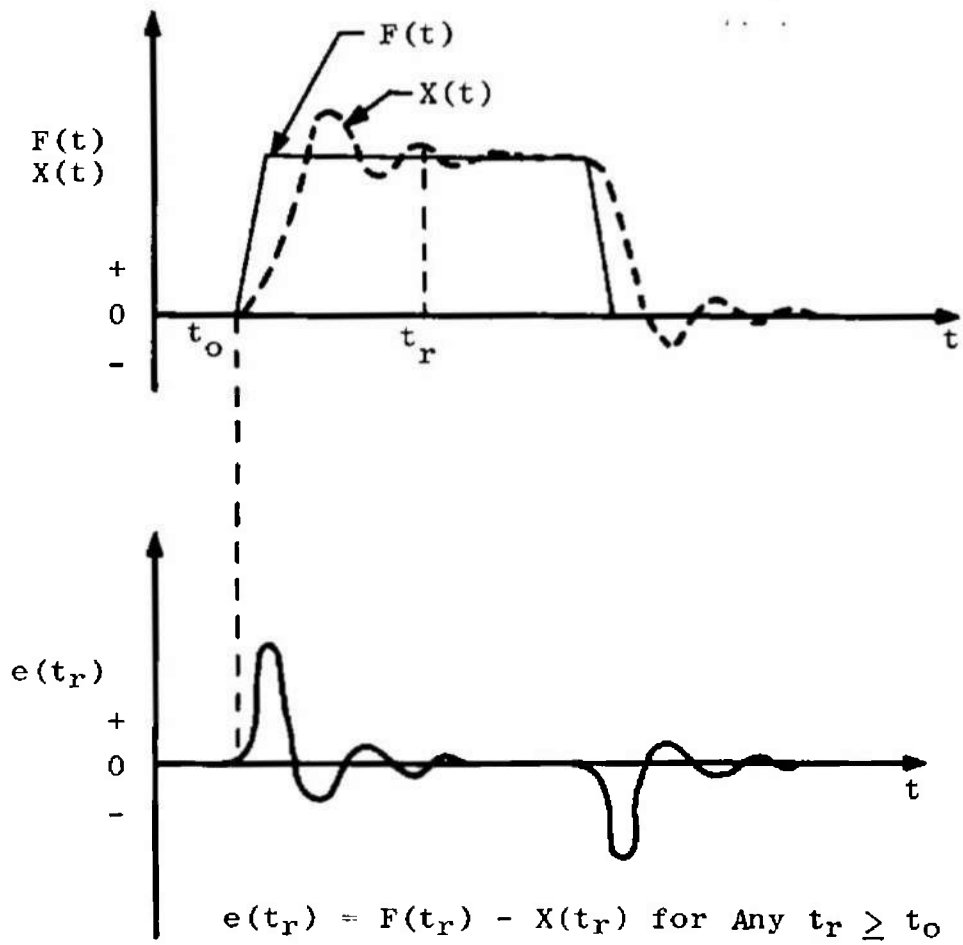


Fig. 8 Instantaneous Tracking Error

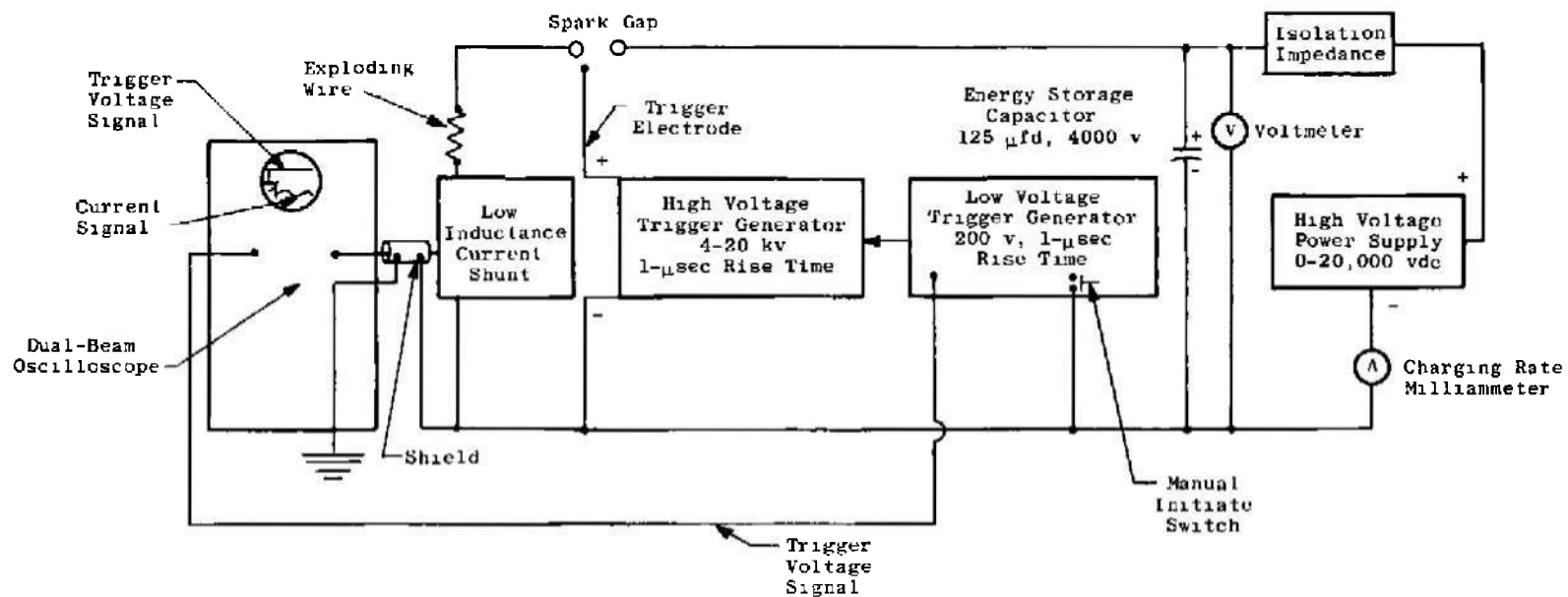


Fig. 9 Schematic of Exploding Wire Device

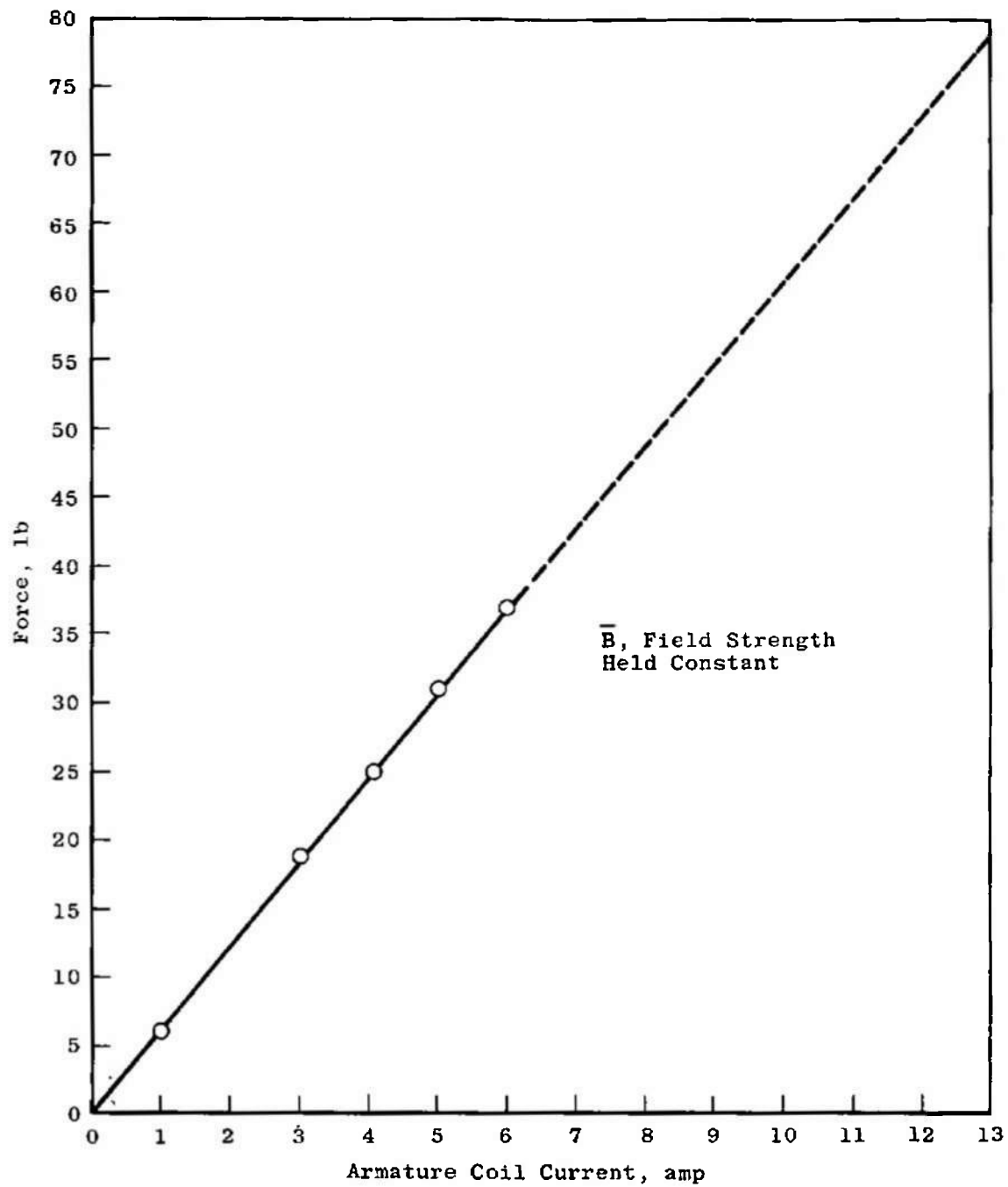


Fig. 10 Force to Armature Coil Current Calibration of Electrodynamic Actuator

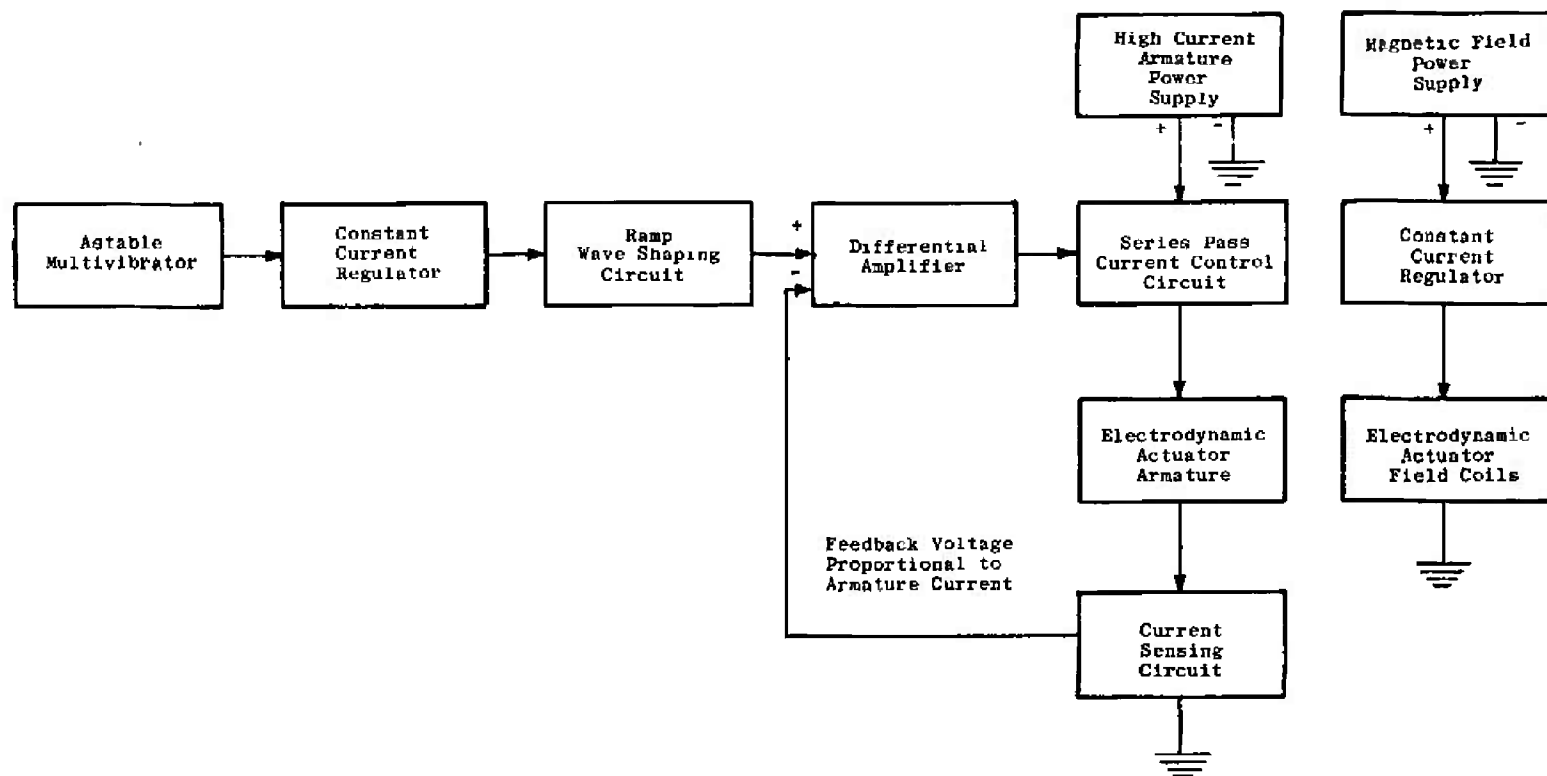
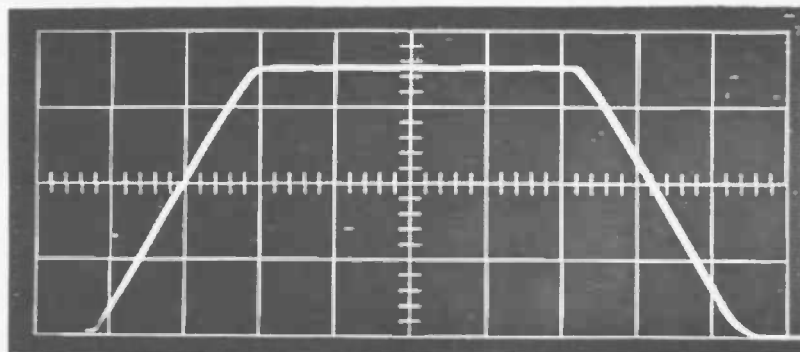


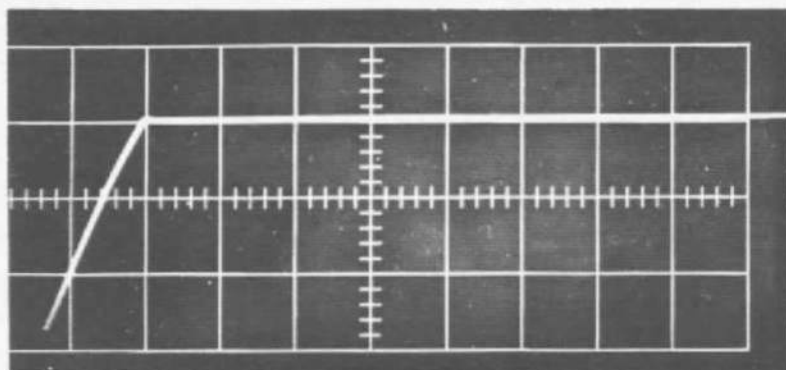
Fig. 11 Block Diagram of Current Function Generator for the Dynamic Force Calibrator



Horizontal Scale - 10 msec/cm
Vertical Scale - 3.28 amp/cm

Current Function
(Force Analog Signal)

a. Dynamic Calibrator Peak Force - 72 lb



Current Function
(Force Analog Signal)

Horizontal Scale - 0.5 msec/cm
Vertical Scale - 1.67 amp/cm

b. Dynamic Calibrator Peak Force - 31.2 lb

Fig. 12 Typical Performance of the Current Function Generator for the Dynamic Force Calibrator

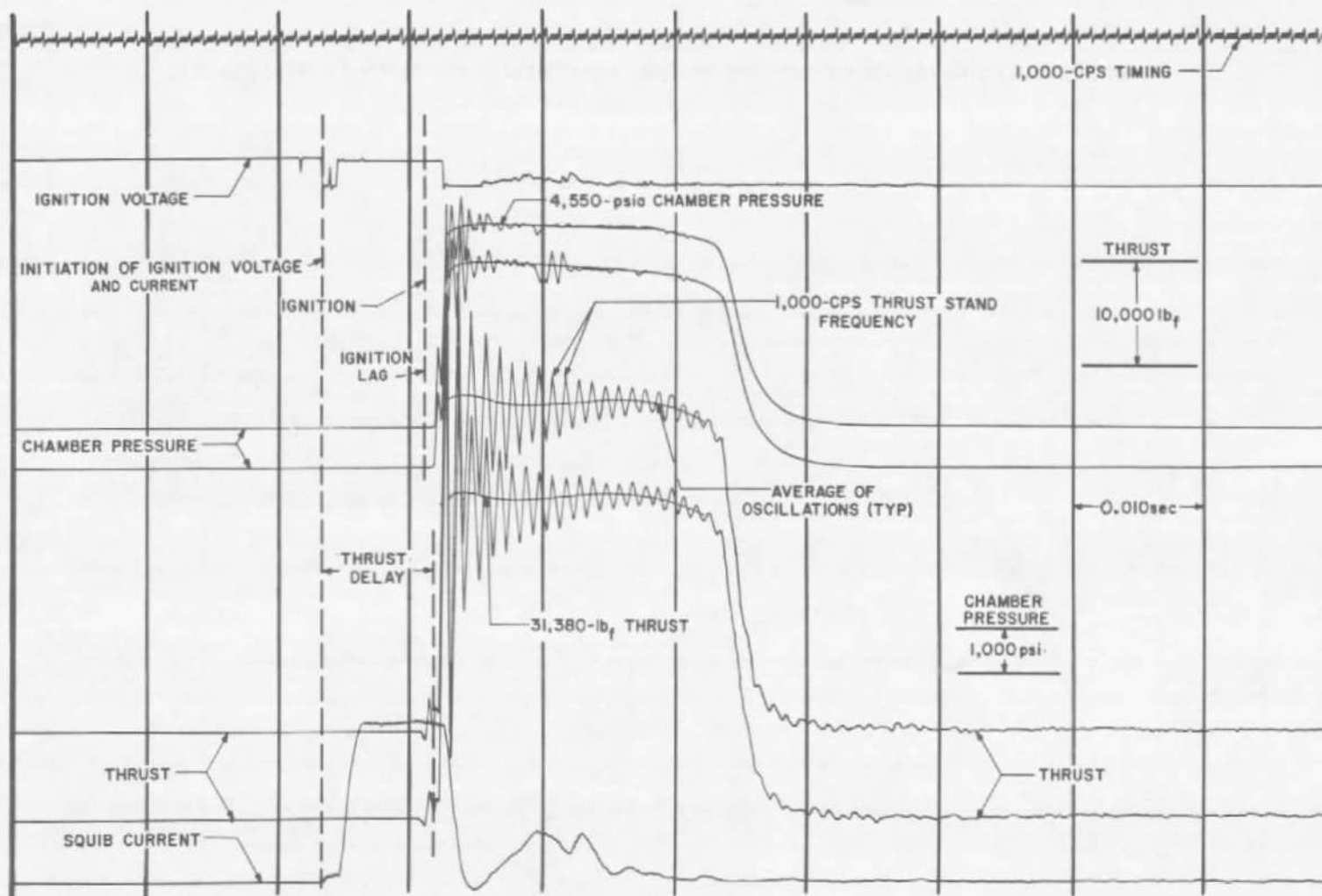


Fig. 13 Rocket Engine Test Data Illustrating Single-Degree-of-Freedom Dynamic Response of the Thrust Measurement System

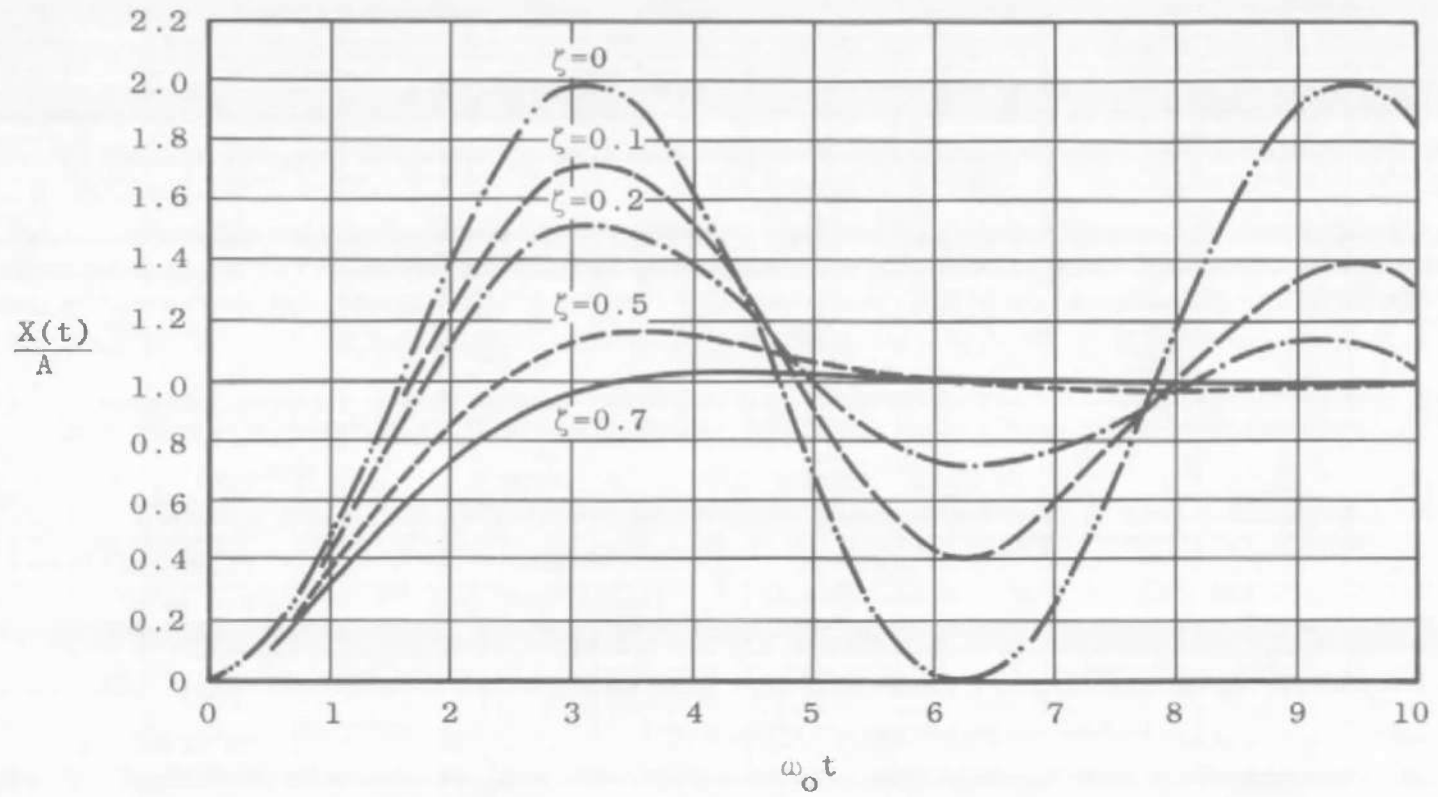
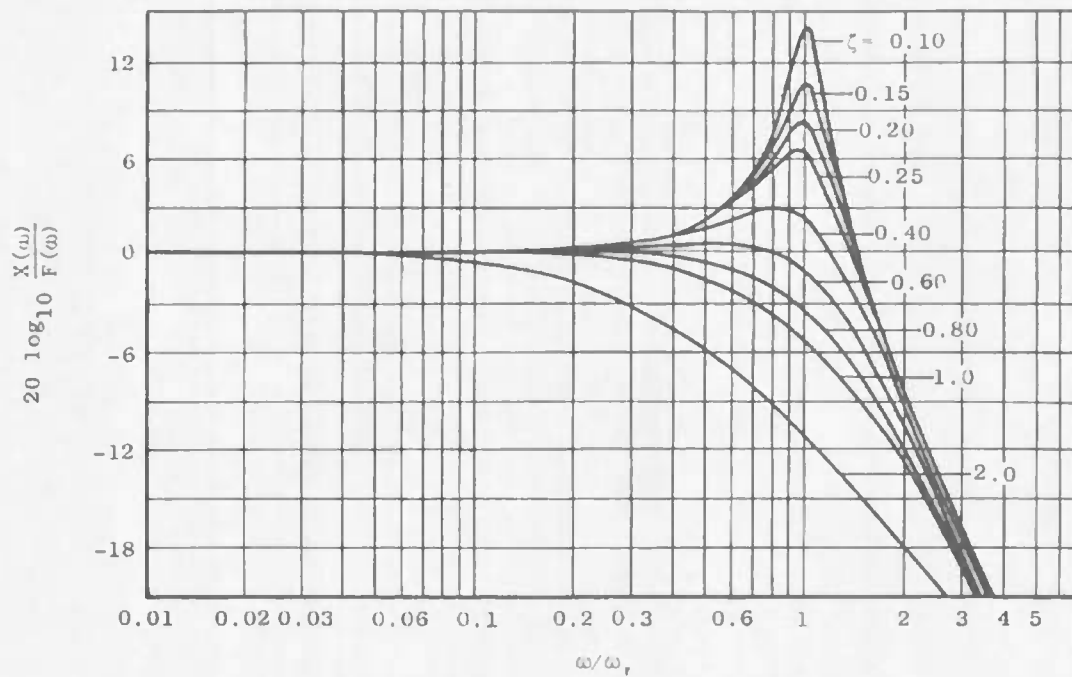
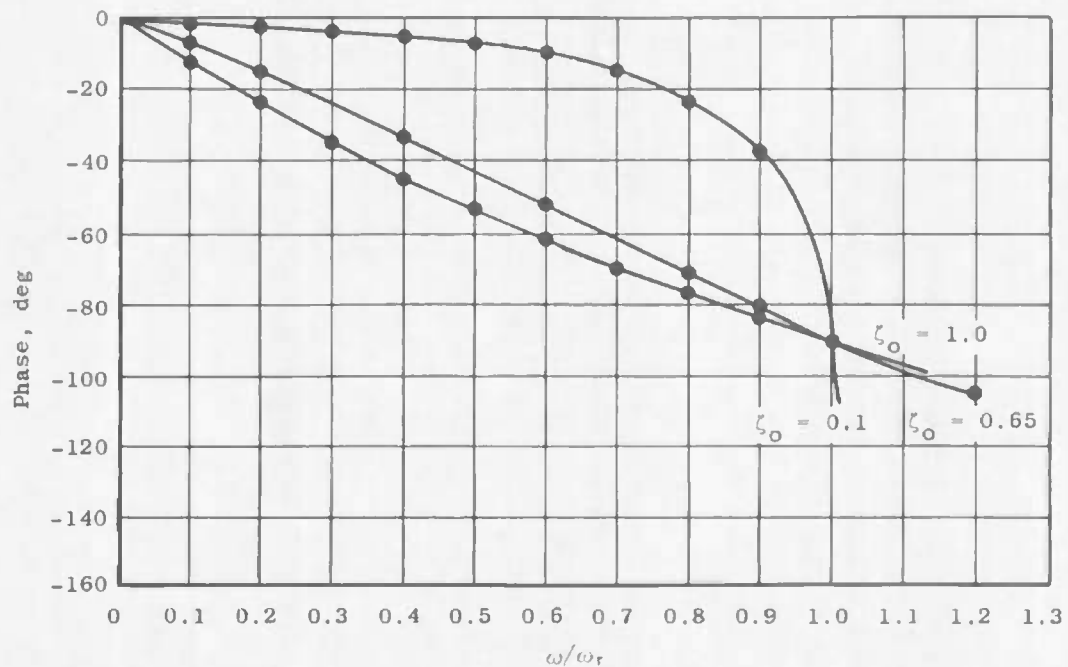


Fig. 14 Step Function Response of Single-Degree-of-Freedom Thrust Measurement System



a. Amplitude Response



b. Phase Response

Fig. 15 Amplitude and Phase Response of Single-Degree-of-Freedom Thrust Measurement System

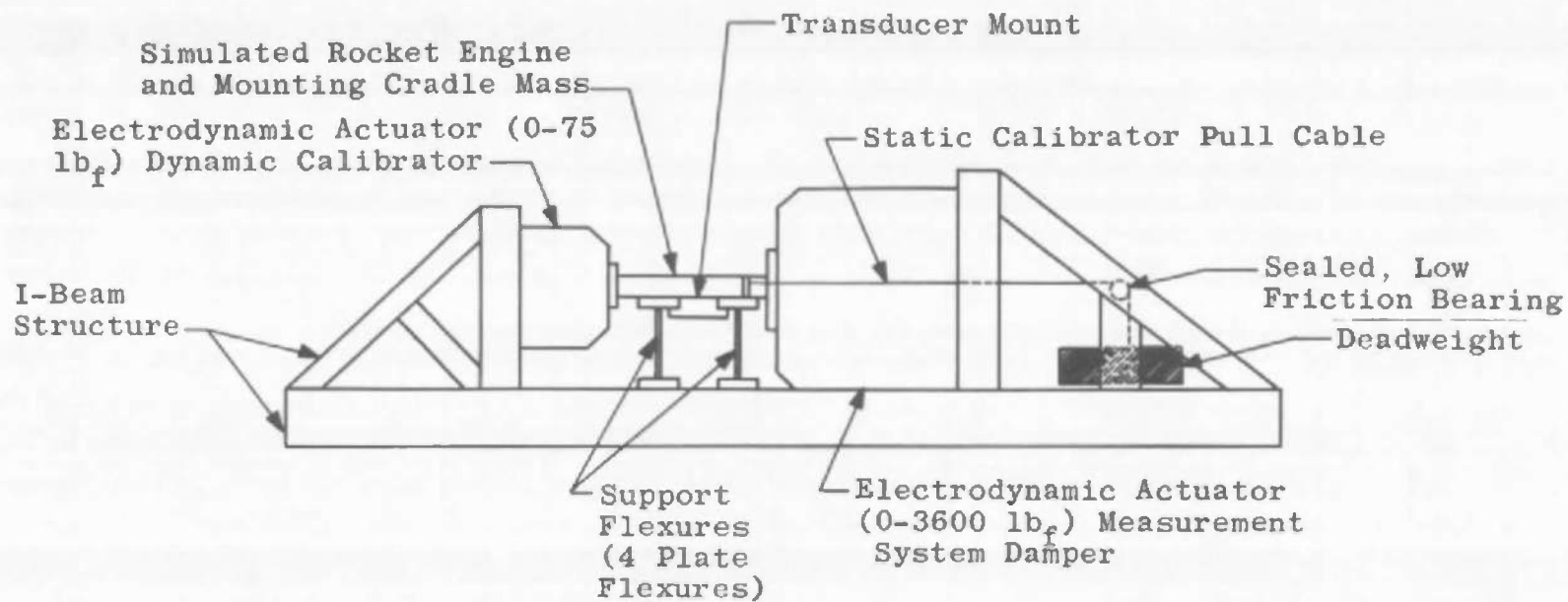


Fig. 16 Mechanical Component Schematic of Optimally Damped Dynamic Thrust Measurement System

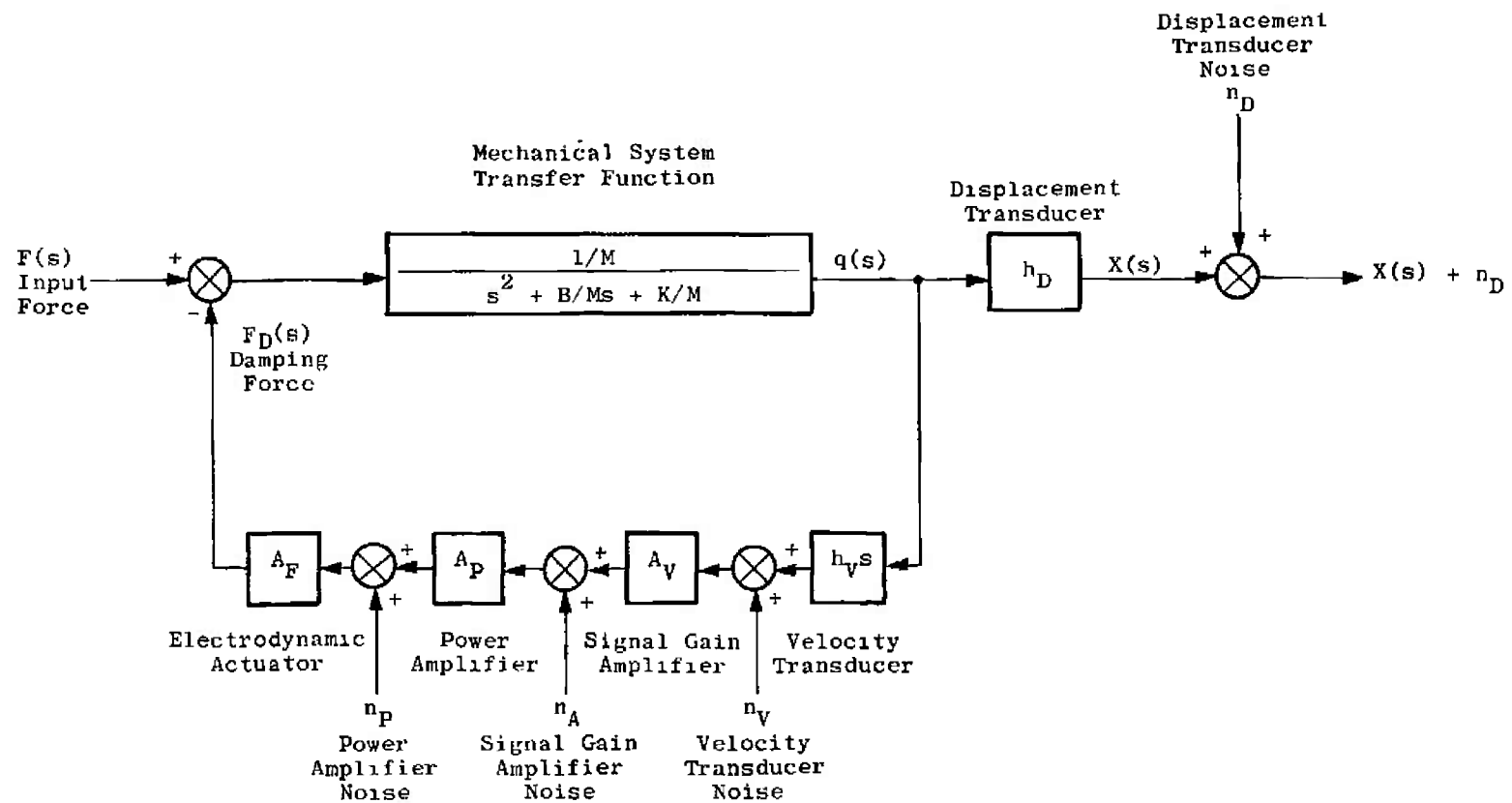


Fig. 17 Block Diagram of Single-Degree-of-Freedom Mechanical System with Velocity Feedback Damping

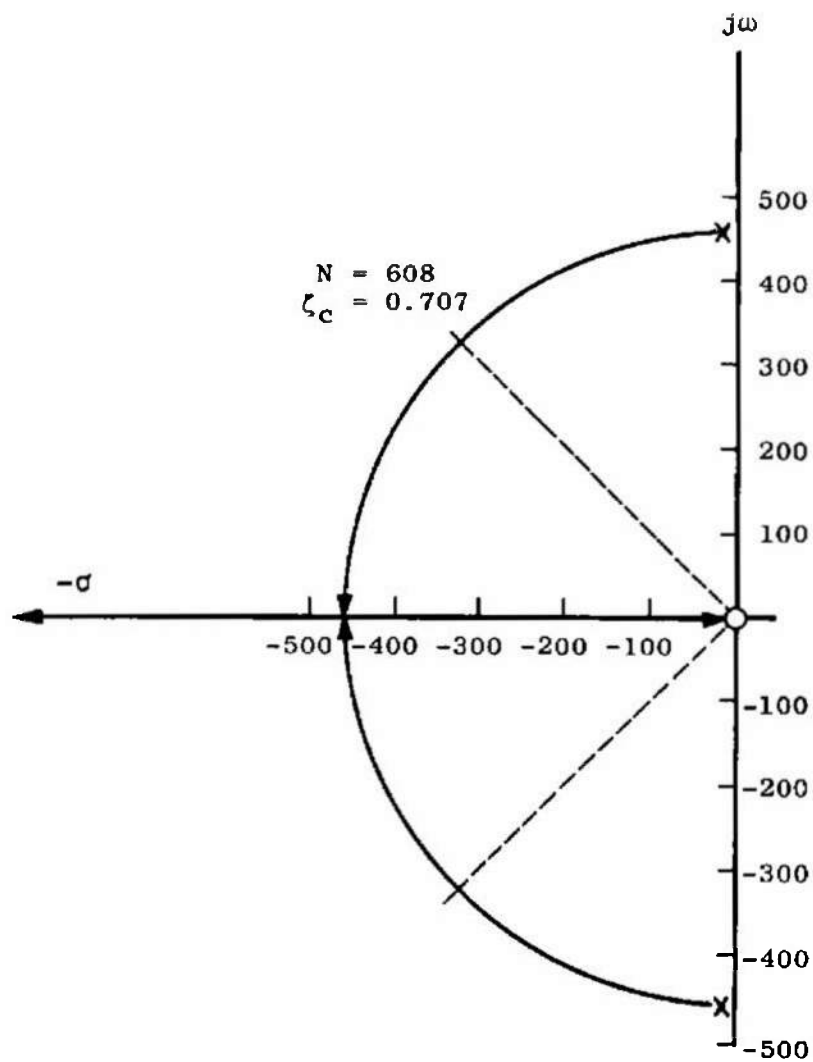


Fig. 18 Root Locus Plot of Open Loop Transfer Function of Velocity Feedback Damped Single-Degree-of-Freedom Mechanical System

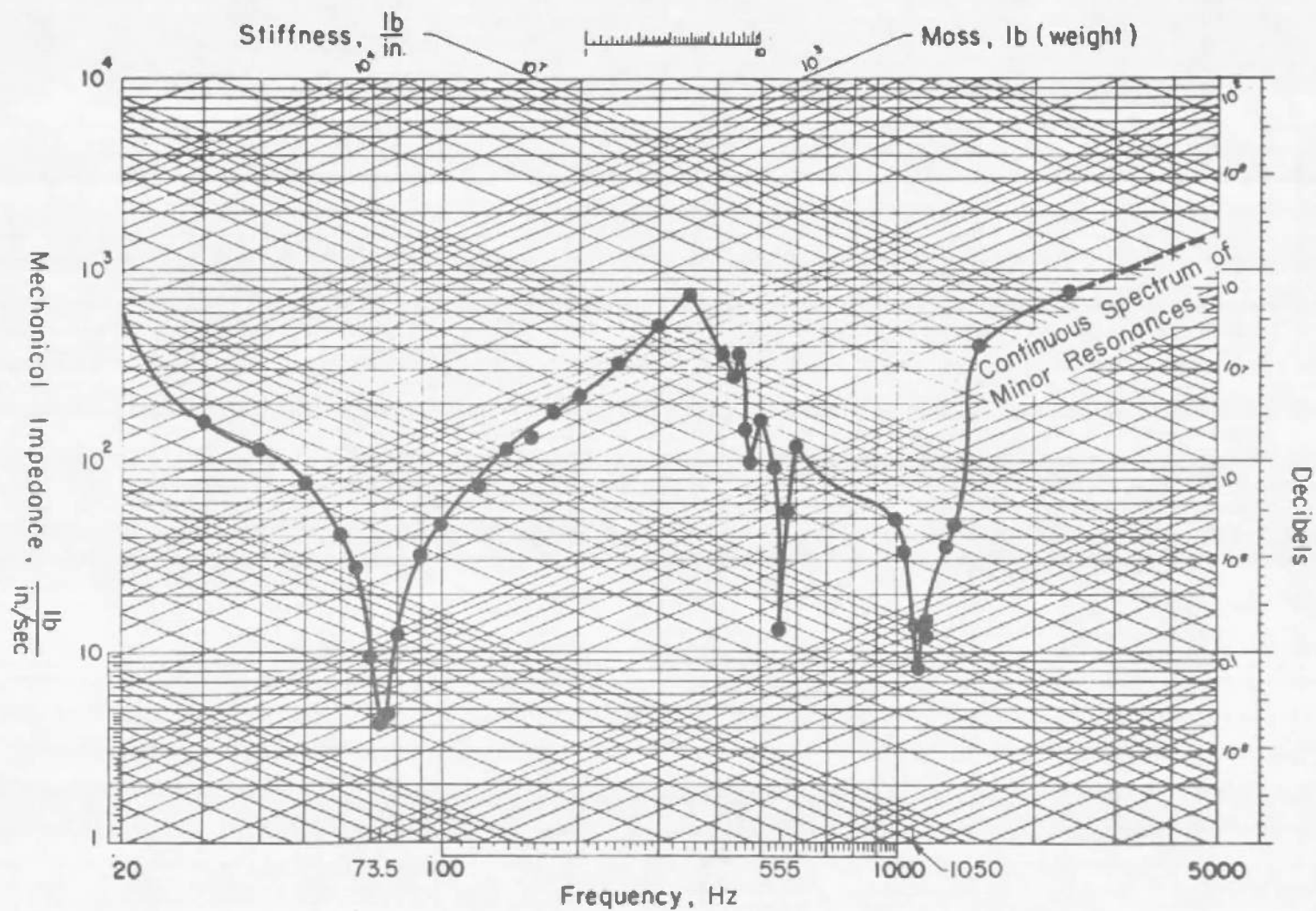
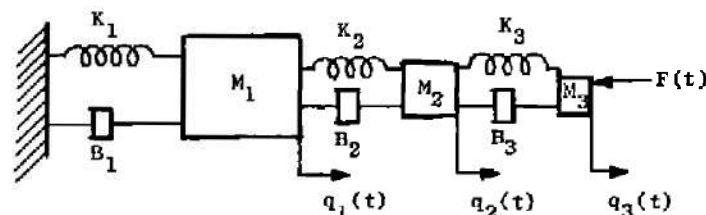
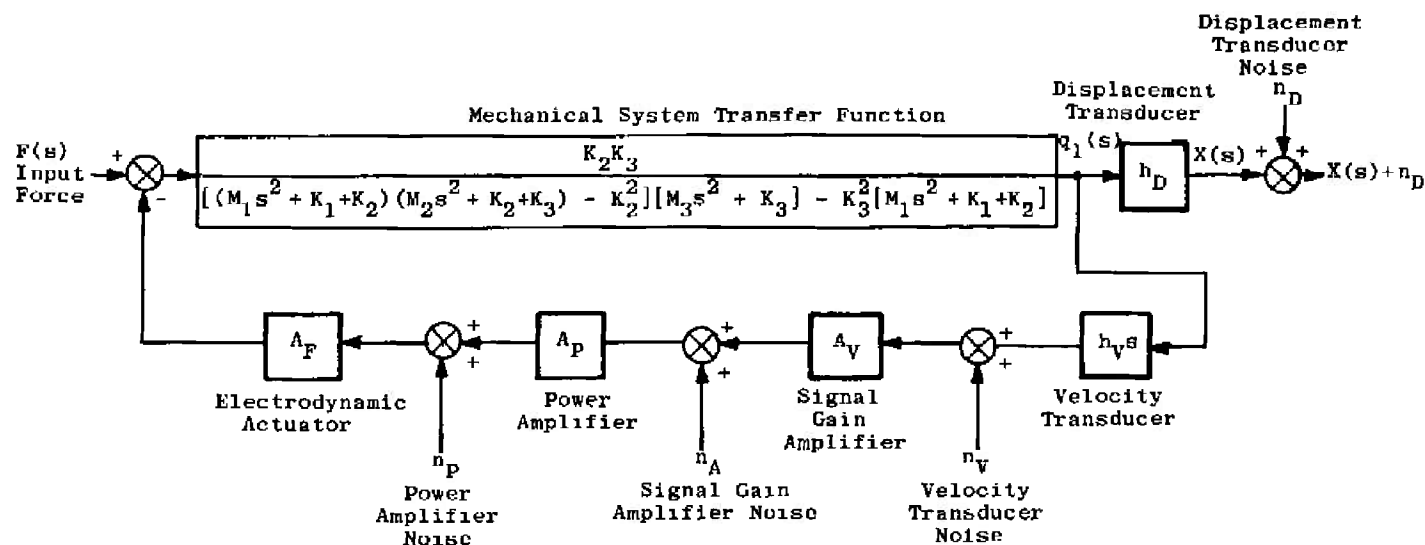


Fig. 19 Transfer Mechanical Impedance Plot (Amplitude Only) for System Shown in Fig. 16



a. Analytical Model



b. Block Diagram

Fig. 20 Analytical Model and Block Diagram of Single Axis, Three-Degree-of-Freedom Mechanical System with Velocity Feedback Damping

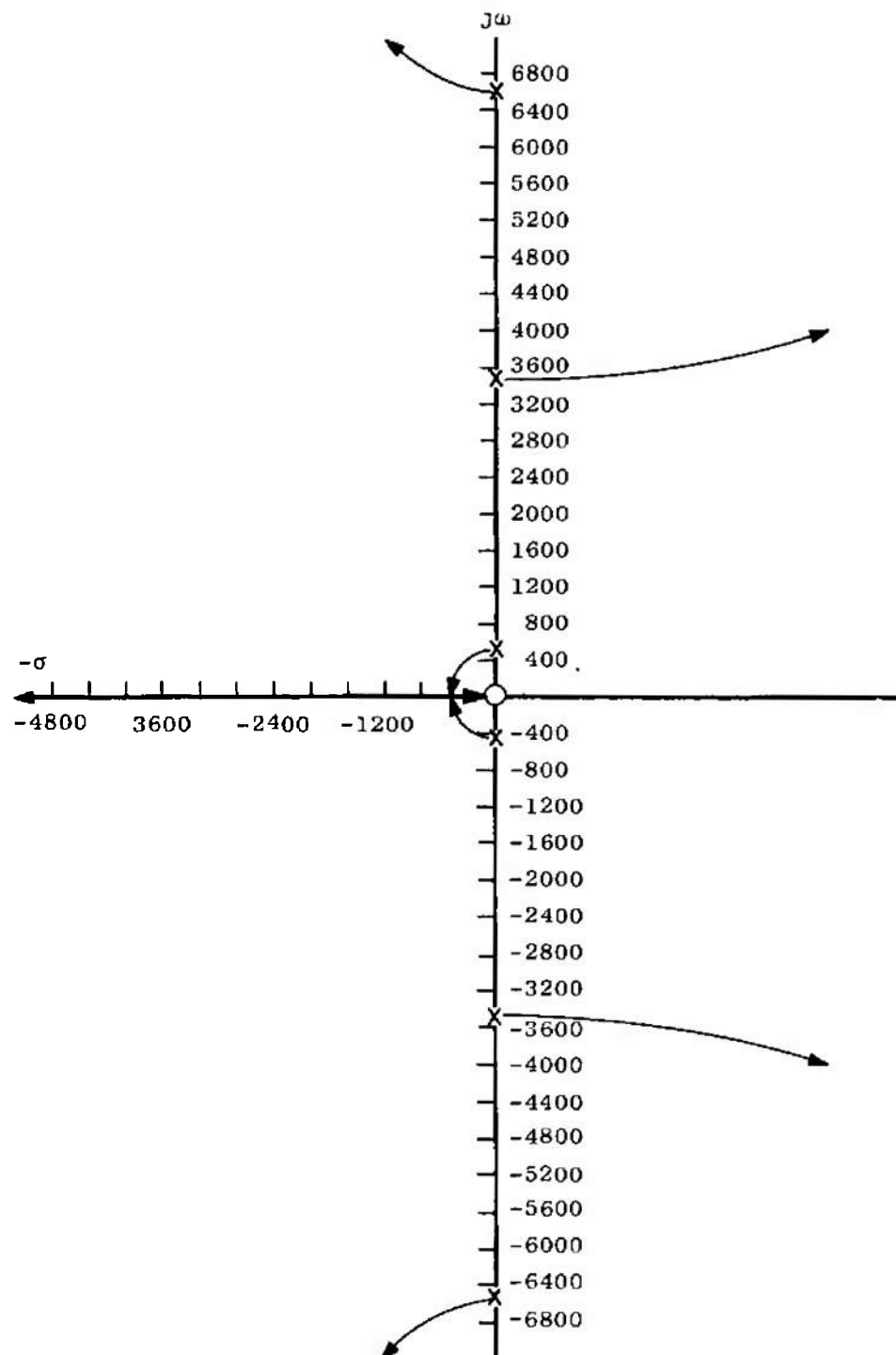
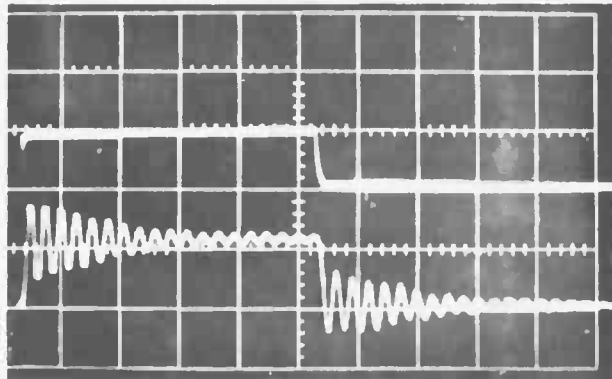


Fig. 21 Root Locus Plot of Open Loop Transfer Function of Velocity Feedback Damped Three-Degree-of-Freedom Mechanical System

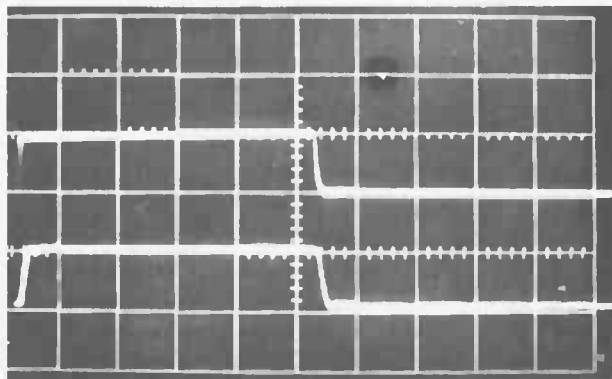


Horizontal Scale - 50 msec/cm
Vertical Scale - 56.4 lb/cm
Input Force Rise Time - 0.5 msec
Fall Time - 0.6 msec

Input Force

Thrust Stand Response

a. System Response without Feedback Damping



Horizontal Scale - 50 msec/cm
Vertical Scale - 56.4 lb/cm
Input Force Rise Time - 0.5 msec
Fall Time - 0.6 msec

Input Force

Thrust Stand Response

b. System Response with Optimum Feedback Damping

Force Imparted to the System with the Electrodynamic
Actuator Dynamic Force Calibrator.

Fig. 22 Optimally Damped Servomechanism System Typical Performance

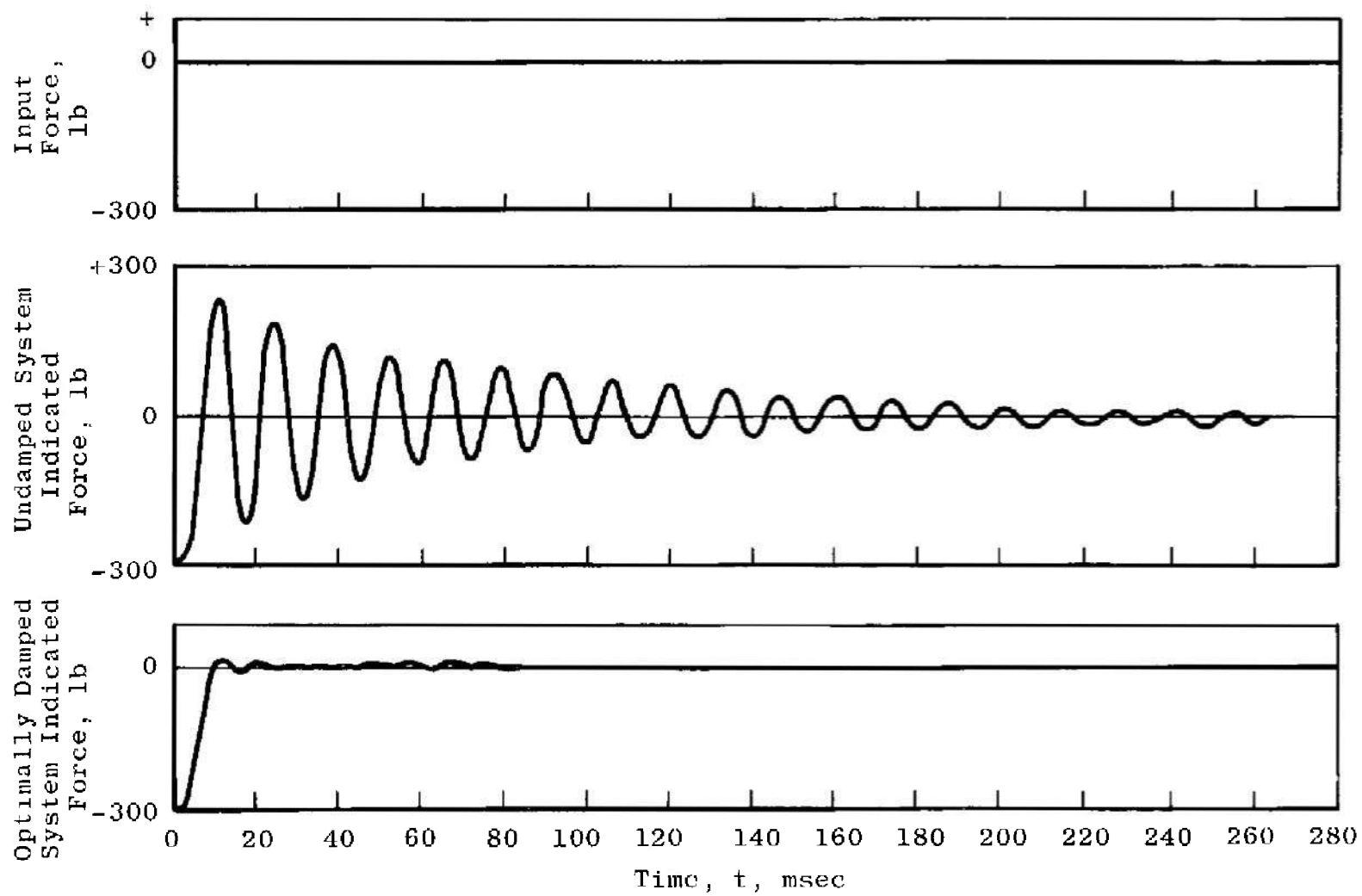


Fig. 23 Optimally Damped Servomechanism System Response to a 300-lb Step Function Force

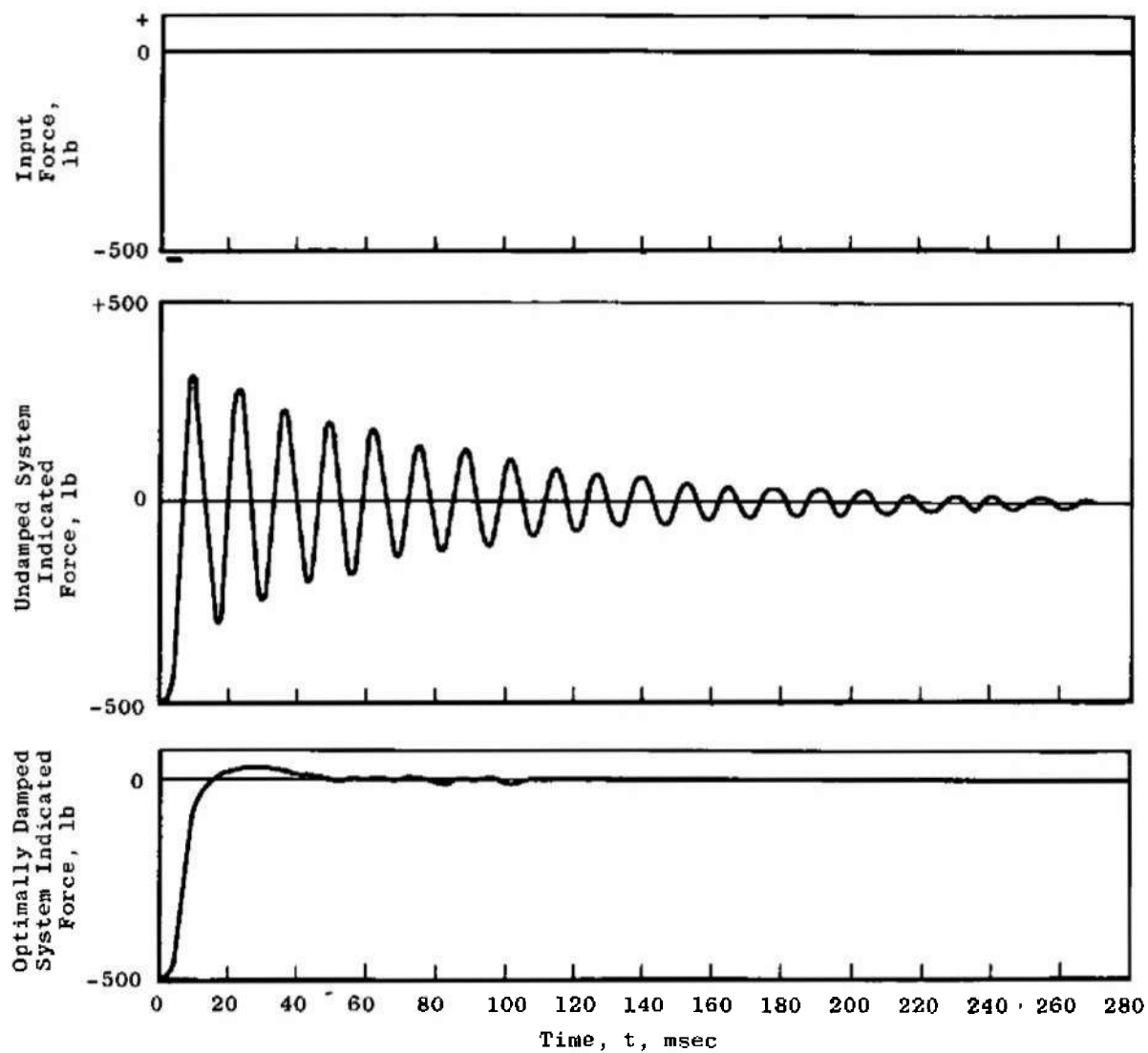
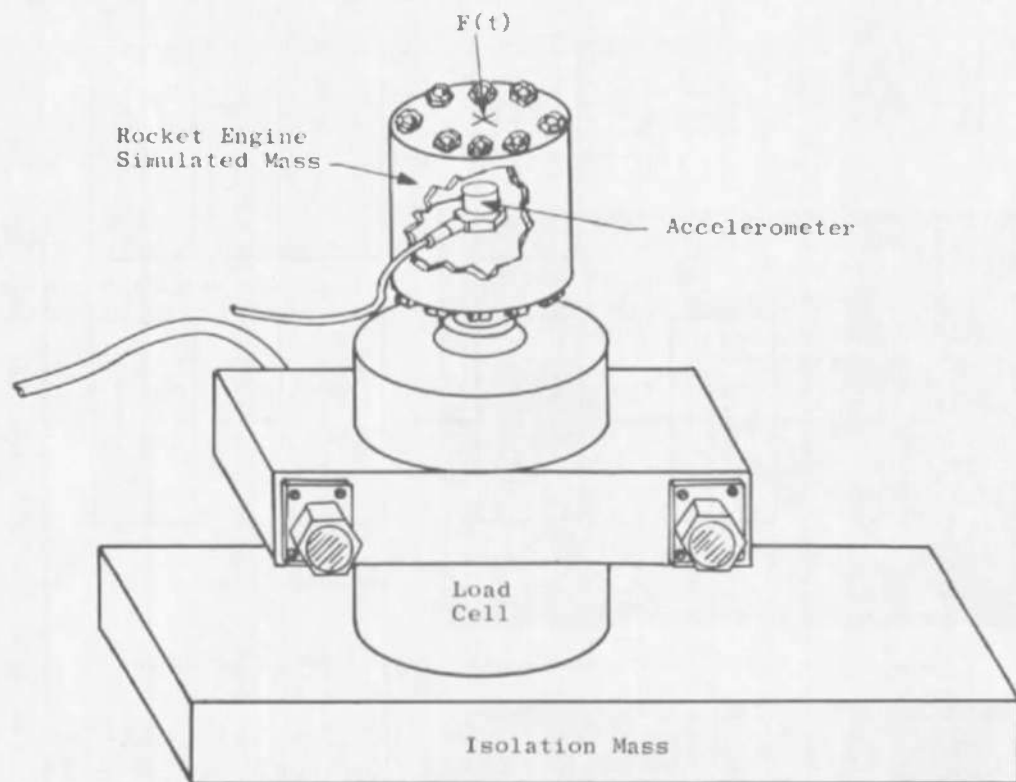
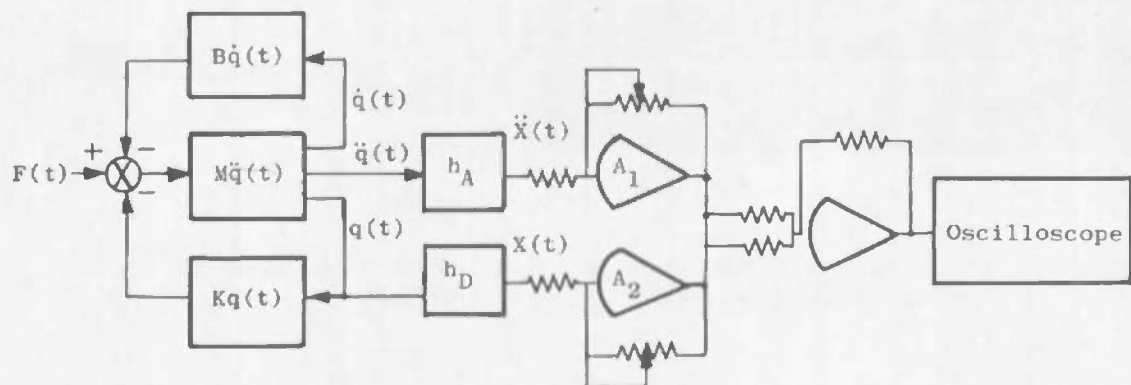


Fig. 24 Optimally Damped Servomechanism System Response to a 500-lb Step Function Force

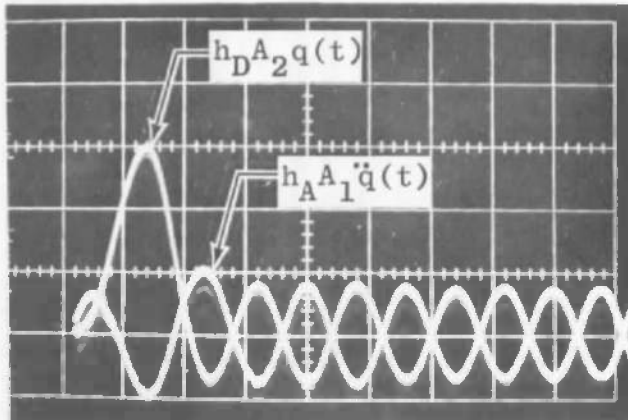


a. System Mechanical Components



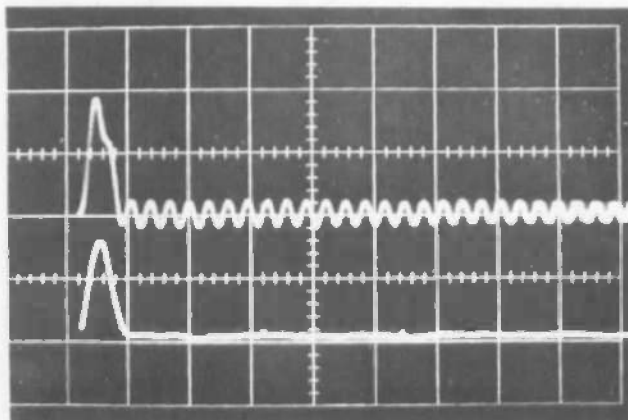
b. Block Diagram

Fig. 25 Reaction Force Summation System



Horizontal Scale - 1 msec/cm
Vertical Scale - 78.1 lb/cm
(Deadweight Calibration)

a. Load Cell and Accelerometer Signals Before Summation



Horizontal Scale - 5 msec/cm
Vertical Scale - 78.1 lb/cm
(Deadweight Calibration)
Peak Input Force - 117.2 lb

← Load Cell Signal

← Load Cell and Accelerometer Signals Summed.

b. Load Cell and Summation Signals

Force Imparted by Striking the System
with a Plastic Tipped Hammer.

Fig. 26 Reaction Force Summation System Typical Performance

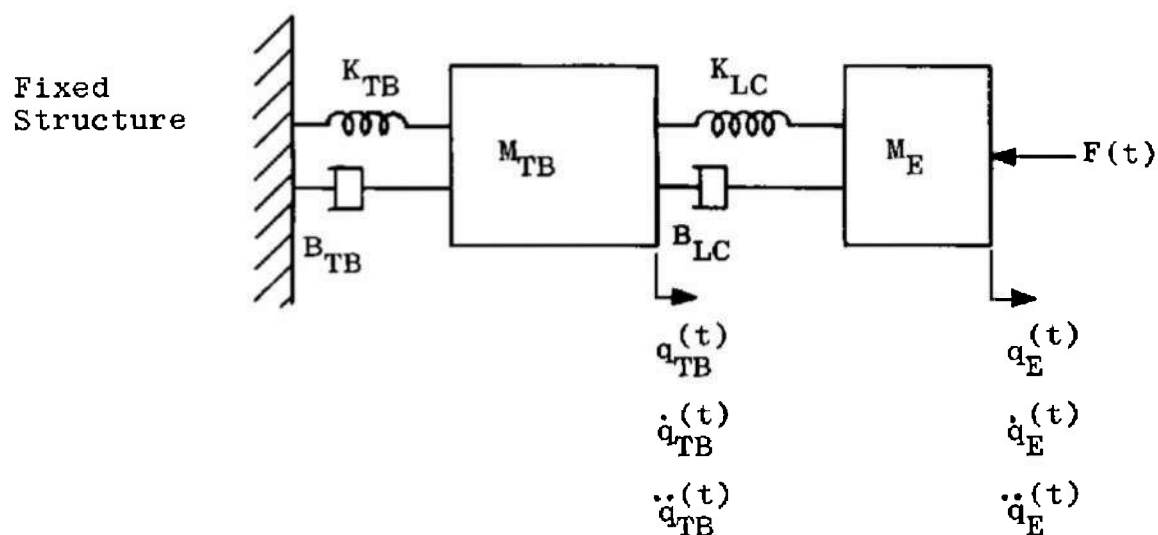


Fig. 27 Analytical Model of a Thrust Measurement System with a Dynamic Degree of Freedom of the Thrust Butt

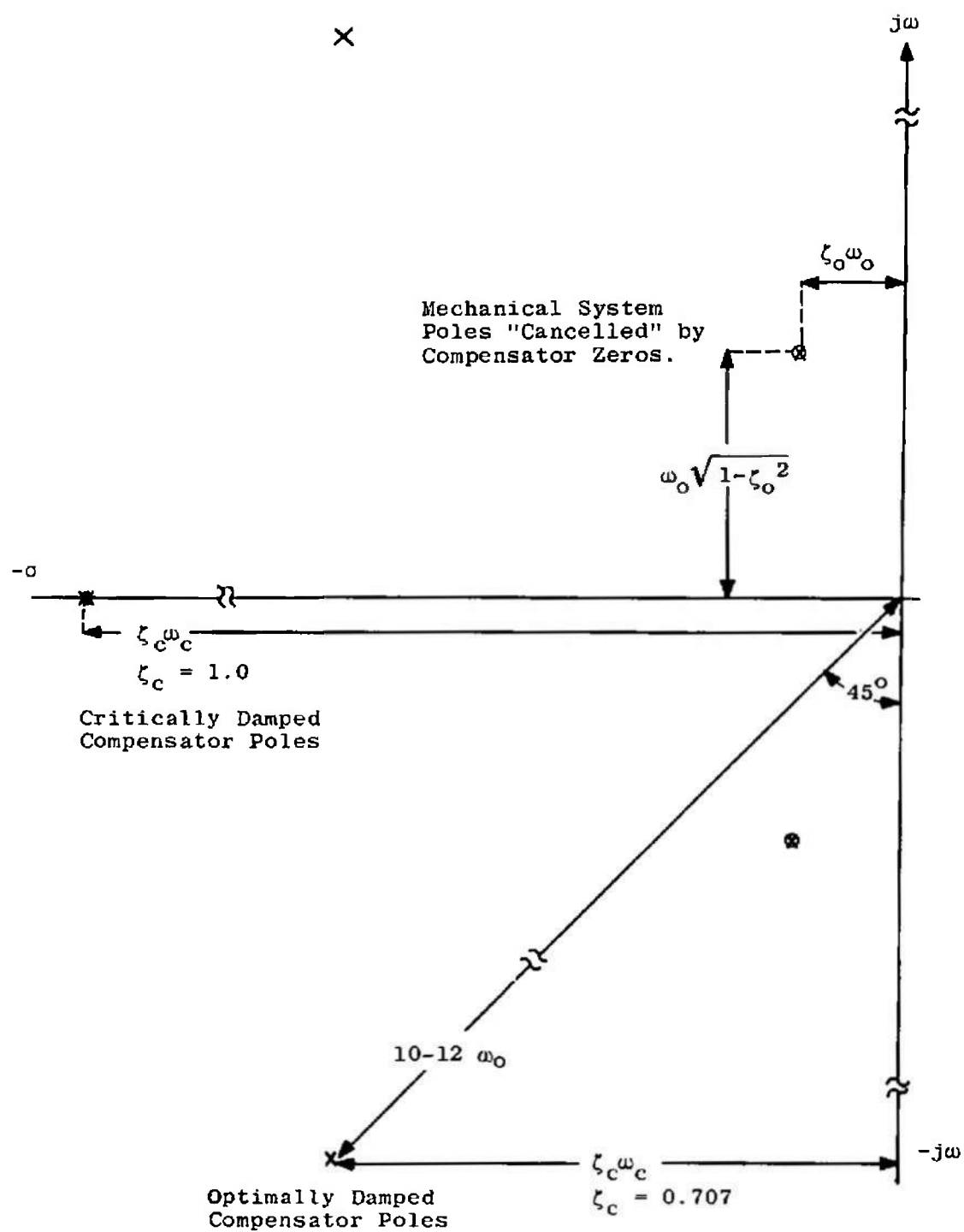


Fig. 28 S-Plane Pole-Zero Plot for Mechanical System and Compensator

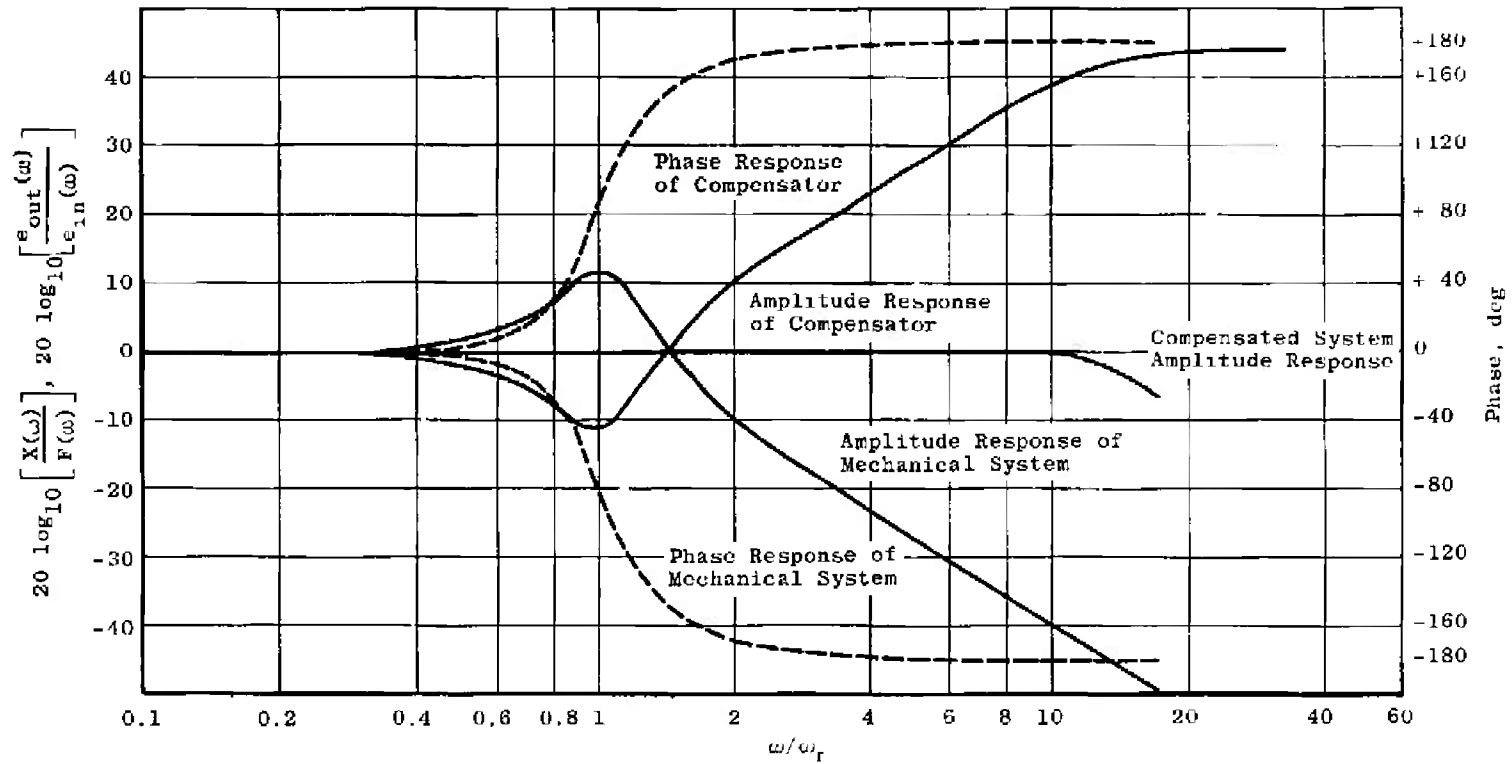
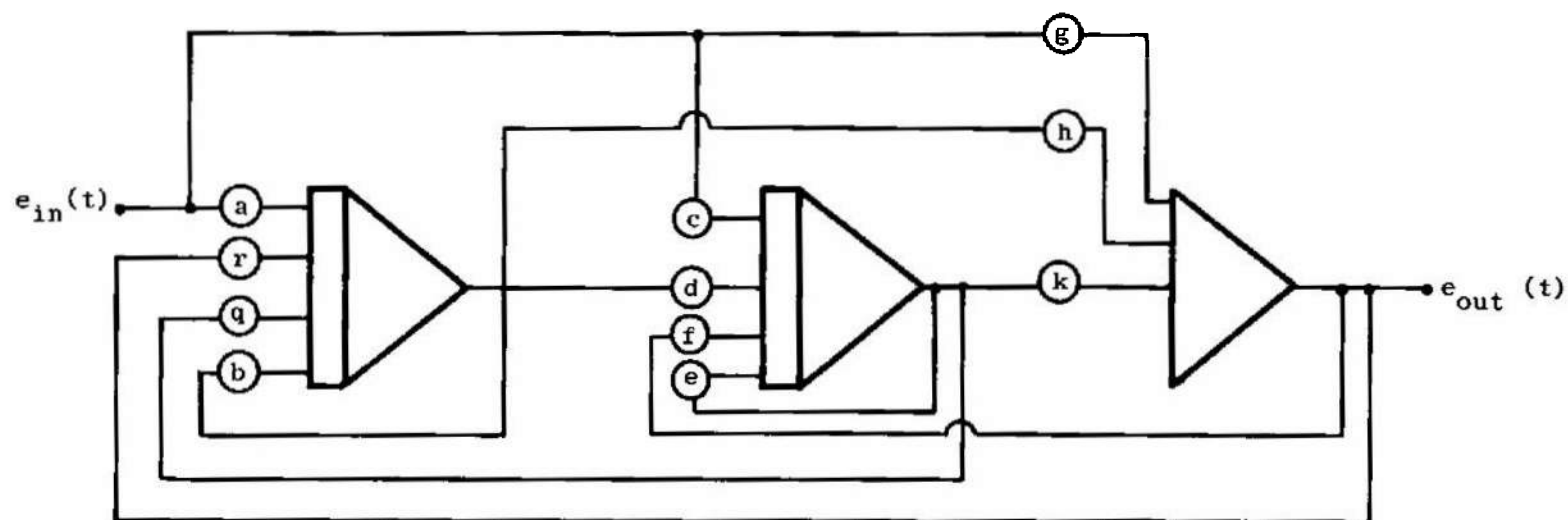


Fig. 29 Frequency Response of Mechanical System, Compensator, and Compensated System



Symbols a through k represent coefficient potentiometers

Fig. 30 Operational Block Diagram of General Three-Amplifier Analog Computer Compensator

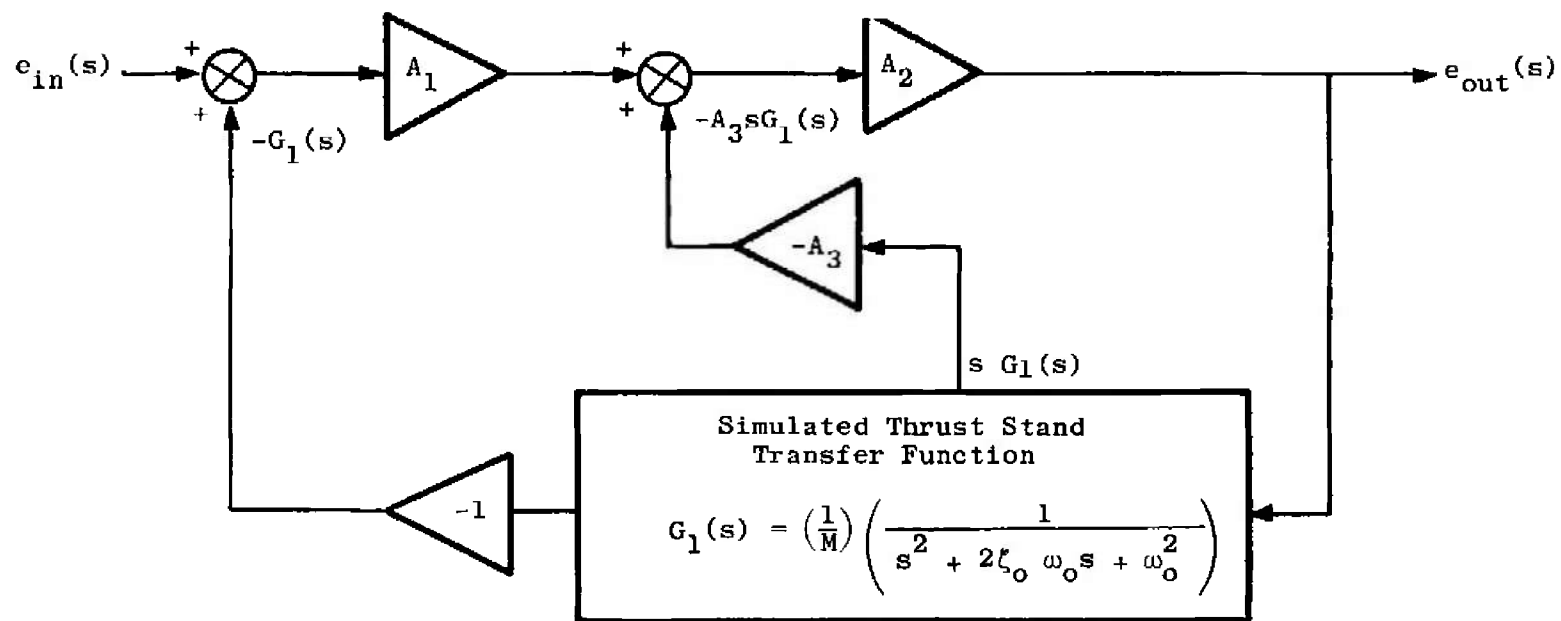


Fig. 31 Operational Block Diagram of Simulated Thrust Stand-Feedback-Type Compensator

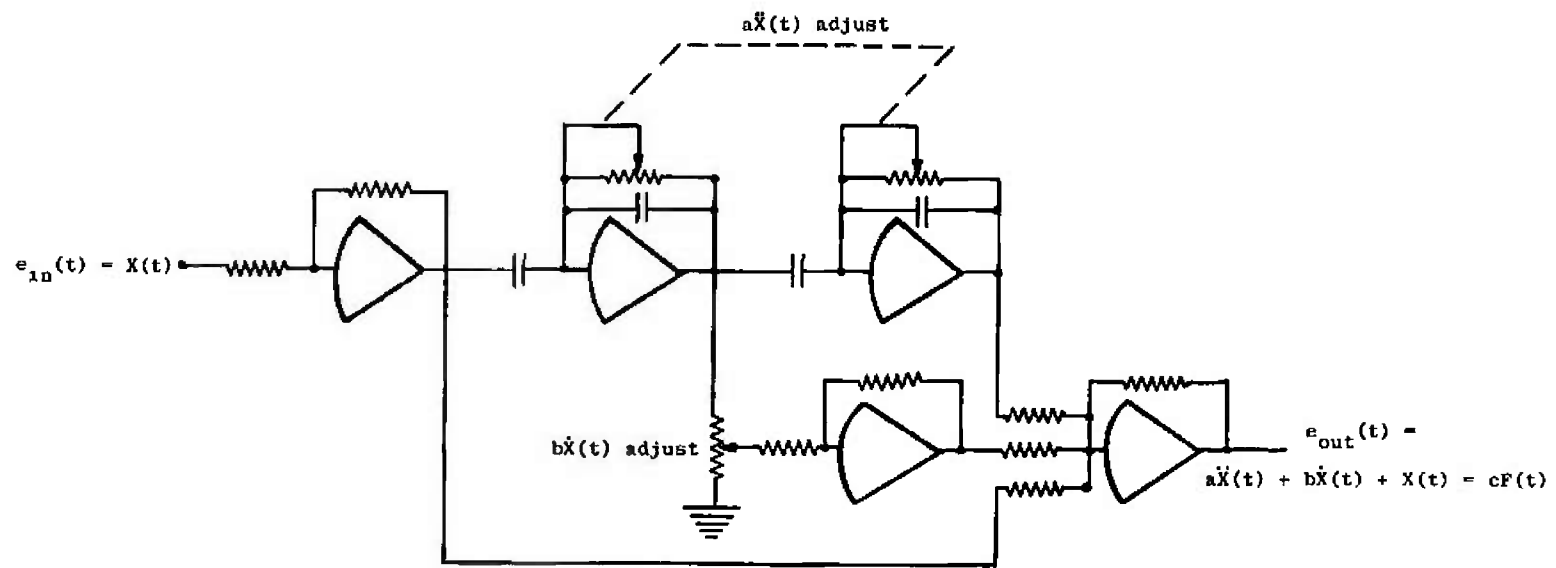


Fig. 32 Simplified Functional Block Diagram of Differentiator-Type Analog Computer Compensator

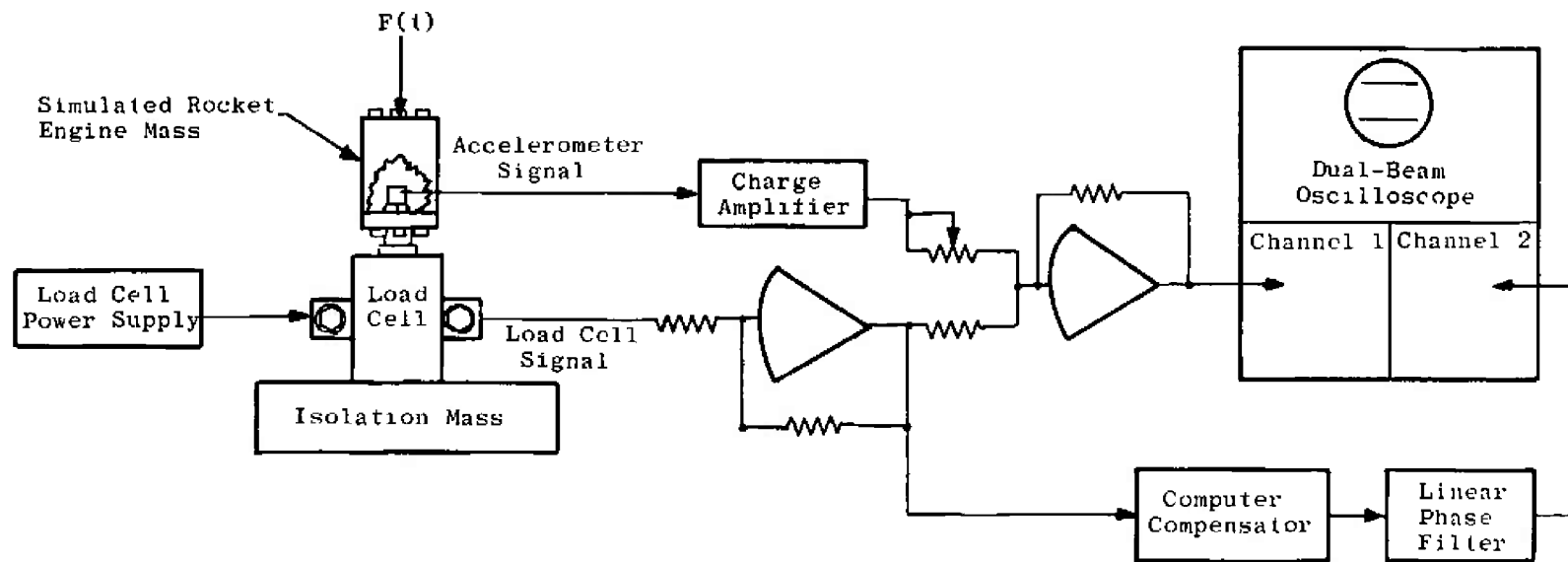


Fig. 33 System for Comparison of Data by Reaction Force Summation and Computer Compensation Techniques

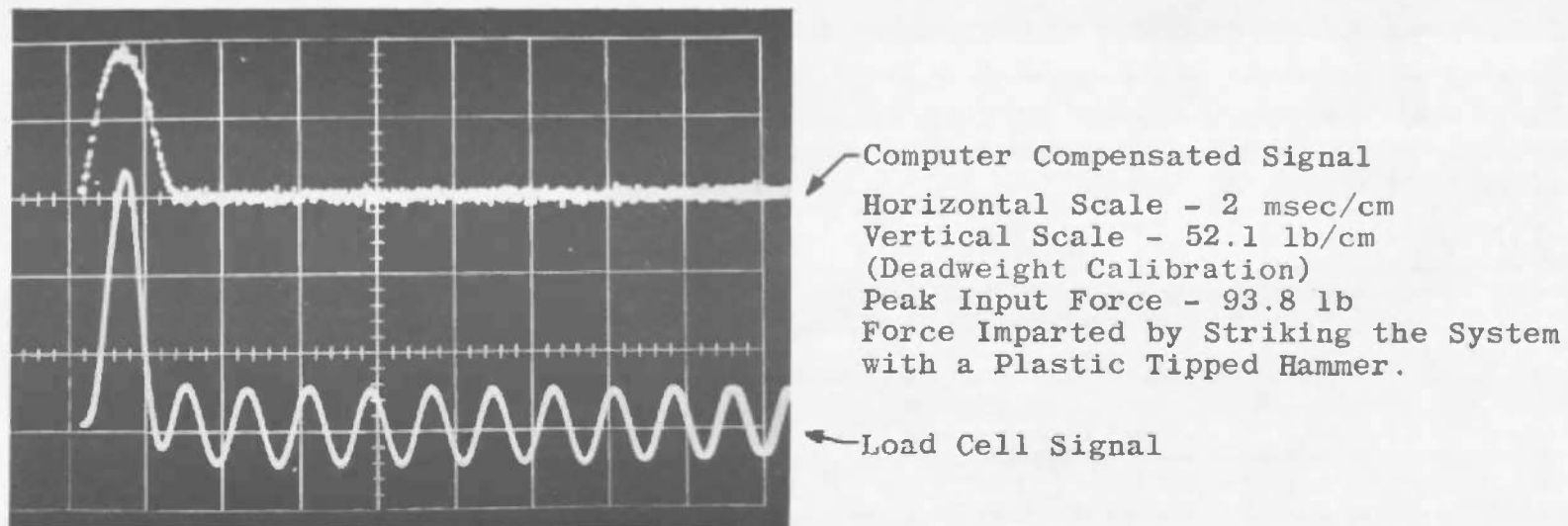
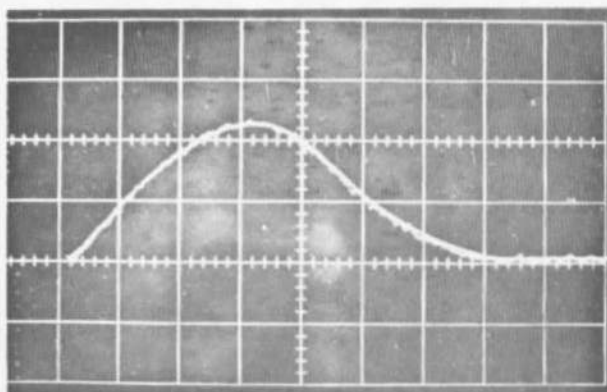
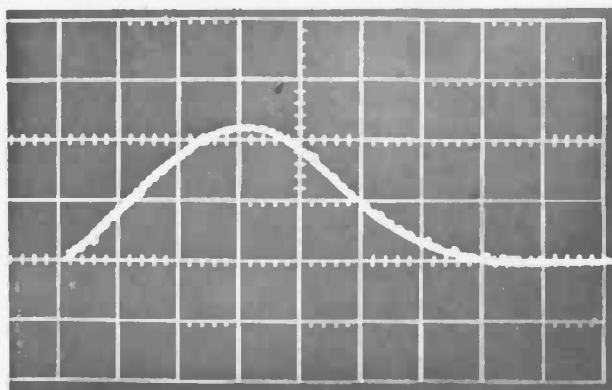


Fig. 34 Computer Compensation System Typical Performance



Horizontal Scale - 0.5 msec/cm
 Vertical Scale - 78.1 lb/cm
 (Deadweight Calibration)
 Peak Input Force - 179.6 lb

a. Reaction Force Summation and Computer Compensation Circuits both Filtered;
 Identical Filters Set with Cutoff Frequency of 5 KHz

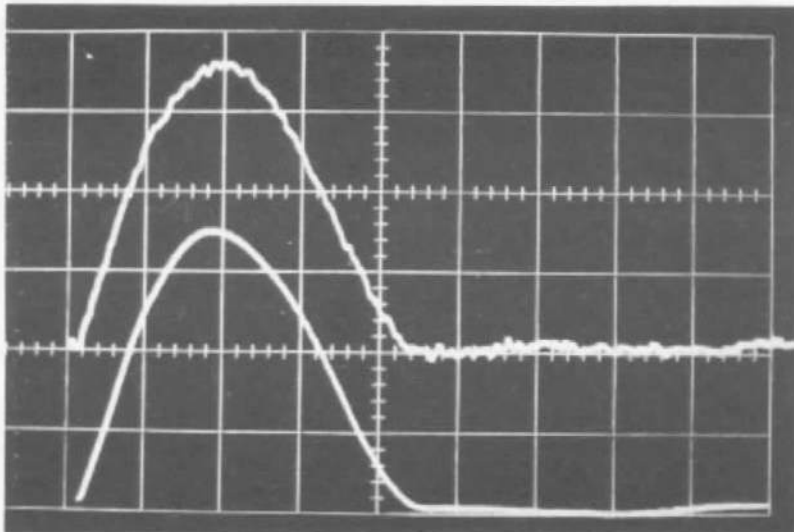


Horizontal Scale - 0.5 msec/cm
 Vertical Scale - 78.1 lb/cm
 (Deadweight Calibration)
 Peak Input Force - 171.8 lb

b. Reaction Force Summation Circuit Unfiltered; Computer Compensation Circuit Filtered

Force Imparted by Striking the System with
 a Plastic Tipped Hammer.
 Signals from Both Techniques Are Superimposed
 on the Oscilloscope.

Fig. 35 Comparison of Performance of Reaction Force Summation and
 Computer Compensation Techniques



Horizontal Scale - 0.5 msec/cm
Vertical Scale - 78.1 lb/cm
(Deadweight Calibration)
Peak Input Force - 273.4 lb

Computer Compensation Filtered
(Filter Cutoff Frequency - 5 kHz)

Reaction Force Summation, Unfiltered

Force Imparted by Striking the System
with a Plastic Tipped Hammer.

Fig. 36 Comparison of Performance of Reaction Force Summation and Computer Compensation Techniques for a High Peak Force Input

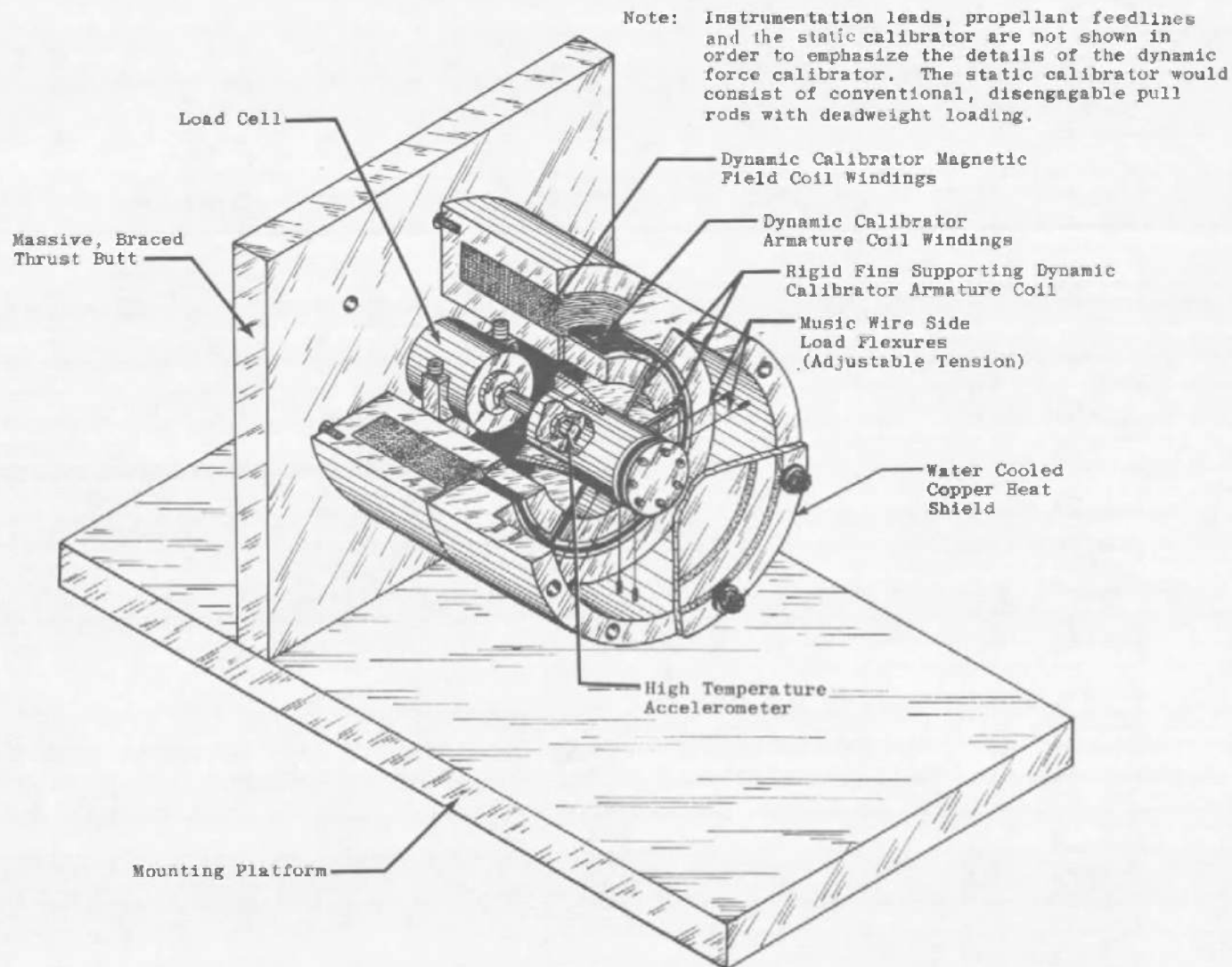


Fig. 37 Conceptual Drawing of Static and Dynamic Thrust Measurement System

APPENDIX II

ANALYTICAL CALCULATION OF MECHANICAL STRUCTURE TRANSIENT RESPONSE

A mechanical structure such as a thrust stand-rocket engine system oftentimes may be adequately represented by a model with constant and lumped parameter components. If the energy dissipation mechanisms are viscous in nature (damping force proportional to velocity) then the equations of motion of relatively simple structures are readily derived by application of D'Alembert's principle. The equations of motion for complex mechanical structures may be derived by application of the Lagrangian formalism:

$$\frac{d}{dt} \left(\frac{\partial L}{\partial \dot{q}_i^*} \right) - \frac{\partial L}{\partial q_i^*} + \frac{\partial D}{\partial \dot{q}_i^*} = Q_i, \quad i = 1, 2, \dots, n, \quad (\text{II-1})$$

where

$L = T - V$ is the Lagrange function,

$T = \frac{1}{2} \sum_i M_i \dot{q}_i^{*2}$ is the system kinetic energy,

$V = \frac{1}{2} \sum_{i,k} K_{ik} (q_i^* - q_k^*)^2$ is the system potential energy,

$D = \frac{1}{2} \sum_{i,k} B_{ik} (\dot{q}_i^* - \dot{q}_k^*)^2$ is the Rayleigh dissipation function.

The terms q_i^* , \dot{q}_i^* , and Q_i are the generalized displacements, generalized velocities, and generalized external forces, respectively; and i and k are coordinate point summation indices.

The solution to the motion problem of a multi-degree-of-freedom system with a large number of coordinates is facilitated by application of the Lagrangian in conjunction with matrix formulation of the equations of motion (Ref. 45):

$$[M] \{\ddot{q}^*\} + [B] \{\dot{q}^*\} - [K] \{q^*\} = \{Q\} \quad (\text{II-2})$$

where $[M]$, the mass and moment of inertia matrix, $[B]$, the damping matrix, and $[K]$, the stiffness matrix are $n \times n$ square matrices, and $\{\ddot{q}^*\}$, $\{\dot{q}^*\}$, $\{q^*\}$, and $\{Q\}$ are single column matrices with n elements, where n is the number of degrees of freedom.

The solution of the homogeneous equation of Eq. (II-2) yields an expression for the natural frequency responses of the q_i coordinates. The solution is of the following form (Ref. 45):

$$q_i = \sum_{r=1}^n A_{ir} e^{\lambda_r t} + \sum_{r=1}^n A'_{ir} e^{\lambda'_r t}, \quad i = 1, 2, \dots, n. \quad (\text{II-3})$$

where $2A_{ir} = C_{ir} e^{j\psi_{ir}}$ and $2A'_{ik} = C_{ir} e^{-j\psi_{ir}}$ are the displacements of the M_i mass point at the q_i coordinate for the $\lambda_r = -\alpha_r + j\omega_r$ and $\lambda'_r = -\alpha_r + j\omega_r$ eigen values.

Equation (I-3) can be expressed in the form:

$$q_i^* = \sum_{r=1}^n C_{ir} e^{-\alpha_r t} \cos(\omega_r t + \psi_{ir}), \quad i = 1, 2, \dots, n, \quad (\text{II-4})$$

where the subscript ir is to be interpreted as the response at coordinate i attributable to the natural frequency r .

When the energy dissipation of a linear system is negligible, the theory of normal mode of vibration is quite useful, since the response problem is amenable to matrix integration methods and digital computer solutions (Ref. 45).

Employing the Langrangian formalism and matrix formulation, the equations of motion can be written as:

$$[M] \{\ddot{q}\} + [K] \{q\} = \{Q\} \quad (\text{II-5})$$

The natural frequencies are determined by assuming solutions of the form:

$$q_i^* = A_j \sin(\omega t + \psi) \quad (\text{II-6})$$

and substituting these solutions into the homogeneous equations of motion:

$$[M] \{\ddot{q}^*\} + [K] \{q^*\} = 0 \quad (\text{II-7})$$

yields

$$\sum_{k=1}^n K_{ik} A_k = M_i \omega^2 A_i, \quad i = 1, 2, \dots, n \quad (\text{II-8})$$

The n homogeneous linear equations have nontrivial solutions if the determinant of the A_i and A_k coefficients vanishes (Ref. 46)

$$|K_{ik} - M_i \omega^2 \delta_{ik}| = 0 \quad (\text{II-9})$$

where δ_{ik} is the Kronecker delta. The solution of Eq. (I-9) for ω^2 yields the natural frequencies. Substituting the $\omega_1^2, \omega_2^2, \dots, \omega_n^2$ values into Eq. (I-8) yields n simultaneous equations for the A_i and A_k . The solution of the homogeneous equation, Eq. (I-7), is given by (Ref. 45):

$$q_i^* = \sum_{r=1}^n A_{ir} \sin(\omega_r t + \psi_{ir}), \quad i = 1, 2, \dots, n. \quad (\text{II-10})$$

DOCUMENT CONTROL DATA - R & D

(Security classification of title, body of abstract and indexing annotation must be entered when the overall report is classified)

1. ORIGINATING ACTIVITY (Corporate author)		2a. REPORT SECURITY CLASSIFICATION	
Arnold Engineering Development Center ARO, Inc., Operating Contractor Arnold Air Force Station, Tennessee		UNCLASSIFIED	
3. REPORT TITLE		2b. GROUP	
INVESTIGATION OF DYNAMIC ROCKET THRUST MEASUREMENT TECHNIQUES		N/A	
4. DESCRIPTIVE NOTES (Type of report and inclusive dates)			
June 1966 to August 1967 - Final Report			
5. AUTHOR(S) (First name, middle initial, last name)			
F. L. Crosswy and H. T. Kalb, ARO, Inc.			
6. REPORT DATE		7a. TOTAL NO. OF PAGES	7b. NO. OF REFS
November 1967		92	46
8a. CONTRACT OR GRANT NO.		9a. ORIGINATOR'S REPORT NUMBER(S)	
AF 40(600)-1200		AEDC-TR-67-202	
b. PROJECT NO. 5730		9b. OTHER REPORT NO(S) (Any other numbers that may be assigned this report)	
c. Program Element 6240518F		N/A	
d. Task 573004			
10. DISTRIBUTION STATEMENT			
This document is subject to special export controls and each transmittal to foreign governments or foreign nationals may be made only with prior approval of AEDC (AETS), Arnold Air Force Station, Tennessee.			
11. SUPPLEMENTARY NOTES		12. SPONSORING MILITARY ACTIVITY	
Available in DDC		Arnold Engineering Development Center, Air Force Systems Command Arnold Air Force Station, Tennessee	

13. ABSTRACT

The dynamic rocket thrust measurement is set forth as a part of the overall ground test problem. Dynamic thrust data obtained with conventional thrust measurement techniques can be distorted because of the transient response of the thrust stand-rocket engine mechanical structure. Distortionless dynamic thrust measurement is shown to be possible if the transfer function of the measurement system satisfies certain criteria. Three independent techniques satisfying the distortionless measurement criteria were investigated both analytically and experimentally, and the results are presented and discussed. The development and use of several dynamic force calibrators are also discussed.

This document is subject to special export controls and each transmittal to foreign governments or foreign nationals may be made only with prior approval of Arnold Engineering Development Center (AETS), Arnold Air Force Station, Tenn.

14.	KEY WORDS	LINK A		LINK B		LINK C	
		ROLE	WT	ROLE	WT	ROLE	WT
	rocket thrust measurement techniques force calibrators						
	1. Rocket motors -- Thrust measurement						
	2 Thrust -- Measurement Techniques						
	16. 3.						